# The Surface Water and Ocean Topography Mission (SWOT) Prior Lake Database (PLD): Lake mask and operational auxiliaries

Jida Wang<sup>1</sup>, Claire Pottier<sup>2</sup>, Cécile Cazals<sup>3</sup>, Marjorie Battude<sup>3</sup>, Yongwei Sheng<sup>4</sup>, Chunqiao Song<sup>5</sup>, Md Safat Sikder<sup>1</sup>, Xiao Yang<sup>6</sup>, Linghong Ke<sup>7</sup>, Marielle Gosset<sup>8</sup>, Rafael Reis Alencar Oliveira<sup>9</sup>, Manuela Grippa<sup>10</sup>, Félix Girard<sup>11</sup>, George H Allen<sup>12</sup>, Sylvain Biancamaria<sup>13</sup>, Laurence Smith<sup>14</sup>, Jean-François Crétaux<sup>15</sup>, and Tamlin M Pavelsky<sup>6</sup>

<sup>1</sup>University of Illinois at Urbana Champaign <sup>2</sup>Centre National d'Études Spatiales (CNES) <sup>3</sup>CS Group <sup>4</sup>Department of Geography, University of California <sup>5</sup>Key Laboratory of Watershed Geographic Sciences, Nanjing Institute of Geography and Limnology, Chinese Academy of Sciences <sup>6</sup>University of North Carolina at Chapel Hill <sup>7</sup>College of Hydrology and Water Resources, Hohai University <sup>8</sup>Institut de Recherche pour le Developpement <sup>9</sup>Ceará State's Foundation for Meteorology and Water Resources (FUNCEME, UFC, UT, GET) <sup>10</sup>Géosciences Environnement Toulouse, Univ. Toulouse, CNRS, IRD, CNES <sup>11</sup>Géosciences Environnement Toulouse (Université de Toulouse, CNRS, IRD, CNES) <sup>12</sup>Virginia Tech <sup>13</sup>CNRS/LEGOS <sup>14</sup>Brown University <sup>15</sup>Laboratoire d'Études en Géophysique et Océanographie Spatiales (LEGOS)

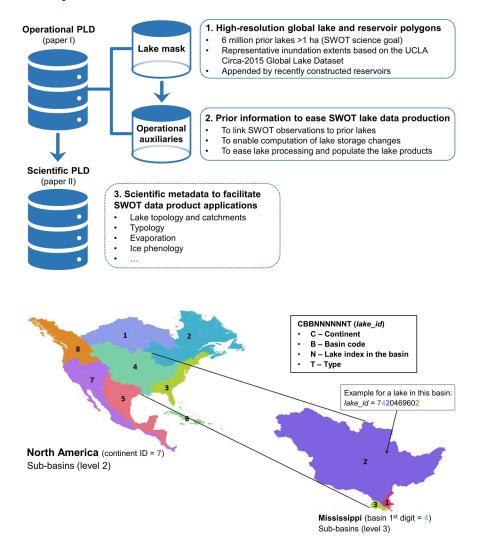
December 14, 2023

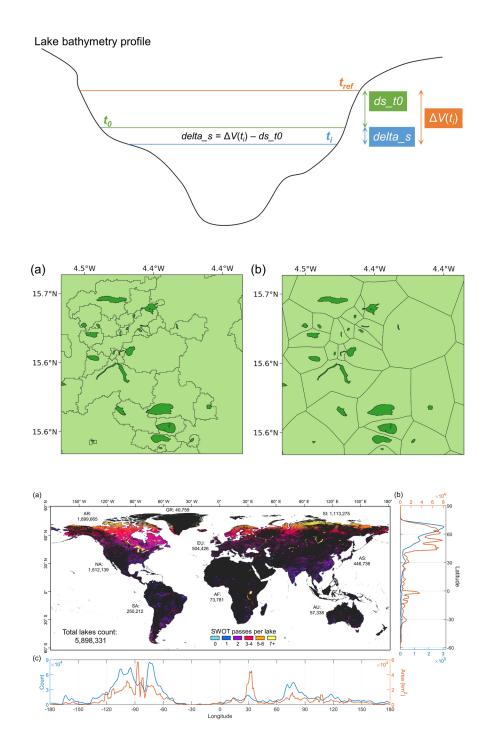
#### Abstract

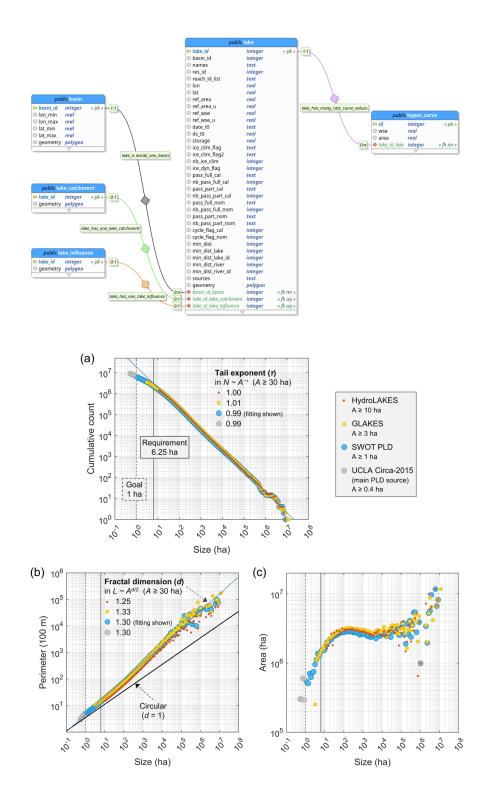
Lakes are the most prevalent and predominant water repositories on land surface. A primary objective of the Surface Water and Ocean Topography (SWOT) satellite mission is to monitor the surface water elevation, area, and storage change in Earth's lakes. To meet this objective, prior information of global lakes, such as locations and benchmark extents, is required to organize SWOT's KaRIn observations over time for computing lake storage variation. Here, we present the SWOT mission Prior Lake Database (PLD) to fulfill this requirement. This paper emphasizes the development of the "operational PLD", which consists of (1) a high-resolution mask of <sup>~</sup>6 million lakes and reservoirs with a minimum area of 1 ha, and (2) multiple operational auxiliaries to assist the lake mask in generating SWOT's standard vector lake products. We built the prior lake mask by harmonizing the UCLA Circa-2015 Global Lake Dataset and several state-of-the-art reservoir databases. Operational auxiliaries were produced from multi-theme geospatial data to provide information necessary to embody the PLD function, including lake catchments and influence areas, ice phenology, relationship with SWOT-visible rivers, and spatiotemporal coverage by SWOT overpasses. Globally, over three quarters of the prior lakes are smaller than 10 ha. Nearly 96% of the lakes, constituting over half of the global lake area, are fully observed at least once per orbit cycle. The PLD will be recursively improved during the mission period and serves as a critical framework for organizing, processing, and interpreting SWOT observations over lacustrine environments with fundamental significance to lake system science.

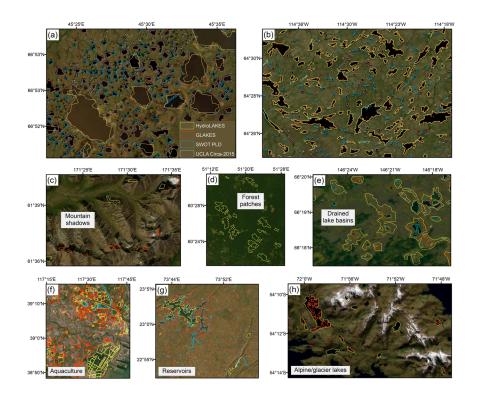
#### Hosted file

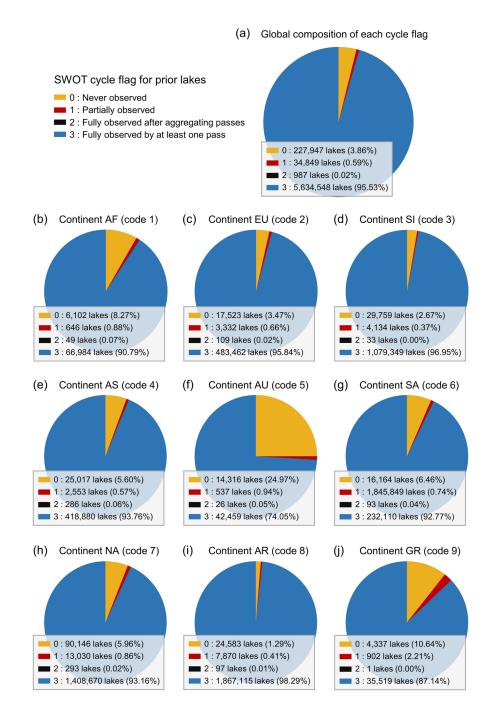
981781\_0\_art\_file\_11674843\_s514gl.docx available at https://authorea.com/users/335717/ articles/693171-the-surface-water-and-ocean-topography-mission-swot-prior-lake-databasepld-lake-mask-and-operational-auxiliaries

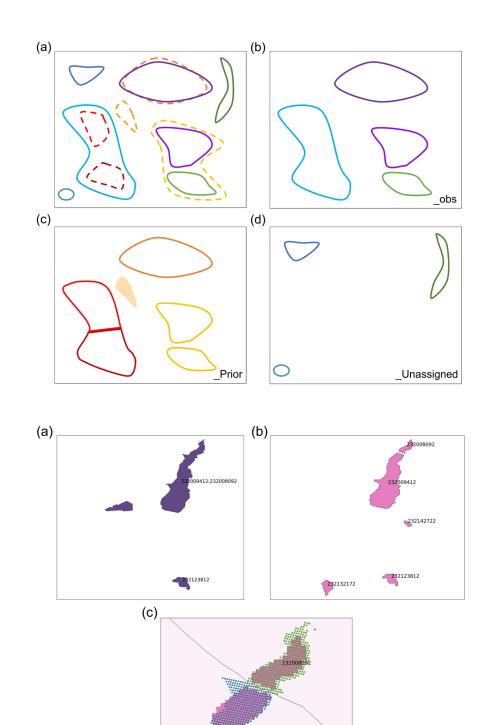












1 The Surface Water and Ocean Topography Mission (SWOT) Prior Lake Database

- 2 (PLD): Lake mask and operational auxiliaries
- 3
- 4 Jida Wang, Claire Pottier, Cécile Cazals, Marjorie Battude, Yongwei Sheng, Chunqiao Song, Md
- 5 Safat Sikder, Xiao Yang, Linghong Ke, Marielle Gosset, Rafael Reis Alencar Oliveira, Manuela
- 6 Grippa, Félix Girard, George H. Allen, Sylvain Biancamaria, Laurence C. Smith, Jean-Francois
- 7 Crétaux, Tamlin Pavelsky
- 8
- 9 Author affiliations:
- 10 Jida Wang: Department of Geography and Geographic Information Science, University of Illinois
- 11 Urbana-Champaign, Urbana, IL, USA. jidaw@illinois.edu
- 12 Claire Pottier: Centre National d'Études Spatiales (CNES), Toulouse, France. <u>Claire.Pottier@cnes.fr</u>
- 13 Cécile Cazals: CS Group, Toulouse, France. <u>cecile.cazals@csgroup.eu</u>
- 14 Marjorie Battude: CS Group, Toulouse, France. <u>marjorie.battude@csgroup.eu</u>
- 15 Yongwei Sheng: Department of Geography, University of California, Los Angeles, CA, USA.
- 16 <u>ysheng@geog.ucla.edu</u>
- 17 Chunqiao Song: Key Laboratory of Watershed Geographic Sciences, Nanjing Institute of Geography and
- 18 Limnology, Chinese Academy of Sciences, Nanjing, China; University of Chinese Academy of Sciences,
- 19 Nanjing, Nanjing, China. cqsong@niglas.ac.cn
- 20 Md Safat Sikder: Department of Geography and Geospatial Sciences, Kansas State University,
- 21 Manhattan, KS, USA. msikder@ksu.edu
- Xiao Yang: Department of Earth Sciences, Southern Methodist University, Dallas, TX, USA.
   xnayang@smu.edu
- Linghong Ke: College of Hydrology and Water Resources, Hohai University, Nanjing, 210098, China;
- State Key Laboratory of Hydrology-Water Resources and Hydraulic Engineering, Hohai University,
   Nanjing, 210098, China. kelinghong@hhu.edu.cn
- Marielle Gosset: Géosciences Environnement Toulouse (Université de Toulouse, CNRS, IRD, CNES).
   <u>marielle.gosset@ird.fr</u>
- Rafael Reis Alencar Oliveira: Ceará State's Foundation for Meteorology and Water Resources
   (FUNCEME, UFC, UT, GET), Fortaleza, Brazil. rafael.reis@funceme.br
- Manuela Grippa: Géosciences Environnement Toulouse (Université de Toulouse, CNRS, IRD, CNES).
   <u>manuela.grippa@get.omp.eu</u>
- Félix Girard: Géosciences Environnement Toulouse (Université de Toulouse, CNRS, IRD, CNES).
   <u>felix.girard@get.omp.eu</u>
- 35 George H. Allen: Department of Geosciences, Virginia Polytechnic Institute and State University,
- 36 Blacksburg, VA, USA. <u>geoallen@vt.edu</u>
- Sylvain Biancamaria: Laboratoire d'Études en Géophysique et Océanographie Spatiales (LEGOS), Centre
   National d'Études Spatiales (CNES), Toulouse, France. sylvain.biancamaria@univ-tlse3.fr
- 39 Laurence C. Smith: Department of Earth, Environmental and Planetary Sciences, Brown University,
- 40 Providence, RI, USA. Laurence Smith@Brown.edu

- 41 Jean-Francois Crétaux: Laboratoire d'Études en Géophysique et Océanographie Spatiales (LEGOS),
- 42 Centre National d'Études Spatiales (CNES), Toulouse, France. jean-francois.cretaux@cnes.fr
- 43 Tamlin Pavelsky: Department of Earth, Marine and Environmental Sciences, University of North
- 44 Carolina, Chapel Hill, NC, USA. pavelsky@email.unc.edu

### 45 Key Points:

- SWOT Prior Lake Database (PLD) provides the foundation for generating SWOT vector
   lake products including area, height, and storage change.
- PLD inventories 6 million lakes with a 1-ha minimum area, 76% of which are smaller
   than 10 ha and 96% are fully observed per orbit cycle.
- PLD contains multiple operational auxiliaries to ease lake assignment, storage change
   computation, and vector lake product distribution.

### 53 Abstract

52

54 Lakes are the most prevalent and predominant water repositories on land surface. A primary

objective of the Surface Water and Ocean Topography (SWOT) satellite mission is to monitor

the surface water elevation, area, and storage change in Earth's lakes. To meet this objective,

57 prior information of global lakes, such as locations and benchmark extents, is required to

organize SWOT's KaRIn observations over time for computing lake storage variation. Here, we

- 59 present the SWOT mission Prior Lake Database (PLD) to fulfill this requirement. This paper
- 60 emphasizes the development of the "operational PLD", which consists of (1) a high-resolution
- mask of ~6 million lakes and reservoirs with a minimum area of 1 ha, and (2) multiple
- 62 operational auxiliaries to assist the lake mask in generating SWOT's standard vector lake
- 63 products. We built the prior lake mask by harmonizing the UCLA Circa-2015 Global Lake
- 64 Dataset and several state-of-the-art reservoir databases. Operational auxiliaries were produced
- 65 from multi-theme geospatial data to provide information necessary to embody the PLD function,
- 66 including lake catchments and influence areas, ice phenology, relationship with SWOT-visible
- rivers, and spatiotemporal coverage by SWOT overpasses. Globally, over three quarters of the
   prior lakes are smaller than 10 ha. Nearly 96% of the lakes, constituting over half of the global
- 69 lake area, are fully observed at least once per orbit cycle. The PLD will be recursively improved
- during the mission period and serves as a critical framework for organizing, processing, and
- interpreting SWOT observations over lacustrine environments with fundamental significance to
- 72 lake system science.

## 73 **1 Introduction**

Natural lakes and manmade reservoirs, hereafter "lakes", are among the most 74 predominant components of land hydrology (Messager et al., 2016; Verpoorter et al., 2014). 75 They collectively store nearly 90% of the liquid freshwater on the Earth's surface, providing the 76 most readily accessible water resource for societal use (Abbott et al., 2019; Oki & Kanae, 2006). 77 78 Lakes also represent diverse and complex aquatic ecosystems, offering unique aesthetic appeals in the landscape and indispensable sources of biodiversity, food, and recreation outlets 79 (Herdendorf, 1984). Although considered as lentic systems, lakes are often dynamic, with water 80 storage and quality reflective of basin-scale hydrology and/or anthropogenic activities (Fergus et 81 al., 2017; Wurtsbaugh et al., 2017; Yang, O'Reilly, et al., 2022). Lakes also sequester a large 82 amount of carbon from the watersheds and modulate terrestrial carbon cycling through water 83 84 storage variation and lacustrine-fluvial interactions (Mendonca et al., 2017; Tranvik et al., 2009). For these reasons, lakes serve as both "sentinels" and "regulators" of climate change (Adrian et 85 al., 2009; Schindler, 2009) and are recognized as an "Essential Climate Variable" by the Global 86 Climate Observing System (GCOS) of the World Meteorological Organization (WMO, 2022). 87 Monitoring the dynamics in global lakes, including water extent and level that are essential to 88 deriving storage variability, has important ramifications to hydrology, ecology, the carbon cycle, 89 and water sustainability (Yao et al., 2023). 90

Our capability to monitor global lake dynamics has been rapidly advancing with the 91 expanding Earth-observing system (Cretaux et al., 2016). But, until recently, individual satellite 92 93 missions for surface hydrology measured either water extent, such as through spectral radiometers and Synthetic Aperture Radar (SAR) imagers, or water surface elevation (WSE), 94 such as through nadir-looking radar and lidar altimeters. This dilemma challenged the 95 monitoring of water storage variation, which requires a synchronous acquisition or coordination 96 of both variables. In addition, conventional radar altimeters usually have coarse footprint sizes 97 (~10 km<sup>2</sup> or greater) and large inter-track distances (~50–100 km or wider), limiting adequate 98 99 measurements to a few thousand largest lakes (Busker et al., 2019; Cretaux et al., 2016; Cretaux et al., 2011; Schwatke et al., 2015; Yao et al., 2023). With improvements of the waveform 100 processing methods, SAR-mode altimeters such as those onboard Sentinel-3A and Sentinel-3B 101 showed potential for measuring WSEs of lakes as small as a few hectares (Boy et al., 2022). 102 103 Smaller footprints (~11–70 m) were also enabled by laser altimeters such as the Ice, Cloud, and land Elevation Satellite (ICESat) and its successor ICESat-2. However, their multi-month repeat 104 105 cycles, along with discrete nadir footprints, limit the temporal density of WSE measurements for medium-sized and small lakes (Cooley et al., 2021; Luo et al., 2022). Fortunately, these technical 106 challenges have been largely overcome by the Surface Water and Ocean Topography (SWOT) 107 108 satellite mission (Biancamaria et al., 2016), recently launched on December 16, 2022.

The main payload of SWOT is a Ka-band (8.6 mm wavelength) radar interferometer 109 (KaRIn). As the first of its kind, KaRIn provides synchronous, wide-swath, and orbital surveys 110 of both surface water extent and elevation, allowing for the derivations of river discharge and 111 lake storage change (Biancamaria et al., 2016; Durand et al., 2010). SWOT's lake observation 112 requirement includes all enclosed water bodies larger than  $250 \times 250 \text{ m}^2$  (i.e., 6.25 ha) between 113 77°N and 77°S covering 90% of the continental surface, and the observation goal is lakes as 114 small as  $100 \times 100 \text{ m}^2$  (i.e., 1 ha) (Biancamaria et al., 2016). Owing to the wide-swath (2×50 km) 115 configuration, more than 90% of the global lakes larger than 1 ha are expected to be observed by 116 SWOT at least once within each 21-day cycle of the three-year science or nominal orbit period 117

(JPL internal document, 2018). While these spatiotemporal coverages will reveal unprecedented

details of global lake storage variability, a prerequisite for facilitating SWOT lake dataproduction is the preparation of a Prior Lake Database (PLD).

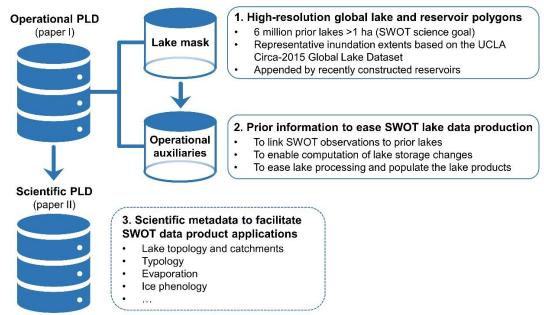
The fundamental purpose of the SWOT PLD is to provide prior data on known lake 121 locations, hereafter "prior lakes", making it possible to link KaRIn observations over time and to 122 123 compute lake storage variation. KaRIn observes terrestrial water features (e.g., lakes and rivers) at a high-rate (HR) mode with fine spatial resolution ( $\sim 5 \text{ m} \times 10-70 \text{ m}$ ) (Biancamaria et al., 124 2016). To accommodate user needs, the HR raw data are processed by the Science Algorithm 125 Software (SAS) to different levels of products, which range from Level 1 single-look complex 126 SAR images (L1B\_HR\_SLC) (JPL internal document, 2022c) intended only for highly 127 specialized applications, to the standard Level 2 vector products delivering readily usable 128 variables specific to rivers and lakes. The initial HR product suitable for general hydrological 129 purposes is "pixel cloud" (L2 HR PIXC) (JPL internal document, 2022d), which consists of 130 geolocated pixel points with measured water heights but is not organized to distinct water 131 features. With the help of the SWOT River Database (SWORD) (Altenau et al., 2021), pixels 132 associated with prior rivers are first extracted to process the standard vector river products (JPL 133 internal document, 2022a, 2022b, 2023). Such river pixels, except those also on SWORD-134 connected lakes, are eliminated from further lake processing. The remaining pixels are then 135 segmented to individual water regions based on statistical clusters of the pixel heights. PIXC 136 geolocations, however, contain noise from the interferogram (Desroches et al., 2016). By 137 smoothing pixel heights across individual water regions, PIXC geolocations are corrected to a 138 less noisy pixel cloud (L2 HR PIXCVec) (CNES internal document, 2022c) for vectorization. 139 With assistance of the PLD, the corresponding water features are processed to the standard 140 vector lake products, which deliver the dynamics and uncertainties of WSE, area, and storage 141 change (when applicable) for each prior lake per orbit pass (L2\_HR\_LakeSP) or cycle 142

143 (L2\_HR\_LakeAvg) (CNES internal document, 2022a, 2022b).

144 Two primary components are required to fulfill the purpose of the PLD (Fig. 1). As lakes are often dynamic over time, their water surface may split and coalesce, and new lakes may 145 emerge whereas others disappear. Without defining lakes a priori, it would be difficult to sort out 146 how water features observed in different periods are spatially related to each other, which would 147 148 then pose a challenge for effectively comparing lake changes. So, the first component of the PLD is a comprehensive prior mask that inventories global lakes larger than SWOT's observation goal 149 (1 ha). Albeit temporally static, this lake mask offers a standardized spatial reference, based on 150 which observed water features can be assigned, aggregated, or partitioned to the corresponding 151 prior lakes. This ensures water dynamics, especially storage change, to be characterized and 152 delivered consistently at the scale of each known lake. On the other hand, the lake mask also 153 identifies observed water features that cannot be assigned to any prior lake. The unassigned 154 features will be used to recursively improve the prior lake mask as SWOT data accumulate and 155 to investigate the changes in wetlands, newly emerged lakes, and other relevant phenomenology. 156 To make the prior lake mask functional, we need the second component of the PLD, namely 157 "operational auxiliaries", which supplement the prior lakes with other necessary attributes, 158 geometries, and logical information. The additional prior information works synergistically to 159 ease the linkage of SWOT observations to the prior lakes, the calculation of lake storage change, 160 and the population of the vector lake products. 161

An accurate and up-to-date prior lake mask is essential to the function of the PLD. We 162 consider a lake mask qualified for the PLD to be "exhaustive" (including all lakes  $\geq 1$  ha), 163 "exclusive" (excluding non-lake features), and "representative" (with lake polygons representing 164 intermediate rather than extreme inundation conditions). At the current stage of the SWOT 165 mission, we prefer intermediate water extent because it presents how a lake normally appears 166 when being observed by SWOT, which eases the spatial linkage of SWOT observations to the 167 prior lake. Despite the recent proliferation of global lake datasets, none of them alone can meet 168 all three criteria. Two fine-resolution and publicly accessible global lake masks are 169 HydroLAKES (v1.0) (Messager et al., 2016), which inventories 1.4 million lakes larger than 10 170 ha, and GLAKES, which comprises 3.4 million polygons depicting the maximum lake water 171 extents large than 3 ha (Pi et al., 2022). The primary data source of HydroLAKES for the 172 landmass below 60° N is the Shuttle Radar Topography Mission Water Body Dataset (SWBD) 173 (Farr et al., 2007), where lake extents were based on water occurrence during February 2000. 174 This timing concurred with the dry winter season across a large proportion of the northern 175 hemisphere, meaning the sizes of many lakes in HydroLAKES are likely skewed towards their 176 seasonal minimums. In addition, SWBD was acquired over twenty years ago, predating the 177 recent prominent lake changes such as the shrinkage of many saline lakes (Wang et al., 2018; 178 Wurtsbaugh et al., 2017), the expansion of glacial lakes (Nie et al., 2017; Shugar et al., 2020; 179 Song et al., 2017), and the boom of new reservoir construction (Wang et al., 2022; Wu et al., 180 181 2023; Yao et al., 2023). Therefore, HydroLAKES may no longer accurately reflect the latest boundaries of many lakes in the world. In comparison, GLAKES used Landsat-derived Global 182 Surface Water Occurrence (GSWO) dataset (Pekel et al., 2016) to extract all-time water area 183 maximum during 1984 to 2019, where non-lake features (e.g., rivers, estuaries, and floodwaters) 184 were removed by a deep-learning algorithm (Pi et al., 2022). While GLAKES is more up to date, 185 the lake polygons correspond to the maximum extreme. Based on our visual inspection, these 186 maximum extents occasionally include inundated riparian zones, floodplains, and paddy fields. 187 Critically, neither dataset reaches a minimum lake size of 1 ha, meaning that lakes potentially 188

189 visible to SWOT are not exhaustively inventoried.



190

191 **Figure 1.** Conceptual structure of the SWOT Prior Lake Database (PLD).

Tailored to the SWOT mission needs, we describe the development of the SWOT PLD in 192 193 a pair of companion papers (Fig. 1). The first paper (this article) emphasizes the prior lake mask and the operational metadata, which constitute the "operational PLD", addressing the above-194 described fundamental purpose for assisting SWOT lake data production. The second paper (in 195 preparation) will focus on the development of a "scientific PLD", which consists of multi-theme 196 scientific metadata to facilitate a wide range of limnological applications of the SWOT lake data 197 products. Following the introduction, we describe the input data sources (section 2) and the 198 methods (section 3) to construct the operational PLD. This is followed by the results (section 4) 199 that present the prior lake mask comparatively with other lake datasets, the theoretical coverage 200 for global lakes during a nominal orbit cycle, and the functionality of the operational metadata. 201 With a primary focus on data development instead of algorithms (SASs), this paper does not 202 elaborate how lake storage change is computed. However, we do describe the purpose of each 203 prior attribute including those for computing lake storage change (section 3) and illustrate how 204 the PLD works to ease SWOT lake data production (section 4). We then conclude the paper by 205

discussing the plans of future PLD improvements and versioning (section 5).

# 207 2 Input data sources

We leveraged multiple data sources to compose the operational PLD. These input datasets and their contributions are summarized in Table 1. The primary data source is the UCLA

210 Circa-2015 Global Lake Dataset (Sheng et al., 2016), which provides most of the polygons in the

211 high-resolution prior lake mask. A collection of other datasets, covering the themes of lake

name, reservoir identity, prior river locations, hydrography, and SWOT orbits, were used to

213 populate the prior attribute information. Details of each input dataset are described below.

Data source	Contribution
UCLA Circa-2015 Global Lake Dataset (Sheng et al., 2016)	Provides the main source of prior lake mask
Georeferenced global Dams And Reservoirs (GeoDAR) dataset v1.1 (Wang et al., 2022) Post2k reservoir dataset (Fan et al., 2023) Other regional reservoirs (see Section 3.2)	Supplements the UCLA Circa-2015 Global Lake – Dataset with additional recently constructed – reservoirs
Global Reservoir and Dam database (GRanD) v1.3 (Lehner et al., 2011)	Provides the identities of large reservoirs
HydroBASINS (Lehner & Grill, 2013)	Populates basin IDs
SWORD (Altenau et al., 2021)	Identifies lakes on prior rivers, which are included for both lake and river data products
SWOT orbits (https://www.aviso.altimetry.fr)	Populates attributes related to the lake coverage by SWOT in the "lake" table
Global Lakes and Wetlands Database (GLWD) (Lehner & Doll, 2004) HydroLAKES v1.0 (Messager et al., 2016) Natural Earth Data (scale 1:30,000,000) (https://www.naturalearthdata.com) OpenStreetMap (OSM;	– – Populates lake names

Table 1. Data sources used to develop the operational PLD

https://www.openstreetmap.org) The IGN Carthage database (BD CARTHAGE®) (https://services.sandre.eaufrance.fr/telecharg ement/geo/ETH/BDCarthage/FXX/2017) Vector Map Level 0 (VMap0) (https://mdl.library.utoronto.ca/collections/ge ospatial-data/vector-map-level-0-vmap0)

## 215 2.1 UCLA Circa-2015 Global Dataset

The foundation of the PLD, i.e., the prior lake mask, mainly comes from the UCLA 216 Circa-2015 Global Lake Dataset (Sheng et al., 2016), or hereafter "Circa-2015" lake dataset. The 217 Circa-2015 lake dataset inventories representative inundation extents of 9.0 million open-water 218 lakes and reservoirs larger than 0.4 ha (i.e., four 30-m-resolution Landsat pixels) in the world. 219 These lakes were mapped from a selection of high-quality Landsat-8 images acquired during the 220 initial 2.5 years of the mission operation (May 2013 to August 2015). The complete mapping 221 procedure, including image selection, water extraction algorithm, quality assurance and quality 222 control (QA/QC), and multi-scene composition, was articulated for the case of Oceania by 223 (Sheng et al., 2016), and the rest of the world was subsequently mapped using the same methods. 224

Compared to other global lake data, a unique merit of the Circa-2015 dataset is the 225 emphasis on representative lake extents, echoing one of the three criteria expected for the SWOT 226 prior lake mask (section 1). Specifically, the images selected for mapping were acquired during 227 the "lake stable season" to minimize the misrepresentation of lake size due to intra-annual 228 inundation extremes. The lake stable season was defined as the period after the rainy season, 229 when inflows equal outflows and the lake thus reaches a stable condition within the annual cycle. 230 To implement this idea, an image selection tool "LakeTime" (Lyons & Sheng, 2018) was 231 developed using long-term climate data to determine the lake stable season independently for 232 each Landsat tile. Cloud-free images were then collected tile by tile during the ideal period for 233 lake mapping. This image selection process rendered a total of ~60,000 Landsat-8 scenes across 234 the continents, with an average of about 6 scenes per tile. 235

For each selected scene, open water was segmented from land using a hierarchical and 236 self-adaptive algorithm to ensure lakes across different landscapes can be mapped as accurately 237 and thoroughly as possible (see (Sheng et al., 2016) for details). Together with a minimum 238 mapping unit of 0.4 ha, the result satisfies the second criterion "exhaustive" for the prior lake 239 mask. Since lakes are diverse aquatic systems, multiple factors such as water turbidity, mineral 240 and chlorophyll contents, ice and snow, and mountain shadows can all complicate their spectral 241 characteristics. To tackle this challenge, the adaptive mapping algorithm was automated to 242 simulate how a human operator segments lakes from the background landscapes (Li & Sheng, 243 2012). In brief, each Landsat scene was first transformed to a normalized difference water index 244 (NDWI) image (McFeeters, 1996) to enhance water appearance and suppress others. Then, the 245 algorithm performs a two-step "global-to-local" segmentation. In the global segmentation, a 246 247 loose preliminary NDWI threshold was used to flag potential lake extents across the entire scene. In the local segmentation, each flagged lake was re-exampled as an object, and the boundary was 248 fine-tuned by an updated NDWI threshold, determined only using the spectral histogram based 249 250 on the vicinity of the lake. The local segmentation was implemented iteratively until the result

converged to a stable water extent. Through this design, the final threshold and lake extent were tailored optimally to the unique spectral condition for each lake.

Following the automated mapping, a rigorous QA/QC process aided by a semi-automated 253 editing tool (Wang et al., 2014) was performed to remove free-flowing river segments and to 254 correct the remaining omission and commission errors. The resultant mapping contained only 255 256 water bodies deemed as lakes and thus satisfies the third criterion "exclusive" for the SWOT prior lake mask. The quality-controlled lake extents from multi-temporal scenes were then 257 composited across the Landsat tiles. With assistance of a previously produced circa-2000 258 reference lake map (Sheng et al., 2016), the median water extent during the lake stable season 259 was selected as the final representative extent for each lake. To comply with SWOT's 260 observation goal, the subset of the Circa-2015 lake dataset with lake size equal to or larger than 1 261 ha was used as the PLD prior lake mask. 262

# 263 **2.2 Additional reservoir polygons**

To ensure that the prior lake mask presents major reservoirs as thoroughly as possible, we 264 supplemented the Circa-2015 lake dataset by another two global reservoir inventories. They are 265 the Georeferenced global Dams And Reservoirs dataset (GeoDAR) v1.1 (Wang et al., 2022) and 266 the Post2k reservoir dataset (Fan et al., 2023). GeoDAR v1.1 consists of 24,783 dam points and 267 their associated reservoir polygons when detectable. The dam points harmonized the Global 268 Reservoir and Dam database (GRanD) v1.3 (Lehner et al., 2011) (see section 2.4) and a 269 georeferenced subset of the World Register of Dams from the International Commission on 270 271 Large Dams (ICOLD; https://www.icold-cigb.org). Reservoir polygons were retrieved for each of the dam points by jointly using the water masks of HydroLAKES v1.0, GRanD v1.3, and the 272 Circa-2015 lake dataset. This led to 21,515 reservoir polygons with a total area of 496,313.8 273  $km^2$ , representing a cumulative storage capacity of 7216.1  $km^3$ . 274

Post2k reservoir dataset contains 6,760 global reservoirs constructed after the year 2000.
These post-2000 reservoirs were detected by comparing composite water occurrence
probabilities before and after 2000, using the multi-decadal remote sensing products Global
Surface Water (GSW) database (Pekel et al., 2016) and the Global Land Analysis and Discovery
(GLAD) database (Pickens et al., 2020). Polygons of the verified post-2000 reservoirs were then
retrieved using the maximum water occurrence maps of GSW and GLAD, such that each
polygon represents the maximum inundation area of the reservoir from the construction to about

282 2020 and has a minimum size threshold of 0.5 km<sup>2</sup>. These post-2000 reservoir polygons have a

total area of  $53,183.9 \text{ km}^2$ , corresponding to a cumulative storage capacity of  $1,287.7 \text{ km}^3$ .

# 284 **2.3 SWORD**

SWORD is the official a priori river database for SWOT (Altenau et al., 2021). It defines 285 the global networks of mainstems and tributaries potentially visible to SWOT (i.e., wider than 50 286 m according to SWOT's observation goal) (Biancamaria et al., 2016) and serves as the 287 288 framework for the SWOT vector river products. Because its primary data source is the Global River Widths from Landsat (GRWL) database (Allen & Pavelsky, 2018), SWORD also contains 289 river reaches with mean annual flow widths as narrow as 30 m. In total, SWORD consists of 290 213,485 river reaches (centerlines) with a median length of 10.5 km, comprising 10.7 million 291 nodes with ~200 m spacing. The SWOT river vector products, which contain WSE, width, slope, 292 and discharge, will be disseminated at the scales of both river reach and node. In addition, 293

294 SWORD also used multiple auxiliary datasets to provide a wide range of hydrological and

morphological attributes such as reach sinuosity, average width, slope, natural and human-

created obstructions, and the topology structure among the reaches and nodes. These attributes

facilitate the processing of SWOT river products as well as their scientific applications. Here we

used SWORD version 15 to identify the PLD lakes that are directly connected to the river

networks visible to SWOT, and the intersecting water bodies will be considered in both lake and

300 river products.

# 301 2.4 GRanD

GRanD is one of the most comprehensive spatial repositories of large dams and
 reservoirs in the world (Lehner et al., 2011). GRanD was constructed by harmonizing a
 collection of open-access dam and reservoir data, including the United Nations Food and
 Agricultural Organization (FAO) AQUASTAT

306 (https://www.fao.org/aquastat/en/databases/dams) and multiple regional inventories and

registers, to form a single, congruent global database. The latest version v1.3 contains 7320

308 georeferenced dams and their associated reservoir polygons when possible. Each reservoir

feature is also provided with over 50 attributes such as reservoir name, storage capacity, and

purpose. While the primary goal is to inventory all reservoirs with a storage capacity greater than

 $0.1 \text{ km}^3$ , GRanD v1.3 includes 3992 smaller reservoirs, leading to a total storage capacity of

 $6881 \text{ km}^3$  in the entire database. The reservoirs also include 119 regulated natural lakes such as

Lake Victoria and Lake Ontario. While a more exhaustive inclusion of smaller and/or newer

reservoirs is important, we used GRanD v1.3 to flag some of the largest manmade reservoirs and

regulated lakes as an a priori attribute for the operational PLD. Polygons in GRanD were not

used to construct the geometry of the PLD lake mask.

# 317 2.5 HydroBASINS

HydroBASINS (Lehner & Grill, 2013) offers a global tessellation of hierarchically nested 318 basins and subbasins at various scales, derived primarily from the HydroSHEDS hydrography 319 dataset at a grid resolution of 15 arc seconds (~500 m at the equator) (Lehner et al., 2008). 320 Following the Pfafstetter coding system (Verdin & Verdin, 1999), the basin hierarchy in 321 HydroBASINS is broken down to 12 nesting levels. They range from level 1 containing 9 322 continental or subcontinental boundaries, to level 12 encompassing about 1.0 million subbasins 323 324 at a scale of only tens of square kilometers. In other words, the basins of a lower level consecutively comprise the subbasins of a higher level. For clarity, the subbasins corresponding 325 to each level are organized as a different data layer. We used the data layers at Pfafstetter levels 326 3 in HydroBASINS v1.c, which contains 291 basin polygons together with their associated 327 Pfafstetter codes at level 2 (corresponding to 62 larger basins) and level 1 (corresponding to 9 328 continental and subcontinental divisions). These level-3 basin boundaries and their Pfafstetter 329 codes were used to help structure the prior lake identifier (*lake id* attribute) and partition the 330 PLD into level-2 basin granules (section 3.1). 331

# 332 **2.6 SWOT orbit files**

The SWOT mission is split in two phases related to two different orbits (JPL internal document, 2022e). The initial Calibration/Validation (Cal/Val) phase, up to July 11st, 2023, was related to a 1-day orbit at an 857 km of altitude: by frequent revisits of specific sites, this phase enabled the calibration of radar system parameters in the shortest time; it also allowed the study

- of rapidly changing phenomena. The science orbit, on which SWOT has been placed since July
- 21st, 2023, is a non-sun-synchronous 21-day orbit, at an 890.6 km of altitude. Combined with the
- 339 swath of the satellite, this orbit allows a quasi-global coverage until 77° of latitude north and
- south and, with its 10-day sub-cycle, is a good compromise for the temporal sampling as a region
- may be observed between once a cycle (at the Equator) to more than ten times a cycle (at the highest latitudes)
- 342 highest latitudes).
- Different from nadir-pointing altimetry missions, which provide measurements just below the satellite, SWOT KaRIn makes observations with a 120 km wide swath, from
- approximately 10 to 60 km of its nadir, on both "right" and "left" sides. The terms "left" and
- <sup>343</sup> approximately 10 to 00 km of its hadn, on both fight and left sides. The terms left and <sup>346</sup> "right" are defined as if one stands on the Earth surface at the spacecraft nadir point facing in the
- direction of the spacecraft velocity vector. The 10 to 60 km width swath orbit file (for the CalVal
- 348 orbit: <u>https://www.aviso.altimetry.fr/fileadmin/documents/missions/Swot/sph\_calval\_swath.zip;</u>
- 349 for the Science orbit:
- 350 <u>https://www.aviso.altimetry.fr/fileadmin/documents/missions/Swot/swot\_science\_orbit\_sept201</u>
- 351 <u>5-v2\_10s\_swath.zip</u>) was considered to compute the observability of each lake by SWOT. It
- provides the full swath per pass. A "pass" is a half revolution of the Earth by the satellite from
- pole to pole (south to north latitudes for ascending passes, and north to south latitudes for
- descending passes). There are 28 passes for the 1-day orbit, and 584 passes for the 21-day orbit.

# 355 **2.7 Databases for lake names**

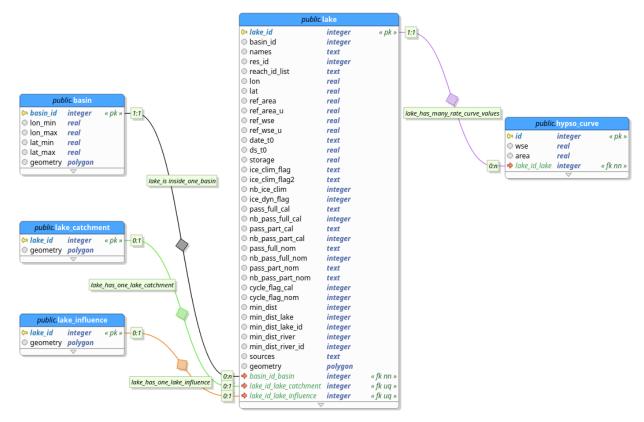
- Multiple databases or open-source online repositories were jointly used to populate lake names for the PLD polygons as thoroughly as possible. These sources include the IGN Carthage database (BD CARTHAGE®) to cover lakes in France (
- database (BD CARTHAGE®) to cover lakes in France (
- 359 <u>https://services.sandre.eaufrance.fr/telechargement/geo/ETH/BDCarthage/FXX/2017</u>), the
- 360 OpenStreetMap (OSM; <u>https://www.openstreetmap.org</u>), the Global Lakes and Wetlands
- 361 Database (GLWD) (Lehner & Doll, 2004), the Natural Earth Data (scale 1:30,000,000)
- 362 (<u>https://www.naturalearthdata.com</u>), the Vector Map Level 0 (VMap0)
- 363 (https://mdl.library.utoronto.ca/collections/geospatial-data/vector-map-level-0-vmap0), and
- HydroLAKES (v1.0) (Messager et al., 2016).

# 365 **3 Database development**

# **366 3.1 Overview of the operational PLD**

Conceptually, the operational PLD is comprised of two primary components (Fig. 1): (1) the prior lake mask, which inventories the polygon geometries of global lakes potentially visible to SWOT (i.e.,  $\geq$ 1 ha); and (2) the operational auxiliaries, which facilitate the linkage of SWOT observations to the prior lakes and assemble prior information necessary to compute lake storage

- change and populate the lake products. Analogously, the prior lake mask sets up the data
- infrastructure, while the operational auxiliaries assist the SAS in embodying the functionality of
- the data infrastructure.



#### 374

Figure 2. Structural model of the operational PLD.

Structurally, the operational PLD is a relational database (Fig. 2) which ties the central 376 "lake" table to four auxiliary tables: "lake catchment", "lake influence", "basin", and 377 "hypso curve". Following the terminology of data science, here "table" refers to an arrangement 378 of records that may contain fields of both geometry (e.g., raw polygons) and non-geometry (e.g., 379 other numeric and text prior attributes). The central "lake" table consists of the polygons of the 380 prior lake mask and a set of attributes for each prior lake. The prior lake mask is used to link 381 SWOT-observed water features to the prior lakes by intersecting their geometries. The other 382 attributes store prior information to calculate lake water storage change and to help populate the 383 vector products at two granule levels, including the standard lake single pass vector product 384 (L2 HR LakeSP) in continental-pass granules (CNES internal document, 2022b) and the 385 standard lake average cycle product (L2\_HR\_LakeAvg) in Pfafstetter level-2 basin granules 386 (CNES internal document, 2022a). The "lake" table also contains an attribute to link the prior 387 lakes and prior rivers (SWORD), such that pixels of lakes connected to the prior river networks, 388 the so-called "connected lakes", are also included in lake data processing. For clarity, we refer to 389 the non-geometric attributes of the "lake" table and the entirety of the other ancillary tables 390 ("lake catchment", "lake influence", "basins", and "hypso curve") as operational auxiliaries, 391 which collectively supplement the prior lake mask to enable the expected functions of the 392 operational PLD. 393

The "lake\_catchment" and "lake\_influence" tables contain ancillary geometries to accelerate the assignment of SWOT observations to the prior lakes. The issue is that the spatial linkage between SWOT-observed water features and the prior lakes does not always follow a one-to-one relationship. Particularly, complexities arise when an observed water feature is intersected by multiple prior lakes, leading to ambiguity regarding how the pixels in the observed

- water feature should be assigned to each of the prior lakes. To tackle the issue, these two
- 400 assignment tables delineate a spatial partition for each prior lake stored in the "lake" table. Each
- lake assignment polygon defines the spatial domain within which the associated prior lake is
   allowed to "expand" before it infringes the domain of another prior lake. In other words, the lake
- 402 answer to expand before it infinges the domain of another phor fake. In other words, the fake 403 assignment polygons disambiguate the vicinity of each prior lake so that lake assignment in
- 404 complex spatial relationships can be eased (see examples in section 4.4). The "lake\_catchment"
- 405 geometries provide a spatial partition that takes into account hydrological constraints and
- topography while "lake\_influence" geometries take into account only distances between lakes.

The "hypso curve" table stores the information of lake hypsometry for computing water 407 storage changes. This ancillary table will be added to the PLD approximately one year into the 408 SWOT mission. More specifically, this table will contain discrete WSE and water area points on 409 the hypsometric curve (i.e., WSE-area relationship) for each prior lake. The curve will be fitted 410 using the pairs of SWOT WSE and water area measurements to be collected from the first valid 411 observation of this lake throughout a certain mission period. Since the hypsometric points 412 account for the variation in lake bathymetry, they will allow for lake storage changes to be 413 estimated in an "incremental" approach (Cretaux et al., 2016) (CNES internal document, 2023a), 414 which is theoretically more accurate than the "direct" approach assuming an invariant 415 416 bathymetric shape.

The operational PLD is organized by HydroBASINS level-2 basins (section 2.5), which 417 results in 61 valid basin-granule PLD files. The "lake" table in each basin-granule PLD includes 418 only the prior lakes intersected by the associated level-2 basin. The "lake catchment" and 419 "lake influence" tables include the catchment and influence polygons intersecting this level-2 420 basin, respectively. The "basin" table delineates the full boundaries of HydroBASINS level-3 421 basins nested within this level-2 basin (section 2.5), together with the associated basin Pfafstetter 422 codes. This table is used to label the observed water features in different continents and basins. 423 424 More details on the development of each table, except "hypso curve", are given in the following subsections. 425

# 426 **3.2 Prior lake mask**

The Circa-2015 lake dataset (Sheng et al., 2016) (section 2.1) was used as the primary source of the prior lake mask. To improve the representation of reservoirs, particularly those constructed after 2015, a few state-of-the-art global and regional reservoir databases (section 2.2) were integrated to the Circa-2015 dataset to form the final prior lake mask.

The reservoirs in GeoDAR v1.1 (Wang et al., 2022) and Post2k (Fan et al., 2023) 431 databases that are not intersected by any Circa-2015 polygon were first added successively to the 432 prior lake mask. The remaining Post2k reservoirs were next investigated based on their spatial 433 relationship with the updated prior lakes. High-resolution Esri and Google Earth imagery were 434 also employed to assist in visual inspection. When a prior lake spatially conflicts with more than 435 one Post2k reservoir, we examined whether this prior lake overshoots the dam location and 436 mistakenly spans multiple reservoirs. If verified, this prior polygon was manually split to 437 multiple reservoirs. When a prior lake intersects with only one Post2k reservoir, we examined 438 whether the Post2k reservoir was substantially overrun by its intersecting prior lake. This 439 possibility was identified when the Post2k reservoir is well included (>75%) by the prior 440 441 polygon but the latter is less well covered (<75%) by the former. We then visually inspected if

this prior polygon mistakenly annexed the reservoir depicted by Post2k; if verified, this prior
polygon was truncated, allowing the Post2k polygon to be added as a new reservoir without
topological conflicts. For the rest of the cases (one Post2k reservoir intersected by one or

445 multiple prior lakes), we classified them based on the spatial agreement between the two data

sources. If their overlapping area covers at least 50% of the lake area in both sources, we

- 447 considered the Post2k reservoir and its intersecting prior lake(s) in good agreement and thus
- excluded them from further investigation. Otherwise, the case was visually inspected, and when necessary, the prior polygon was split or replaced by the intersecting Post2k reservoir.

The improved prior lakes were next compared with the remaining GeoDAR reservoirs. 450 The procedure was overall similar to the one for Post2k reservoirs, except that we employed a 451 more qualitative approach in comparing GeoDAR and prior polygons, and that the comparison 452 was focused on large reservoirs only. This was because many small and medium-sized reservoir 453 polygons in GeoDAR are already sourced from the Circa-2015 lake dataset, and the other 454 polygons sourced from HydroLAKES and GRanD usually exhibit coarser shorelines (Wang et 455 al., 2022). Nevertheless, when a GeoDAR polygon shows a major superiority in representing the 456 reservoir integrity (e.g., with improved shoreline connectivity and reduced surface water 457 patchiness), the GeoDAR polygon was used to replace the intersecting prior lake(s). In 458 occasional cases where a single source is not a sufficient solution, we performed manual 459 digitization to modify and merge multiple sources. The data sources and harmonizing methods 460 were reflected in the attribute *source* of the prior lake mask (Table 2). 461

462 Additional regional improvements were further made on the prior lake mask after the integration of global reservoir databases. In particular, we included nearly 7,000 reservoirs in the 463 Crateús and Banabuiú basins of Brazil to refine the completeness and accuracy of reservoir 464 mapping in this hotspot region. These Brazilian reservoirs were mapped from Landsat surface 465 reflectance images using water index spectral thresholds as in (Fisher et al., 2016) to represent 466 the interannual water area maximum during 2008 to 2019. We also improved the mapping of 467 468 several critical reservoirs in semi-arid western Africa, which are typically covered by aquatic vegetation and difficult to delineate using global algorithms. These reservoirs were extracted 469 following a supervised classification of Sentinel-2 images using the Active Learning for Cloud 470 Detection (ALCD) algorithm (Papa et al., 2023) and/or spectral thresholding of the modified 471 472 NDWI (MNDWI) with an ad hoc threshold for each lake (de Fleury et al., 2023). Finally, the updated prior lakes were post-processed such that polygons sharing a common vertex were 473 474 concatenated by a narrow channel and polygons sharing a common border were separated by a small gap. This post-processing reduced the number of original prior polygons by a minor extent 475 but improved the connectivity of lake surface and eliminated topological ambiguity. 476

477 **Table 2.** Key attributes in the operational PLD tables.

Attribute name	Description		
"lake" table			
lake_id	Unique identifier (ID) of the prior lake.		
lat / lon	Latitude and longitude (in decimal degree) of the centroid of the prior lake		
names	Known name(s) of the prior lake. If one lake has several names, the names are separated by semicolons.		
res_id	Reservoir ID from the Global Reservoir and Dam database (GRanD v1.3), if the prior lake intersects a GRanD reservoir		

reach_id_list	List of the IDs of the SWORD reaches that intersect the prior lake. If there are mor than one reach, the IDs are concatenated by semicolon.
ref_area / ref_area_u	Maximum area and the associated uncertainty (in $m^2$ ) of the prior lake. Values
· - <u>j _</u> · · · , · · <u>· · _</u>	correspond to the same state as <i>ref_wse</i> .
ref_wse / ref_wse_u	Maximum water surface elevation (WSE) and the associated uncertainty (in m) of
<i>y</i>	the prior lake, with respect to the reference geoid (EGM 2008).
date_t0	Reference date from which the storage change is computed. The reference date will
	be populated as the date of the first SWOT observation of the lake.
ds_t0	Storage change (in m <sup>3</sup> ) between the lake at the maximum WSE ( <i>ref_wse</i> ) and the
—	lake state at the reference date ( <i>date_t0</i> ).
storage	Maximum water storage variation (in m <sup>3</sup> ) observed by SWOT, i.e., the storage
0	difference between the maximum and minimum WSEs observed by SWOT
ice_clim_flag /	Flag characterizing the presence of ice covering the lake during each day of a
ice_clim_flag2	calendar year based climatological data:
	0: never frozen
	1: can be frozen
	2: always frozen
	ice_clim_flag is a text string containing the ice flags from January 1st to June 30th
	and ice_clim_flag2 contains information from July 1st to December 31st.
pass_[full/part]_[cal/nom]	List of the IDs of the SWOT passes fully or partially covering the prior lake during
puss_[juit puri]_[cut nom]	a calibration or nominal orbit cycle. The IDs are separated by semicolons.
cycle_flag_[cal/nom]	Flag characterizing the scenario of lake observation by SWOT during a calibration
eyete_ftug_feut.nomf	or nominal orbit cycle.
	0: never observed
	1: only partially observed
	2: fully observed after aggregating partial observations in multiple passes
	3: fully observed by a single pass at least once
min_dist_[lake/river][_id]	Geodesic distance (in m) to the closest lake or river and the corresponding <i>lake_id</i>
mm_disi_fiake/fiverjf_laj	or reach_id
sources	Data source of the prior lake polygon
"lake_catchment" table	
lake_id	ID of the prior lake that the lake_catchment polygon encompasses
"lake_influence" table	
lake_id	ID of the prior lake that the lake_influence polygon encompasses
"hypso_curve" table (expec	cted to be generated approximately one year into the SWOT mission)
id	ID of the WSE-area pair
lake_id	ID of the prior lake with which the WSE-area pair is associated
wse /area	WSE (in m) and water area (in $m^2$ ) values of a discrete point on the hypsometric
	curve of the prior lake. The hypsometric curve is fitted using available SWOT
	measurements of the lake WSE and water area since the first observation of this
	prior lake.
<b>"basin" table</b> basin_id	ID of the HydroBASINS Pfafstetter level-3 basin
	ID of the HydroBASINS Pfafstetter level-3 basin Minimum and maximum latitudes (in decimal degree) of the basin boundary

# 478 **3.3 Attributes in "lake" table**

The attributes in the "lake" table (Table 2) provide multi-theme information for each prior lake polygon, which covers basic lake identities, relationship with drainage basins and prior rivers, reference WSE and water area for deriving lake storage change, and SWOT overpass

482 statistics to enable data processing and product distribution. Accompanying the attribute

definitions in Table 2, we provide additional details that are necessary for understanding the

attribute format, purpose, and populating method.

## 485 3.3.1 Lake identities

The primary key, *lake\_id*, is a ten-character string in the format CBBNNNNNNT, where 486 487 C is a one-digit continent code (Table 3), BB a two-digit basin code, NNNNNN a zero-padded, six-digit sequence representing the ordinal index of the lake within its associated basin, and T a 488 one-digit code indicating the water body type (Table 4). Only integers 0 to 9 are allowed for each 489 digit. The first three digits (CBB) are based on the Pfafstetter coding system used in 490 HydroBASINS. The continental code (C) corresponds to level-1 divisions (Table 3), and BB 491 concatenates the codes of level-2 and level-3 basins representing increasing drainage details. 492 493 This hierarchy organized the global prior lakes to 291 subbasins at the scale of Pfafstetter level 3 (see section 3.5), and the coding assignment was based on geometric intersection with 494 HydroBASINS boundaries. Following the Pfafstetter coding system, prior lakes within each 495 level-3 basin are then indexed from 000001 to a maximum of 999999 based on a random order. 496

Continent code (ID)	Continent name	Lake count	Lake area (ha)	Mean / median area (ha)	Lake density (%)
1 (AF)	Africa	73,781	24,377,083.2	330.4 / 3.2	0.8
2 (EU)	Europe and Middle East	504,426	28,023,908.5	55.6 / 3.7	1.6
3 (SI)	Siberia	1,113,275	28,945,547.3	26.0 / 4.0	2.2
4 (AS)	Central and Southeast Asia	446,736	23,450,116.9	52.5 / 2.5	1.1
5 (AU)	Australia and Oceania	57,338	7,332,072.6	127.9 / 3.8	0.7
6 (SA)	South America	250,212	16,435,120.5	65.7 / 3.6	0.9
7 (NA)	North America and Caribbean	1,512,139	82,537,606.4	54.6 / 3.9	5.2
8 (AR)	North American Arctic	1,899,665	47,750,812.6	25.1 / 3.5	7.6
9 (GR)	Greenland	40,759	894,185.3	21.9 / 3.3	0.4
Global		5,898,331	259,746,453.3	44.0 / 3.6	1.9

497	<b>Table 3.</b> PLD lake abundance in each Pfafstetter level-1 continental divisions.
-----	---

The last digit in *lake\_id* classifies global prior lakes to two water body types based on their geometric connectivity with prior rivers (Table 4). The same water body type codes are also used for the primary key in SWORD (Altenau et al., 2021). As listed in Table 4, each prior lake was categorized to either a connected lake (T = 3) or a disconnected lake (T = 2). A connected lake is defined as any prior lake polygon intersected by one or more prior reaches and is included in both river and lake data processing. It is worth noting that this connectivity was determined specifically in relation to SWORD. This means a "disconnected" prior lake may also be 505 hydrologically connected to a river, but the river is too narrow to be observed by SWOT and is

506 therefore not inventoried in SWORD.

Type code (T)	Water body type		
1	River (only applicable to SWORD)		
2	Disconnected lake		
3	Connected lake		
4	Dam (only applicable to SWORD)		
5	No topology (only applicable to SWORD)		

507 **Table 4.** Water body type codes in the prior lake and river IDs

508 Figure 3 illustrates an example to help interpret the hierarchy of *lake\_id*. This example

509 covers the Pfafstetter coding system in the North American continent (C = 7), which

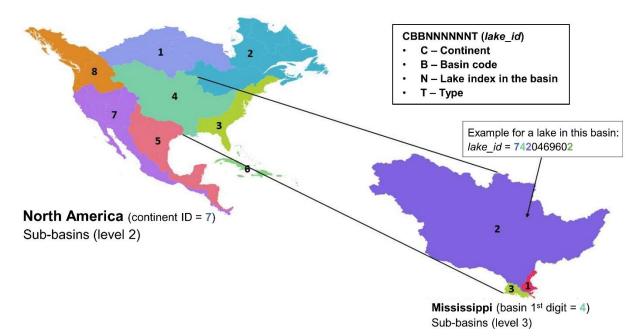
encompasses eight level-2 basins. One of them (first B = 4) contains the Mississippi River Basin

(second B = 2) at level 3. There are 109,861 prior lakes in the Mississippi River Basin, which all

share "742" as the first three digits in *lake\_id*. Among them is an example lake "7420469602",

indicating that this lake is indexed to be the  $46960^{\text{th}}$  in the basin (NNNNNN = 046960) and is

514 disconnected from any prior rivers in SWORD (T = 2).



515

- **Figure 3.** Hierarchical structure of the 10-character *lake\_id* for prior lakes. The example is given
- to a disconnected prior lake (T = 2) in a Pfafstetter level-3 basin (BB = 42, the Mississippi River Basin) of the North American continent (C = 7).

519 The *names* attribute inventories the known names of global prior lakes as thoroughly as 520 possible for the convenience of PLD and SWOT science data users. The lake names were 521 populated through "spatial join" from multiple open-source atlases and databases, including the

- 522 IGN Carthage database for France, OSM, GLWD, the Natural Earth Data, VMap0, and
- 523 HydroLAKES (v1.0) (section 2.7; Table 1). All names are in capital letters to avoid accents and

other spelling discrepancies. The same name can be shared by several prior polygons if they are disconnected portions of the same lake due to either mapping issues or seasonal variation. From

this aspect, the *names* attribute is potentially useful for dissolving patchy water bodies with

527 known lakes to improve the integrity of their prior extents and the completeness of storage

change estimates. A total of 152,260 lake names were assigned to 329,376 prior lake polygons,

529 which account for 5.6% of the global lakes by count and 61.8% by area.

The prior lake polygons include both natural lakes and artificial reservoirs. While 530 classifying lake typology is not the priority of the operational PLD, the "lake" table does provide 531 a res id attribute, which flags about 7300 large reservoirs using the IDs of GRanD v1.3. These 532 IDs were populated by intersecting the prior lakes with GRanD reservoir polygons. If a prior lake 533 intersects more than one reservoir, only the ID of the GRanD reservoir containing the prior lake 534 centroid was used. Although GRanD focuses on the world's largest reservoirs (e.g., with storage 535 capacity exceeding 0.1 km<sup>3</sup>), this flag allows for a preliminary attribution of SWOT-measured water 536 storage changes to either climate or human regulation. More comprehensive information about 537 reservoirs and other lake types is available in the "scientific PLD". 538

# 539 3.3.2 Relations with SWOT-visible rivers

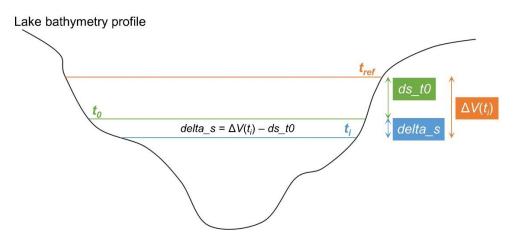
The *reach\_id\_list* attribute identifies each river-connected prior lake by the IDs of the 540 intersecting SWORD reaches. For each identified prior reach, SWOT-detected water pixels that 541 correspond to the lake portion are kept for both lake and river data processing whereas the other 542 pixels on the reach are eliminated from further lake processing. The specific reach IDs will also 543 544 facilitate a potential synergy of SWOT lake and river data products. One example is the LakeFlow algorithm (Riggs et al., 2023), which uses both products and the concept of lake-river 545 mass conservation to improve the estimates of lake inflow and outflow. The reach\_id\_list 546 attribute identified 16,499 prior lakes connected to 43,247 prior river reaches, and these 547 connected lakes account for 38.4% of the global lake area. More advanced information on lake 548 drainage topology and lake-river connectivity will be available in the "scientific PLD". 549

550 3.3.3 Prior information for computing lake storage change

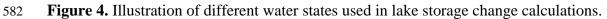
551 An essential role of the operational PLD is to assist the SAS in turning lake area and WSE repeatedly measured by SWOT to lake water storage variation. For this purpose, the "lake" table 552 553 reserves several attributes associated with the reference water state for each prior lake, based on which water storage change (i.e., the output variable *delta\_s* in the lake products) can be 554 computed. These attributes start with *date\_t0*, which defines the date of the first valid SWOT 555 observation of each prior lake. The WSE and water area on this initial date set up the reference 556 state for computing *delta\_s*. In other words, even though lake storage algorithms in the SAS vary 557 in bathymetrical model (linear or quadratic) and integration approach (direct or incremental), the 558 output *delta\_s* conceptually always represents the storage change from the observed state (i.e., 559 WSE and water area at a given time  $t_i$ ) to the reference state defined by *date* t0 (see Fig. 4). 560

For practical reasons in bathymetric and hypsometric modeling, the calculation is first performed for the lake storage change  $(\Delta V(t_i))$  between  $t_i$  and a high water level state defined by the *ref\_wse* and *ref\_area* attributes. Specifically, *ref\_wse* quantifies the maximum WSE of the prior lake during a certain SWOT observation period, and *ref\_area* stores the inundation area corresponding to *ref\_wse*. Their associated uncertainties are given in *ref\_area\_u* and *ref\_wse\_u*, which are needed for propagating storage change errors. The storage difference between the two states (i.e., the high level state and the reference state on *date\_t0*) is provided in the *ds\_t0* attribute. This way, *delta\_s* can be derived by subtracting *ds\_t0* from  $\Delta V(t_i)$  (Fig. 4). Technical details on lake storage change algorithm and error propagation are beyond the scope of this paper but are available in the Algorithm Theoretical Basis Document (CNES internal document, 2023a).

572 It is important to note that the reference state on *date\_t0* does not necessarily correspond to the minimum level of the prior lake. However, the "lake" table provides another attribute 573 storage, which quantifies the storage change between the maximum and minimum WSEs for 574 each lake during the same period for calculating *ref wse* and *ref area*. This attribute estimates 575 the magnitude of possible storage variation per prior lake, which is needed for assessing the 576 scales of intermediate storage variation relative to the maximum storage change magnitude. 577 Lacking sufficient SWOT observations so far, ref area is temporarily populated as the area of 578 the prior lake polygon whereas the other attributes are filled with "no data" and will be populated 579 at the first major update of the operational PLD (see section 5). 580



#### 581



### 583 3.3.4 SWOT overpasses and lake coverage

Lastly, the "lake" table contains a few more attributes that describe SWOT's coverage of 584 the prior lakes in relation to orbit passes. These attributes inform how well each prior lake can be 585 observed under a single pass or after aggregating multiple passes during a calibration or nominal 586 orbit cycle. The *pass\_full* and *pass\_part* attributes list the IDs of the passes covering each prior 587 lake fully and partially, respectively. Their values were configured by intersecting the prior lakes 588 and the orbit passes with swaths covering 10-60 km from nadir (section 2.6). The intersection 589 applied a 5-km buffer to take into account SWOT orbit jitter. These two attributes can be used to 590 quantify how many times each lake can be observed partially, completely, or both during an orbit 591 cycle (see section 4.3). Using this information, the cycle\_flag attribute summarizes SWOT's lake 592 coverage into four scenarios. Scenario "0" flags the prior lakes that will never be observed by 593 SWOT. This was determined by the lakes where both *pass\_full* and *pass\_part* values are empty. 594 Scenario "1" indicates that the lake will only be partially observed even after aggregating all 595 596 passes over a cycle, and scenario "2" indicates that the lake can be fully observed by SWOT, but only after pass aggregation over a cycle. In both scenarios, *pass\_part* has valid pass IDs while 597 pass\_full is empty. Finally, scenario "3" flags all prior lakes that will be observed fully by at 598

least one single pass. This was determined by the prior lakes where *pass\_full* has valid pass IDs regardless of *pass\_part*.

601 3.3.5 Lake ice flag

The goal of *ice\_clim\_flag* (climatological ice flag) is to help the data user make decisions on removing potentially ice-affected SWOT lake products, and to allow the SAS to calculate the *ice\_clim\_f* attribute (i.e., a climatological flag indicating whether the lake is ice-covered on the day of the observation based on *ice\_clim\_flag*) in the vector lake product (CNES internal document, 2022b). Climatological ice flags are estimated ice conditions for a typical year, averaging ice conditions between January 1st 2010 and January 1st 2020. Here we briefly describe the two steps taken to develop the lake ice flag.

609 Development of a lake ice fraction empirical model. To develop a priori ice conditions for all prior lakes, we applied an empirical lake ice fraction model by matching same-day ice 610 fractional data derived from Landsat 5, 7, and 8 images, whenever cloud-free conditions were 611 observed, with daily surface air temperature from ERA5 climate reanalysis data (Copernicus 612 Climate Change Service, 2017). The lake ice fraction was calculated based on the lake ice 613 detection algorithm (SLIDE) (Yang, Pavelsky, et al., 2022) for each prior lake polygon. By 614 modeling the lake ice fraction with daily-mean air temperature, we identified the following 615 logistic regression: 616

$$\log(odds(P_{ice})) = -0.46 \cdot SAT_{30} - 0.02 \cdot SAT_{30} \cdot Period + 0.85$$
(1)

where  $P_{ice}$  denotes the lake ice area fraction;  $SAT_{30}$  denotes the prior 30-day mean surface air temperature; and *Period*, a categorical variable, denotes whether the calculation was carried out during the breakup months (*Period* = 1 when Julian day is between [70, 227]; *Period* = 0 otherwise). Adding the variable *Period* allowed the model to accommodate the difference in ice dynamics during the breakup and freeze-up, a difference that has been previously identified in other types of freshwater bodies (Lacroix et al., 2005).

*Estimating lake ice flag.* For each point geometry representing the prior lake centroid, 624 625 and for each day during the period between January 1st 2010 and January 1st 2020, we estimated the ten-year mean lake ice fraction by inputting daily mean surface air temperature from ERA5 626 reanalysis database (variable: mean\_2m\_air\_temperature) to the empirical lake ice model above. 627 Then, a climatological mean lake ice fraction was estimated by averaging lake ice fraction across 628 the ten years for each Julian day. At last, the continuous ice fraction was converted to three 629 discrete integer values to represent ice conditions for SWOT ice flag: mean ice fraction < 0.2: 0; 630 631  $0.2 \leq \text{mean ice probability} \leq 0.8$ : 1; and mean ice probability  $\geq 0.8$ : 2.

This flag can suggest likely ice cover conditions at the given time of year for a given prior lake based on modeled historical ice conditions. However, factors such as interannual variability for ice phenology, multiple freeze-thaw events during cold seasons, and nonstationarity in climate mean that users are encouraged to seek ice conditions that are more recent and locally relevant whenever those sources are available. When no other sources are available, the climatological flag provides a reasonable representation of the average ice condition.

## 638 **3.4 "Lake\_catchment" and "lake\_influence" tables**

639

The "lake\_catchment" and "lake\_influence" tables store the assignment polygons for

each of the prior lakes referenced in the "lake" table. By definition, a lake assignment polygon

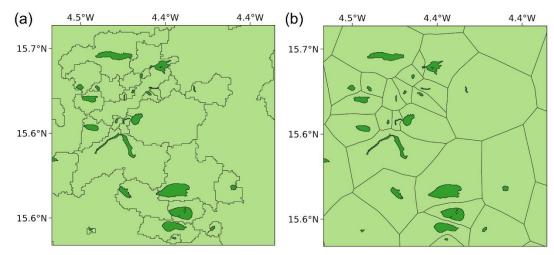
- should encompass the associated prior lake as well as its water fluctuation zone; meanwhile, it
- should not overlap those of any other prior lakes but collectively, the assignment polygons
- 643 partition the entire continental surface. This way, when it is unclear how a SWOT-detected water 644 region should be assigned to the prior lakes using the prior lake geometry alone, the assignment
- region should be assigned to the prior lakes using the prior lake geometry alone, the assignment polygons can help determine the rule for executing lake assignment (see sections 3.1 and 4.4). In
- 645 polygons can help determine the rule for executing lake assignment (see sections 3.1 and 4.4 646 addition to the geometries, each assignment polygon is also indexed by the ID of the
- 647 encompassed prior lake, *lake\_id* (section 3.3.1), which links the "lake\_catchment" and
- 648 "lake\_influence" tables to the "lake" table.

We considered two rationales for constructing lake assignment polygons. The first rationale 649 follows the concept of lake hydrological catchment, which defines the sub-basin between the 650 outlets of a prior lake and its immediate upstream prior lake(s). If a prior lake is in the headwater 651 (meaning no lakes further upstream), the catchment is then the entire watershed upstream to the 652 outlet of this lake. As water dynamics in a lake are confined by its own catchment boundary, this 653 rationale complies with the ideal definition of lake assignment polygons described above. To 654 implement this rationale, we applied the algorithm recently developed for the global Lake 655 Topology and Catchment (Lake-TopoCat) database (Sikder et al., 2023) on the prior lake mask and 656 the 90-m-resolution MERIT-Hydro hydrography data (Yamazaki et al., 2019). Results of the 657 algorithm are fine-detailed catchments for each of the prior lakes, which compose the geometries 658 of the "lake catchment" table. A regional example is given for part of western Africa in Fig. 5a. 659

660 The second rationale relies on geometric vicinity. Specifically, we employed the Voronoi tessellation (Aurenhammer, 1991) to partition the continental surface into proximal regions based 661 on the geodesic distance to the prior lakes, and the resultant regions, also known as Voronoi cells 662 or Thiessen polygons, are the geometries of the "lake influence" table (see the example of Fig. 663 5b). Mathematically, the Voronoi tessellation decomposes a plane with a finite number of objects, 664 or the so-called "seeds", into the same number of Thiessen polygons. Each Thiessen polygon 665 corresponds to one seed object, e.g., a prior lake in our case, and every virtual point within this 666 polygon is closer to its seed prior lake than to any other prior lake. Because of this proximal 667 characteristic, Thiessen polygons are often regarded as the "areas of influence" in computational 668 geometry and have been widely applied in hydrology, meteorology, and geo-statistics (Evans & 669 Jones, 1987). Although these influence features do not follow the exact lake catchment boundaries 670 (Fig. 5), it is important to note that assignment polygons are not needed for every case of lake 671 assignment. When they are indeed needed, the Thiessen polygons provide a computationally 672 efficient alternative to ease the linkage of SWOT observations to the prior lakes. An example of 673 when lake assignment polygons are required and how they function to ease lake linkage is given in 674

675 section 4.4.

#### manuscript submitted to Water Resources Research



676

**Figure 5.** An example of SWOT prior lakes in part of western Africa (deep green) and their associated assignment domains (light green). (a) Lake hydrological catchments as in the "lake catchment" table. (b) Lake influence features as in the "lake influence" table.

### 680 **3.5 "Basin" table**

The "basin" table contains the geometries of Pfafstetter level-3 basins corresponding to a 681 level-2 basin granule (see section 3.1 for PLD organization). The basin boundaries were 682 retrieved from the HydroBASINS dataset, with a total number of 291 level-3 basins on the global 683 continents except Antarctica. Each basin feature in this table is provided with five attributes as 684 listed in Table 2. The basin id attribute is the basin identifier, containing the level-3 Pfafstetter 685 code from HydroBASINS. The value of this attribute is identical to the first three digits in 686 lake id (i.e., CBB) of the "lake" table, which links each prior lake to its associated basin. The 687 basin geometries and *basin id* values are used to separate the water features observed by SWOT. 688 including those not intersected by any prior lakes, to different continents and basins, which is 689 needed for populating the vector lake products at different granule scales. 690

### 691 4 Results and discussion

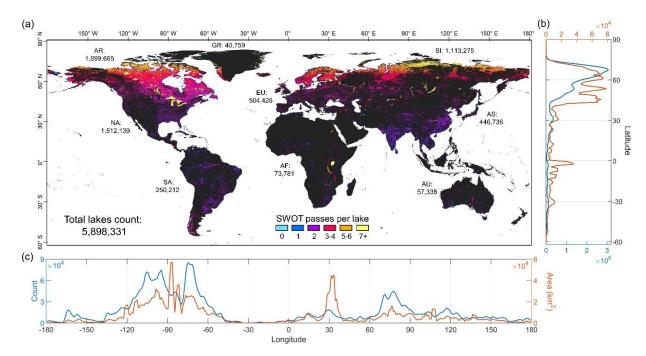
## 692 **4.1 Prior lake abundance and distribution**

As the primary component of the SWOT PLD, the prior lake mask contains 5,898,331 polygons larger than 1 ha (Fig. 6), mostly representing the intermediate water extents of global lakes during their stable seasons. These prior lakes have a total area of 2,597,464.5 km<sup>2</sup>, covering about 2% of the global land surface excluding Antarctica. The Caspian Sea, including the Garabogazköl lagoon, is excluded from the PLD due to its large size and dual characteristics of both lake and ocean (Zimnitskaya & Geldern, 2011).

Table 3 summarizes the lake abundance in each of the nine Pfafstetter-1 continental divisions. The lake count ranges from less than 80,000 per division in Africa (AF), Australia and Oceania (AU), and Greenland (GR) to more than 1 million in Siberia (SI), North America and Caribbean (NA), and North American Arctic (AR). In general, the divisions with larger lake counts also tend to exhibit a greater total lake area and lake density. Despite a global average of 1.9%, lake density varies substantially from only 0.4–0.8% in GR, AU, and AF, to 5.2% in NA and as high as 7.6% in AR. On a continental scale, lake abundance appears to be negatively correlated to aridity and positively correlated to the degree of glaciation or periglacial processes
(except GR). The divisions with less lake abundance, however, tend to have a greater mean lake
size (e.g., 127.9 ha in AU and 330.4 ha in AF), implying fewer but larger lakes are more likely to
develop in arid regions. On the other hand, the lake-dense circum-Arctic regions (AR and SI) are
dominated by smaller lakes with an average size of 25.1 ha, substantially below the global
average 44.0 ha. In comparison, the median lake sizes are more consistent among the continents
and range subtly between 2.5 ha to 4.0 ha

and range subtly between 2.5 ha to 4.0 ha.

With a minimal lake size of 1 ha, the prior mask reveals an unprecedented detail of global 713 lake distribution. About 65% of the total lake count or 40% of the total lake area is clustered in 714 the sparsely populated high-latitude regions above 55°N (Fig. 6b), where glacial activities 715 prevailed in the last ice age. Lakes are particularly ubiquitous across the Canadian Shield and 716 717 Scandinavia as a result of glacial erosions during the Pleistocene (Shilts et al., 1987) and the boreal permafrost lowlands (e.g., in Siberia and Alaska) associated with thermokarst (Kokelj & 718 Jorgenson, 2013; Manasypov et al., 2014; Smith et al., 2005; Wik et al., 2016). While lake count 719 gradually declines southward, lake area continues to plateau till 40°N, owing to the presence of 720 some of the most gargantuan lakes in the world such as the Laurentian Great Lakes, Lake 721 Balkhash, and Lake Baikal. As a result, more than 70% of the global lake area is concentrated 722 above 40°N, a latitudinal belt accounting for only one-third of the global landmass (excluding 723 724 Antarctica). In comparison, the temperate and tropical zones between  $40^{\circ}$ N and  $40^{\circ}$ S are home to about 85% of the global population (estimated based on the Gridded Population of the World 725 (GPW v4) (CIESIN, 2018)) but only 16% of the global lake count or a quarter of the lake area, 726 highlighting the unequal spatial distribution of lake water resources. Longitudinally, 64% of the 727 global lakes (or 59% by area) are distributed in the land-lacking western hemisphere (Fig. 6c) 728 due to disproportionate lake densities in Alaska, the Canadian Shield, the Amazon floodplain, 729 and alpine Patagonia. A spike of lake area is also seen around 30°E, which is associated with 730 Lake Victoria and a few elongated large lakes in the East African Rift System such as Lakes 731 Tanganyika and Malawi. Another cluster of lake abundance occurs in the longitudinal belt of 732 733  $60^{\circ}$ E to  $90^{\circ}$ E, which is contributed by thousands of thermokarst lakes across the North Siberian Lowlands and the alpine and glacial lakes on the Tibetan Plateau. 734



735

Figure 6. Global map and distribution of the SWOT prior lakes. (a) Global map of prior lakes, 736 with numbers labeling the count of lake polygons per Pfafstetter level-1 division and colors 737 displaying the number of SWOT overpasses per lake during each 21-day orbit cycle. (b) Count 738 and total area of the PLD lakes per latitudinal degree. (c) Count and total area of the PLD lakes 739 per longitudinal degree. The location of a lake polygon was determined by the latitude and 740 longitude coordinates of the centroid of the lake polygon. Values in both latitudinal and 741 longitudinal histograms (b and c) were smoothed by a 3-degree average window to enhance 742 743 aesthetic appearance and take into account that lakes can span multiple 1-degree intervals.

### 744 4.2 Comparison with other global lake masks

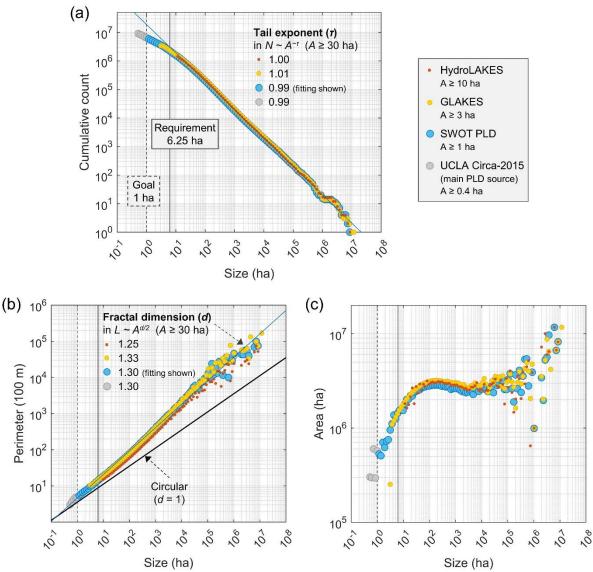
We compare the PLD prior lake mask with HydroLAKES, GLAKES, and the entirety of 745 the Circa-2015 lake dataset, to further understand the capability of the PLD in helping SWOT 746 achieve its science objectives for global lake monitoring. The comparison emphasizes the 747 characteristics of lake size distribution, shoreline fractality, and lake mask accuracy across 748 different landscapes, in addition to summary statistics on global lake abundance. While the prior 749 lake mask is, to a large extent, a subset of the Circa-2015 lake dataset (section 2.1), we include 750 the latter for comparison in order to understand the abundance of small lakes that are inventoried 751 but beyond SWOT's science goal (<1 ha). 752

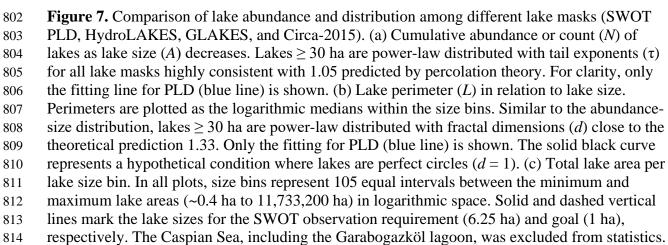
As shown in Fig. 7a, all datasets concur that the distribution of the Earth's lake area is 753 asymmetric and lake abundance increases as lake size decreases. When lakes are larger than a 754 scale of  $\sim 100$  ha (1 km<sup>2</sup>), the size-abundance relationship conforms to a power-law or Pareto 755 distribution, where the cumulative lake count increases linearly with the decrease of lake size in 756 logarithmic space. Lakes smaller than this scale, however, gradually deviate from a power-law 757 distribution. Since 100 ha well exceeds the minimum lake size in any of the four datasets, the 758 power-law deviation is not attributable to incomplete mapping of small lakes, but instead 759 suggests that lakes behave as self-similar fractals until a lower size limit is reached (Mandelbrot, 760 1982). Cael and Seekell (Cael & Seekell, 2016) explained that such a lower size limit exists 761

because topographic characteristics at sub-kilometer scales are less self-similar, and that the development of small lakes is more subject to external dynamics that are scale dependent. Pi et al. (Pi et al., 2022) also noted that lakes <100 ha, despite accounting for only ~15% of the global lake area, dominated the lake area variability over the past four decades, further highlighting the unique roles of small lakes in representing regional geomorphic processes and regulating surface water dynamics.

For the above reasons, the capability of characterizing small lake abundance is critical to 768 the SWOT PLD. Through experimentation based on the PLD, we suggest the lower size limit of 769 the power-law distribution to be 30 ( $\pm$ 5) ha, where the fitting slope as a function of lake size 770 threshold reaches the inflection point and remains stable. Using the subset of lakes  $\geq 30$  ha, we 771 fitted a power-law function for each of the lake datasets (fitting for the PLD shown in Fig. 7a), 772 773 which rendered a similar tail exponent of  $\sim 1.00$ , close to 1.05 predicted by percolation theory (Cael & Seekell, 2016). While this consistency suggests that the four datasets are comparable in 774 representing the abundance of large lakes, the major difference is their capabilities of 775 characterizing smaller lakes that deviate from a power-law distribution. As shown in Fig. 7a, the 776 pattern of how this deviation develops becomes increasingly clear as the minimum lake size 777 decreases from 10 ha in HydroLAKES, 3 ha in GLAKES, 1 ha in PLD, to 0.4 ha in the Circa-778 2015 lake dataset. Put in the context of SWOT, the deviation is to the extent that there are 55% 779 780 fewer lakes meeting SWOT's science requirement ( $\geq 6.25$  ha) than would be expected if the lakes conformed to power law across the entire size range, and the deviation was amplified to a 781 factor of two (221% fewer lakes) for the lakes meeting SWOT's science goal ( $\geq 1$  ha). 782

Besides size distribution, the perimeter-area scaling relations are plotted in Fig. 7b to 783 compare lake shoreline convolutedness (complexity) among the datasets. As fractals are self-784 similar and scale-invariant, their perimeters and areas are related to each other by power law 785 (Cheng, 1995). The exponent, equivalent to the slope of perimeter-area scaling in logarithmic 786 space, defines the fractal dimension (d) measuring how irregular the fractal boundaries are 787 788 relative to perfect circles (d = 1). As expected, the perimeters and areas of lakes  $\geq 30$  ha in all datasets conform to power-law relationships. The fitted d ranges from 1.25 for HydroLAKES, 789 1.30 for PLD (fitting shown in Fig. 7b) and Circa-2015, to 1.33 for GLAKES, which are overall 790 791 consistent with 1.33 predicted by percolation theory (Cael & Seekell, 2016). The smaller d for 792 HydroLAKES was likely because the scales of some of the source data (e.g., the MODerate resolution Imaging Spectro-radiometer (MODIS) MOD44W water mask (Carroll et al., 2009)) 793 794 underrepresented real shoreline complexity, in combination with additional shoreline smoothing during data post-processing (Messager et al., 2016) (Fig. 8). As the area and fractality decrease 795 among lakes < 30 ha, the lake masks with finer resolutions, particularly the PLD and the Circa-796 797 2015 dataset, reveal a subtle transition of d towards 1 (Fig. 7b), echoing the finding of (Cael & 798 Seekell, 2016) based on high-resolution Swedish lakes that the shapes of small lakes are less convoluted. This comparison highlights the advantage of PLD in representing reliable shoreline 799 morphology for both sizable and small lakes. 800





We further compare the lake masks using their summary statistics (Table 5) and discuss 815 the implications of discrepancies among them. The total lake count in the PLD (~6.0 million  $\geq 1$ 816 ha) is nearly double that in GLAKES (3.4 million  $\geq$  3 ha) and more than quadruple that in 817 HydroLAKES (1.4 million  $\geq$  10 ha). These multi-fold differences reflect an unparalleled ability 818 of the PLD to characterize the sheer number of small but SWOT-visible lakes. This improvement 819 is exemplified by two high-latitude lake-rich regions: one in the Kanin Peninsula of Russia 820 dotted with circularly shaped thermokarst lakes and bogs (Fig. 8a), and the other in the interior of 821 the Canadian Shield, which is dominated by more convoluted, elongated lakes largely controlled 822 by structural geology (Fig. 8b). In both examples, the PLD shows superiority in representing 823 local lake density, geolocations, and shoreline morphology. The Circa-2015 lake dataset includes 824 another 3.1 million lakes in the world beyond SWOT's observation goal (< 1 ha), although these 825 tiny lakes and ponds add only 3% to the total lake area. Despite a significantly greater lake 826 population in the PLD, its total lake area (2,597,464.5 ha) is 7% lower than that of GLAKES 827 (2,787,115.5 ha) and exceeds that of HydroLAKES (2,537,863.1 ha) by only 2%. 828

For more detailed comparisons, we broke down the statistics into size classes determined 829 by the minimum lake areas of each of the datasets as well as SWOT's observation requirement 830 (Table 5). For lakes smaller than 6.25 ha and larger than 3 ha (the minimum size in GLAKES), 831 the abundance in the PLD exceeds that in GLAKES by ~2% for both count and area. Based on 832 our visual comparisons, we attribute this difference to an overall greater omission error for small 833 lakes in GLAKES (e.g., Fig. 8a and Fig. 8b), probably related to a conservative nature of its non-834 parametric "expert system" for water detection (Pekel et al., 2016). For lakes  $\geq 6.25$  ha, however, 835 the total abundance in the PLD becomes 6-9% less than that in GLAKES and 1-4% less than 836 that in HydroLAKES. To investigate if such lower abundance is skewed to any individual lakes 837 or size groups, we calculated how the total lake area and population (count) are distributed across 838 detailed size bins (Fig. 7c). The patterns are highly consistent among the datasets: as lakes grow 839 in size, their population decreases monotonically, but the total lake area exhibits a three-phase 840 change. In phase one, the total lake area increases as the size grows towards ~100 ha, suggesting 841 842 for smaller lakes, the area gain due to size growth outpaces the area loss due to population decline. In phase two, the total lake area decreases subtly and then stabilizes as the size grows to 843  $\sim 10,000$  ha, suggesting for medium-sized lakes, the area gain due to size growth generally 844 compensates for the area loss due to population decline. In phase three, the total area rapidly 845 increases again when lake size exceeds 10,000 ha, indicating a dominant impact of large lakes on 846 area statistics albeit a limited population. Regardless of this multi-phase pattern, the relative 847 difference in lake abundance between the PLD and the other datasets remains overall uniform 848 across the size bins: excluding lakes  $\leq 6.25$  ha, both area and count in the PLD are centered 849 around ~10% less than those in GLAKES and 5% less than those in HydroLAKES. 850

around  $\sim 10\%$  less than those in GLAKES and 5% less than those in HydroLAKES.

851	Table 5. Statistical comparison among	SWOT PLD, HydroLAKES,	GLAKES, and Circa-2015
-----	---------------------------------------	-----------------------	------------------------

lake dataset. The Caspian Sea, including the Garabogazköl lagoon, was excluded from thestatistics.

Statistics Minimum lake size (ha)		HydroLAKES	KES GLAKES SWOT PLD C	Circa-2015	
		10	3	1	0.4
G	All	1,427,686	3,426,387	5,898,331	9,092,158
Count	1–3 ha			2,590,538	2,659,773

#### manuscript submitted to Water Resources Research

	3–6.25 ha		1,302,135	1,327,205	1,345,113
	6.25–10 ha		616,915	574,923	573,042
	≥10 ha	1,427,686	1,507,337	1,405,665	1,414,396
	All	2,537,863.1	2,787,115.5	2,597,464.5	2,596,665.3
	1–3 ha			46,076.6	47,276.0
Area (km <sup>2</sup> )	3–6.25 ha		56,509.8	57,583.0	58,326.4
(KIII)	6.25–10 ha		48,665.5	45,276.0	45,020.6
	≥10 ha	2,537,863.1	2,681,940.1	2,448,529.0	2,425,359.2

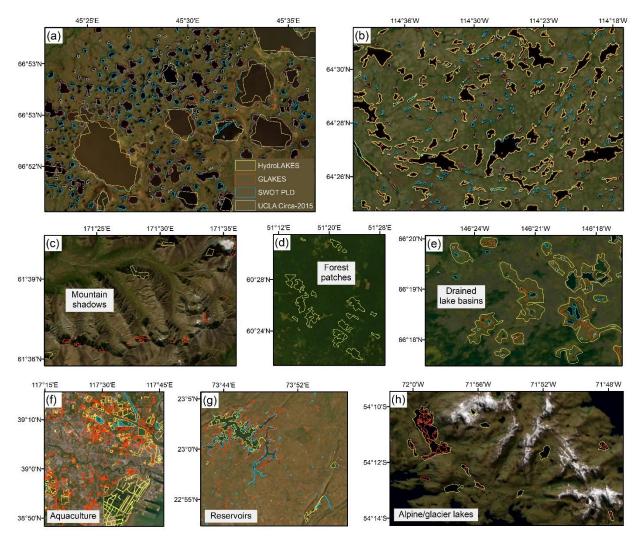
854 The discrepancy in the lake abundance for lakes  $\geq 6.25$  ha reflects the differences in mapping standard, quality, timespan, and reference sources among the datasets. A higher lake 855 abundance in GLAKES is expected because its polygons represent all-time water area maximum 856 during 1984 to 2019 whereas most lakes in the PLD depict intermediate water extents during 857 circa 2015. Although both datasets were derived from Landsat imagery, the differences in 858 mapping period and standard, in theory, led to not only a larger lake area in GLAKES, but also a 859 860 greater lake quantity given that not all intermittent lakes were inundated during circa 2015. While the Circa-2015 lake dataset was supplemented by recently constructed reservoirs (sections 861 2.2 and 3.2), natural lakes that disappeared before or emerged after circa 2015 are not included in 862 the PLD. On the other hand, HydroLAKES was a compilation of eight independent lake sources 863 with publication dates spanning a decade (Messager et al., 2016). Variation among these data 864 sources may contribute intricately to a higher abundance (for lakes  $\geq 10$  ha) in HydroLAKES 865 than the PLD. 866

For instance, the acquisition time of SWBD (February 2000), a major source of 867 HydroLAKES for 56°S to 60°N, may explain the smaller areas in the reservoirs of northwestern 868 India (Fig. 8g), where water levels were low during the drier monsoon season. In another 869 relevant case, a number of important reservoirs in western Africa were built after February 2000. 870 These include the Ziga Reservoir (completed in July 2000) in Burkina Faso (12.5°N, 1.1° W) 871 that is absent from HydroLAKES 1.0. On the other hand, this acquisition time of SWBD 872 coincided with the warmer season in the southern hemisphere. Meanwhile, SWBD as a radar-873 874 derived product (Slater et al., 2006) is less sensitive to surface spectral disturbance such as remnant lake ice and snow. Both factors might lead to a more complete inventory of glacier lakes 875 in HydroLAKES across the southern Andes (Fig. 8h). 876

Another example in Fig. 8e highlights a portion of the Yukon River Valley in Alaska,
where thermokarst lakes and their drained lake basins develop dynamically atop the permafrost
(Grosse et al., 2013). While the PLD polygons appear highly consistent with the recent
thermokarst lake extents, HydroLAKES depicts the much larger drained thaw lake basins. These
outdated lake boundaries are sourced from the US National Hydrography Dataset (U.S.Geological-Survey, 2013) and contribute partially to an overestimated area abundance in
HydroLAKES.

In addition, part of the higher abundance in HydroLAKES and GLAKES may be ascribed to commission errors such as mountain shadows and forest patches, as shown in the examples of Fig. 8c and Fig. 8d. Such commission errors were largely eliminated from the PLD owing to a rigorous QA/QC procedure (Sheng et al., 2016) (section 2.1). Other factors such as lake definition and mapping objective could also lead to discrepancies in lake abundance. In Fig. 8f,

- 889 GLAKES and HydroLAKES include a large quantity of aquaculture ponds in coastal China,
- 890 which were not considered as lakes in the PLD.



891

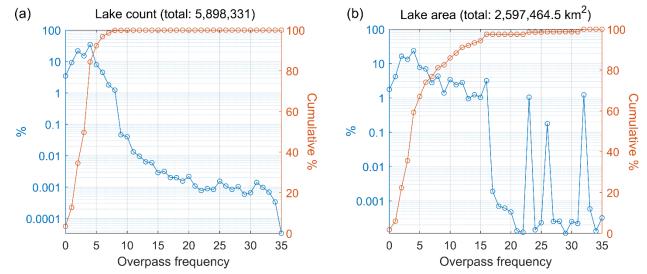
Figure 8. Regional comparisons among the PLD, HydroLAKES, GLAKES, and the Circa-2015 892 lake dataset. (a) Thermokarst lakes in the southern Kanin Peninsula, the Nenets Autonomous 893 Okrug, Russia. (b) Structurally controlled lakes in the Canadian Shield, Northwest Territories, 894 Canada. (c) Commission errors (mountain shadows misclassified as lakes in HydroLAKES and 895 GLAKES) in Kamchatka Krai, Siberia, Russia. (d) Commission errors (forest patches 896 misclassified as lakes in HydroLAKES) in southern Komi Republic, Russia. (e) Thermokarst 897 lakes and drained thaw lake basins in the Yukon River Valley, eastern Alaska. (f) Aquaculture 898 ponds near the Bohai coastline, Tianjin, China. (g) Reservoirs in eastern Gujarat, India. (h) 899 Alpine and glacier lakes in the southern Andes. 900

# 901 **4.3 Lake spatiotemporal coverage**

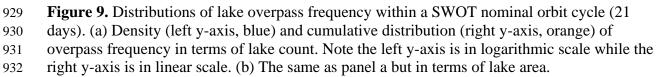
SWOT coverage for the land surface is determined jointly by orbit characteristics, the KaRIn swath width ( $2 \times 50$  km), the nadir gap width (20 km) between the two swaths, and the orbit crossover density which is a function of latitude (Biancamaria et al., 2016). In addition, the spatiotemporal coverage for lakes also depends on the size and shape of each lake. With all these factors considered, Fig. 6a shows the frequency of SWOT observations over each prior lake

- during every 21-day orbit cycle, which was calculated by summing the counts of unique
- overpasses in both *pass\_full\_nom* and *pass\_part\_nom* attributes (section 3.3.4). As summarized
- in Fig. 9, 96.5% of the global lakes, covering 98.2% of the total lake area, are observed by
  SWOT at least once per orbit cycle. More than 65% of the global lakes, covering nearly 80% of
- the lake area, are observed at least weekly on average (i.e., three times per cycle). About 3.5% of
- the global lakes, or 1.8% of the lake area, may never be observed due to a combination of nadir
- gaps and orbit intertrack gaps. This lake coverage complies with the SWOT science
- requirements, which states that "SWOT shall collect data over a minimum of 90% of all ocean
- and land area covered by the orbit inclination for 90% of the operation time" (JPL internal
- 916 document, 2018).

917 Despite complexity in the global pattern (Fig. 6a), lake observation frequency tends to increase with higher latitudes and larger lake sizes. As latitude increases, the orbit crossover 918 densifies and the overlap among adjacent swaths increases. This gradually leads to the closure of 919 orbit intertrack gaps at 25°S/N and then the closure of nadir gaps at about 60.5°S/N. As lake size 920 increases, the chance of one lake overlapped by multiple passes also increases. As a result, 921 unobserved lakes between 10°S and 10°N account for about 10% of the local lakes (in terms of 922 both count and area), but the proportion decreases to less than 1% (0.9% in lake count and 0.5% 923 924 in lake area) over the latitudes above  $60^{\circ}$ S/N. Since lake abundance is skewed towards higher latitudes in both count and size (section 4.1), these factors also explain why SWOT's coverage 925 gap for global lake area (1.8%; Fig. 9b) is significantly smaller than that for the entire land 926 surface (3.6%) (Biancamaria et al., 2016). 927

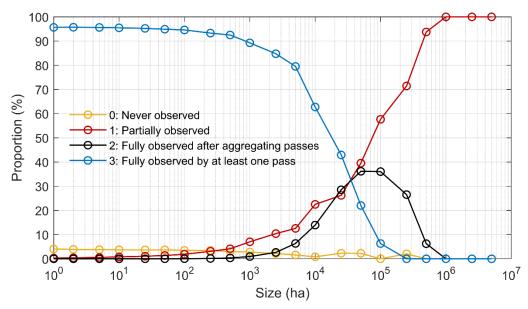


928



Globally speaking, the median observation frequency is maintained at about twice per orbit cycle for lakes between 50°S and 50°N and smaller than 100 km<sup>2</sup>. The median frequency increases to three times per cycle for larger lakes over this latitudinal band and for lakes between 50–60°N/S regardless of the lake size. The median frequency increases further to four times per cycle above 60°N. On the other hand, some of the highest observation frequencies are found in
the world's largest lakes regardless of latitudinal distribution. For example, nearly all lakes larger
than 10,000 km<sup>2</sup>, except Lake Malawi with an elongated shape parallel with SWOT passes (Fig.
6a), are observed from six times per cycle to more than twenty times per cycle (i.e., every day).

A higher overpass frequency does not always warrant a better spatial coverage. Nearly 941 942 6% of the prior lakes, constituting 67.3% of the global lake area, fall on the edge of at least one overpass. These lakes will appear incomplete in some of the granules of the single-pass product 943 (L2\_HR\_LakeSP). However, with a higher overpass frequency, there is an increasing chance that 944 the lake can be observed fully by at least one pass per cycle, or the aggregation of multiple 945 passes can lead to a full extent to represent the average inundation condition during the cycle. 946 The latter reflects the value of the cycle-average product (L2\_HR\_LakeAvg). To evaluate how 947 lakes are spatially covered per cycle, we calculated the percentage of lakes for each of the 948 cycle\_flag\_nom scenarios (section 3.3.4) and how the percentages vary in lake size. As shown in 949 Fig. 10, smaller lakes, albeit overall less frequently observed, are easier to be seen with a full 950 extent. About 90% of the lakes smaller than 10 km<sup>2</sup> are fully observed at least once per cycle 951 (scenario 3). As lake size increases, the proportion of scenario 3 monotonically declines; 952 meanwhile, lakes that are observed fully only after pass aggregation (scenario 2) and lakes that 953 remain observed partially after pass aggregation (scenario 1) increase at similar paces. The three 954 scenarios cross at  $\sim 300 \text{ km}^2$ , beyond which lakes of scenario 3 are no longer the majority. The 955 proportion of scenario-2 lakes peaks at nearly 40% around 500 km<sup>2</sup>. Lakes larger than this size 956 are gradually dominated by scenario 1 until 10,000 km<sup>2</sup>, beyond which lakes can only be 957 observed partially despite very high overpass frequencies. The proportion of lakes that can never 958 be observed (scenario 0) remains less than 5% regardless of size, and more than 97% of them are 959 smaller than  $1 \text{ km}^2$ . 960

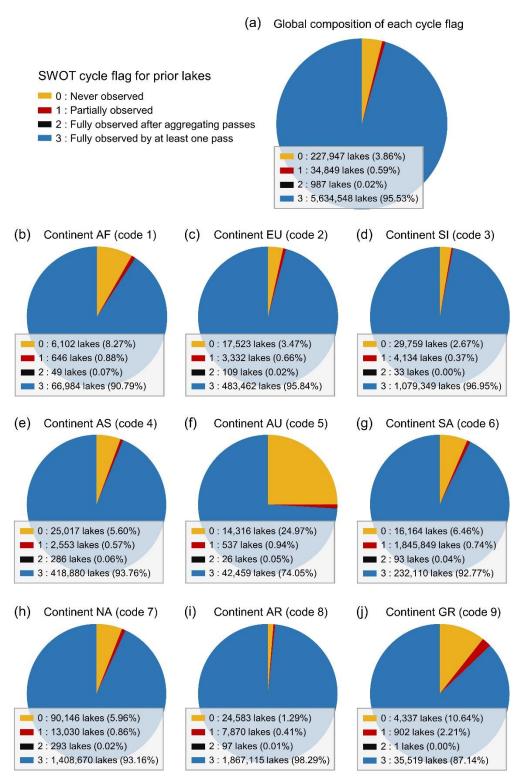


961

Figure 10. Lake spatial coverage (*cycle\_flag\_nom*) as a function of lake size during each SWOT
 nominal orbit cycle.

Synthesizing all lake sizes, Fig. 11 shows that 95.5% of the global prior lakes, constituting 50.4% of the total lake area, are fully observed during a nominal cycle, and 3.9% (or 1.9% by

- area) are never seen. Less than 1,000 prior lakes, accounting for 8.7% of the global lake area, can
- be fully covered after aggregating multiple passes per cycle, whereas the remaining 0.6%
- 968 (34,849) lakes, accounting for 38.9% of the global lake area, cannot be fully covered in a cycle.
- 969 For these partially observed lakes, complete water areas could be estimated with assistance of
- other sensors and/or an auxiliary water probability or contour map (such as GSWO (Pekel et al.,
  2016)). In each of the Pfafstetter-1 (sub)continents, the proportion of lakes that are partially
- observed is lower than 1% except GR. In SI and AR, more than 96% of the prior lakes are fully
- covered by a single pass, while in AU, this proportion is only 74.1%, and a quarter of the lakes,
- most of which are small, are not observed by SWOT at all. It is also worth noting that lakes in AU
- will be observed by the low-rate (LR) products but not by the HR products. Despite this regional
- 976 limit, the LR products can still be useful, especially for understanding the dynamics in larger lakes.

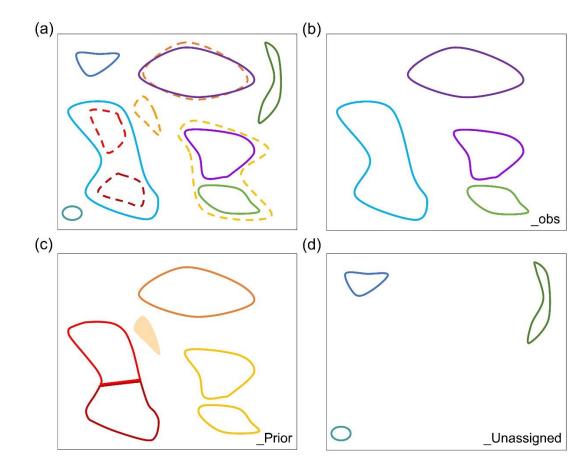


977

**Figure 11.** Distributions of lake coverage scenarios during a SWOT nominal orbit cycle for each continent or subcontinent.

### 980 **4.4 Example of linking SWOT observations**

Here we provide a conceptual example to demonstrate how the operational PLD assists 981 the SAS in linking KaRIn observations to the prior lakes and generating the L2\_HR\_LakeSP 982 vector product. More technical details are given in the Algorithm Theoretical Basis Document 983 (CNES internal document, 2023a). As introduced in section 1, the lake processing pipeline starts 984 985 from the subset of the pixel cloud (L2\_HR\_PIXC) after the removal of pixels associated with prior rivers. The remaining non-river pixels are segmented to distinct water regions based on 986 height clusters, and the pixel geolocations are further regularized by the average height per 987 region. The resulting pixels with height-constrained geolocations are used to vectorize water 988 regions, and the attributes such as water area and average WSE are computed for each vectorized 989 water feature. These processes are directly based on SWOT observations and are independent 990 from the PLD. 991



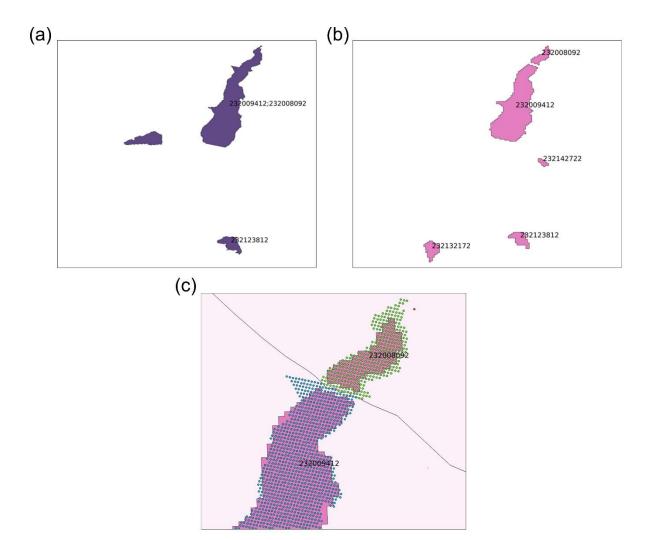
992

993 Figure 12. Illustration of how the PLD is used to organize SWOT-observed water features into the three vector files of the L2 HR LakeSP product. (a) Observed water features (solid) and 994 prior lakes (dashed) in a hypothetical region. Different colors represent different water features 995 996 or prior lakes. (b) Result of the observation-oriented file (L2 HR LakeSP Obs). (c) Result of the PLD-oriented file (L2 HR LakeSP Prior). The unobserved prior lake is an empty geometry 997 with only prior attributes, shown as a filled polygon. An observed feature intersecting two prior 998 lakes is partitioned to two feature entities (red and dark red), whereas two observed features 999 intersecting the same prior lake (yellow) are dissolved to a multipart entity. (d) Result of the 1000 observation-oriented unassigned file (L2 HR LakeSP Unassigned). 1001

1002 The observed water features are next compared with the prior lake polygons to establish 1003 spatial linkage between them. Depending on the relationship, the observed water features are organized into three product files (Fig. 12): L2\_HR\_LakeSP\_Obs, L2\_HR\_LakeSP\_Prior, and 1004 1005 L2 HR LakeSP Unassigned. As illustrated in Fig. 12a, observed water features (solid) and prior lake polygons (dash) do not always exhibit a one-to-one relationship. A linkage is considered 1006 1007 valid if an observed feature intersects at least one prior lake with sufficient overlap, typically 1008 defined as 2% or larger (CNES internal document, 2023b). In this case, the water feature is 1009 considered a lake and stored in L2\_HR\_LakeSP\_Obs (Fig. 12b). Otherwise, the feature is gathered in L2\_HR\_LakeSP\_Unassigned (Fig. 12d). Both product files are observation-oriented, 1010 1011 meaning that the water features maintain the geometries as observed by SWOT, and the output attributes, such as area and WSE, are the same as those of the input observed features. 1012

1013 To enable storage change calculation, each observed water feature must be linked to a reference water state. However, reference states are only provided for prior lakes (section 3.3.3), 1014 which often exhibit complex topological relations with observed features. Such spatial 1015 inconsistency requires water features in L2\_HR\_LakeSP\_Obs to be reorganized (grouped or 1016 1017 split) according to the prior lakes, so that the resulting features and the prior lakes have a one-toone relationship. The resulting features are gathered in L2 HR LakeSP Prior (Fig. 12c). This 1018 1019 process is straightforward when the original feature intersects only one prior lake. In this case, 1020 the geometry of the water feature remains unchanged, and the intersected prior lake with its water reference state is assigned to this water feature. When a prior lake intersects more than one 1021 water feature, all intersected features are grouped to a multipart geometry (i.e., an entity 1022 composed of several distinct polygons that represent only one set of attributes), and this prior 1023 lake is assigned to the multipart feature. 1024

A more complicated case is one observed water feature intersecting multiple prior lakes. 1025 When this occurs, the assignment polygons of the intersected prior lakes in either the 1026 "lake catchment" table or the "lake influence" table can be utilized to split the observed water 1027 1028 feature. Figure 13 illustrates an example using the "lake influence" table. In this example, an observed feature in the northeast overlaps two prior lakes (lake\_id 232008092 and 232009412). 1029 1030 To partition this feature, each of its PIXC pixels is assigned to the prior lake whose influence 1031 area contains the pixel (Fig. 13c). Since the influence areas are Thiessen polygons (section 3.4), 1032 this assignment essentially groups the water pixels based on the closest prior lake. The pixels are then re-vectorized based on their prior lake assignment to form separate water features, and the 1033 1034 corresponding WSE and water areas are recalculated. Eventually, water storage change for each feature is computed using the reference water state of the prior lake assigned to the feature. Any 1035 1036 prior lake that is not observed under an overpass, such as an intermittent lake during the dry 1037 season, is also added to L2\_HR\_LakeSP\_Prior but as an empty geometry with only prior 1038 attributes. Water storage change is not calculated for L2 HR LakeSP Unassigned where 1039 features are not linked to any prior lake, thus lacking a reference water state to effectively derive 1040 storage change.



1041

- **Figure 13.** Example of lake assignment using the operational PLD. (a) SWOT-observed water features in a hypothetical region. (b) Associated prior lakes. Prior lakes 232142722 (*lake\_id*) and 232132172 are not observed by this overpass and will be gathered by L2\_HR\_LakeSP\_Prior as empty geometries with only prior attributes. The observed water feature in the central east is linked to no prior lake and will be gathered by L2\_HR\_LakeSP\_Unassigned. The observed water feature in the northeast intersects both prior lakes 232008092 and 232009412. It will be a single
- 1048 feature in L2\_HR\_LakeSP\_Obs but will be split into two separated features in
- 1049 L2\_HR\_LakeSP\_Prior. The observed feature associated with prior lake 232123812 will be
- 1050 gathered by both L2\_HR\_LakeSP\_Obs and L2\_HR\_LakeSP\_Prior with identical geometry. (c)
- 1051 Zoom-in of the case where one observed feature intersects two prior lakes and how the pixels of
- 1052 this water feature are reorganized by the assignment polygons in the "lake\_influence" table.

### 1053 **5 Versioning plan**

1054 The operational PLD introduced in this paper represents the initial version that is used to 1055 generate the official SWOT vector lake products. With the accumulation of SWOT observations 1056 throughout the mission period, the PLD will be recursively updated to improve the functionality 1057 and quality, according to the versioning plan currently configured below.

### 1058 **5.1 Five update levels**

We envision five levels (Levels 0 to 4) of PLD update depending on the quality of the 1059 1060 prior lake polygons and the attributes computed from the SWOT vector lake products. Level 0 refers to manual inputs from data users. Level 1 updates lake storage parameters, i.e., ref\_wse, 1061 ref\_area, date\_t0, and ds\_t0. As described in Section 3.3.3, ref\_area in the initial PLD version is 1062 1063 populated as the area of the prior lake polygon, and *ref\_wse* are filled with "no data". With SWOT measurements being available, these two attributes will be updated using the values of 1064 wse and area\_total attributes in the LakeSP product (CNES internal document, 2022b) 1065 corresponding to the 80th percentile of the time series for each prior lake during the update cycle 1066 (see timeline in Section 5.3). Accordingly, the storage change parameters at the reference state 1067 (date\_t0 and ds\_t0) will be computed with reference to the date of the first valid SWOT 1068 1069 observation of the prior lake. Level 2 generates and updates the hypso curve table. The hypso\_curve table will be generated by fitting the (wse, area) pairs in the LakeSP product from 1070 the first valid observation for the prior lake (section 3.1). Each time the table is updated, the 1071 fitting will be redone using all (wse, area) pairs available from the first valid observation to the 1072 1073 end of the update cycle. Level 3 updates the geometry of each existing prior lake. This will be done by intersecting the polygons associated with the three highest wse values, of this prior lake 1074 1075 in the LakeSP Prior product. Level 4 adds new prior lakes that are absent from the previous 1076 PLD version. New prior lakes will be obtained from the water features that are observed to be persistent in the LakeSP\_Unassigned product. 1077

### 1078 **5.2 Three priority categories**

1079 Along with the five update levels, we will classify the prior lakes into three categories (P1 to P3) based on how easy or complex the update can be, with consideration of the prior lake 1080 1081 geometry, SWOT coverage, and relationship with SWOT-observed water features. These classes will be used to guide the update priority. Class P1 represents the "easiest" prior lakes and is 1082 defined as any lake that satisfies the following criteria: (1) having a size compliant with the 1083 1084 SWOT observation requirement (*area\_total* in the vector lake product > 6.25ha); (2) being fully observed by SWOT at least once per cycle ( $cycle_flag = 3$ ); (3) being fairly isolated from other 1085 lakes (*min\_dist* > 300 m); and (4) exhibiting low complexity in relation to SWOT observation, 1086 i.e., one prior lake generally corresponds to one SWOT-observed lake feature. Class P2 contains 1087 1088 the prior lakes that have the same first three criteria as Class P1 but exhibit higher complexity in 1089 relation to SWOT observation, where one prior lake corresponds to many SWOT-observed lake 1090 features. Class P3 refer to all the other prior lakes.

### 1091 **5.3 General timeline**

The first major update of the PLD will be applied only on the prior lakes overflown 1092 1093 during the Cal/Val phase (under the 1-day fast-track orbit) using the initial validated product. This update is expected to occur around 16 months after the launch of SWOT (i.e., April 2024, 1094 1095 about one year into the mission after the Cal/Val phase), when the initial validated product is 1096 released. Prior lakes of Class P3 will go through a Level-0 update (manual inputs); lakes of Class 1097 P2 will experience a Level-1 update (populating ref\_wse, ref\_area, date\_t0, and ds\_t0 attributes); and lakes of Class P1 will have a Level-2 update (generating the *hypso\_curve* table). 1098 1099 The second major update of the PLD will occur approximately one year after the first update. This update will involve prior lakes that are covered by the nominal orbit, using the same 1100

- 1101 methodology described for the first major update. Level-3 (geometry) and Level-4 (new lakes)
- 1102 updates will not be considered before the third major update of the PLD, which may occur
- approximately 3 years after the launch of SWOT (i.e., December 2025 or later). These expected
- 1104 PLD updates will reflect an improved understanding of global lake distribution and dynamics as
- 1105 SWOT observations accumulate, and in return, the updated PLD will also improve the
- 1106 processing of SWOT vector lake products. In addition to facilitating SWOT data production, the
- 1107 PLD, with its high-resolution lake mask and multiple operational tables, can be applied to
- benefiting a wide range of disciplines such as limnology, hydrological modeling, ecology, and
- 1109 climate science.

### 1110 Acknowledgements

This work is in part funded by the NASA Surface Water and Ocean Topography (SWOT)
Science Team grant (#80NSSC20K1143).

### 1113 Data Availability Statement

- 1114 The operational SWOT PLD is freely accessible for download from the Hydroweb-next
- 1115 website (<u>https://hydroweb.next.theia-land.fr</u>) under Etalab 2 license
- 1116 (https://www.etalab.gouv.fr/wp-content/uploads/2018/11/open-licence.pdf).

### 1117 Open Research

All underlying data required to produce the operational PLD are openly accessible from the respective download sources specified in Table 1 and Section 2 of this paper. Codes and algorithms used in PLD production and analysis are available upon request.

### 1121 **References**

- Abbott, B. W., Bishop, K., Zarnetske, J. P., Minaudo, C., Chapin, F. S., Krause, S., ... Pinay, G. (2019). Human domination of the global water cycle absent from depictions and perceptions. *Nature Geoscience*, *12*(7), 533-540. https://doi.org/10.1038/s41561-019-0374-y
- Adrian, R., O'Reilly, C. M., Zagarese, H., Baines, S. B., Hessen, D. O., Keller, W., ... Winder, M. (2009). Lakes as sentinels of climate change. *Limnology and Oceanography*, 54(6), 2283-2297.
  https://doi.org/10.4319/lo.2009.54.6\_part\_2.2283
- Allen, G. H., & Pavelsky, T. M. (2018). Global extent of rivers and streams. *Science*, *361*(6402), 585-587.
  https://doi.org/10.1126/science.aat0636
- Altenau, E. H., Pavelsky, T. M., Durand, M. T., Yang, X., Frasson, R. P. D., & Bendezu, L. (2021). The Surface
  Water and Ocean Topography (SWOT) Mission River Database (SWORD): A global river network for
  satellite data products. *Water Resources Research*, *57*(7), e2021WR030054.
  https://doi.org/10.1029/2021WR030054
- 1134Aurenhammer, F. (1991). Voronoi diagrams a survey of a fundamental geometric data structure. Computing1135Surveys, 23(3), 345-405. https://doi.org/10.1145/116873.116880
- Biancamaria, S., Lettenmaier, D. P., & Pavelsky, T. M. (2016). The SWOT Mission and Its Capabilities for Land
   Hydrology. *Surveys in Geophysics*, *37*(2), 307-337. https://doi.org/10.1007/s10712-015-9346-y
- Boy, F., Cretaux, J. F., Boussaroque, M., & Tison, C. (2022). Improving Sentinel-3 SAR mode processing over lake
  using numerical simulations. *IEEE Transactions on Geoscience and Remote Sensing*, 60, 5220518.
  https://doi.org/10.1109/Tgrs.2021.3137034
- Busker, T., de Roo, A., Gelati, E., Schwatke, C., Adamovic, M., Bisselink, B., . . . Cottam, A. (2019). A global lake
  and reservoir volume analysis using a surface water dataset and satellite altimetry. *Hydrology and Earth System Sciences*, 23(2), 669-690. https://doi.org/10.5194/hess-23-669-2019
- Cael, B. B., & Seekell, D. A. (2016). The size-distribution of Earth's lakes. *Scientific Reports*, *6*, 29633.
   https://doi.org/10.1038/srep29633

1146	Carroll, M. L., Townshend, J. R., DiMiceli, C. M., Noojipady, P., & Sohlberg, R. A. (2009). A new global raster
1147	water mask at 250 m resolution. International Journal of Digital Earth, 2(4), 291-308.
1148	https://doi.org/10.1080/17538940902951401
1149	Cheng, Q. M. (1995). The Perimeter-Area Fractal Model and Its Application to Geology. Mathematical Geology,
1150	27(1), 69-82. https://doi.org/Doi 10.1007/Bf02083568
1151	CIESIN. (2018). Gridded Population of the World, Version 4 (GPWv4): Population Count, Revision 11 Version
1152	Revision 11) NASA Socioeconomic Data and Applications Center (SEDAC).
1153	https://doi.org/10.7927/H4JW8BX5
1154	CNES internal document (2022a). Level 2 KaRIn high rate lake average vector product (short name:
1155	L2_HR_LakeAvg), Revision A. Surface Water and Ocean Topography (SWOT) Project Product
1156	Description Document. SWOT-TN-CDM-0676-CNES, September 30, 2022. Accessed from
1157	https://archive.podaac.earthdata.nasa.gov/podaac-ops-cumulus-docs/web-
1158	misc/swot mission docs/pdd/SWOT-TN-CDM-0676-
1159	CNES_Product_Description_L2_HR_LakeAvg_20220930_RevA.pdf on October 16, 2023.
1160	CNES internal document (2022b). Level 2 KaRIn high rate lake single pass vector product (short name:
1161	L2_HR_LakeSP), Revision A. Surface Water and Ocean Topography (SWOT) Project Product Description
1162	Document. SWOT-TN-CDM-0673-CNES, September 30, 2022. Accessed from
1163	https://archive.podaac.earthdata.nasa.gov/podaac-ops-cumulus-docs/web-
1164	misc/swot mission docs/pdd/SWOT-TN-CDM-0673-
1165	CNES_Product_Description_L2_HR_LakeSP_20220930_RevA.pdf on October 16, 2023.
1166	CNES internal document (2022c). Level 2 KaRIn high rate pixel cloud vector attribute product (short name:
1167	L2_HR_PIXCVec), Revision A. Surface Water and Ocean Topography (SWOT) Project Product
1168	Description Document. SWOT-TN-CDM-0677-CNES, September 30, 2022. Accessed from
1169	https://archive.podaac.earthdata.nasa.gov/podaac-ops-cumulus-docs/web-
1170	misc/swot mission docs/pdd/SWOT-TN-CDM-0677-
1171	CNES_Product_Description_L2_HR_PIXCVec_20220930_RevA.pdf on October 16, 2023.
1172	CNES internal document (2023a). Level 2 KaRIn high rate lake single pass science algorithm software: Level 2
1173	processing (short name: SAS_L2_HR_LakeSP: Level 2 processing), Initial Release. Surface Water and
1174	Ocean Topography (SWOT) Project Algorithm Theoretical Basis Document. SWOT-NT-CDM-1753-
1175	CNES, July 26, 2023. Accessed from https://archive.podaac.earthdata.nasa.gov/podaac-ops-cumulus-
1176	docs/web-misc/swot mission docs/atbd/SWOT-NT-CDM-1753-
1177	CNES_ATBD_LakeSP_20230726_Initial_w-sigs.pdf on October 16, 2023.
1178	CNES internal document (2023b). Level 2 KaRIn high rate lake tile auxiliary parameter file (short name:
1179	Param_L2_HR_LakeTile). Surface Water and Ocean Topography (SWOT) Project Auxiliary Data
1180	Description Document. 2023, to be released.
1181	Cooley, S. W., Ryan, J. C., & Smith, L. C. (2021). Human alteration of global surface water storage variability.
1182	Nature, 591(7848), 78-81. https://doi.org/10.1038/s41586-021-03262-3.
1183	Copernicus Climate Change Service (C3S) (2017). ERA5: Fifth generation of ECMWF atmospheric reanalyses of
1184	the global climate.
1185	Cretaux, J. F., Abarca-del-Rio, R., Berge-Nguyen, M., Arsen, A., Drolon, V., Clos, G., & Maisongrande, P. (2016).
1186	Lake Volume Monitoring from Space. Surveys in Geophysics, 37(2), 269-305.
1187	https://doi.org/10.1007/s10712-016-9362-6
1188	Cretaux, J. F., Jelinski, W., Calmant, S., Kouraev, A., Vuglinski, V., Berge-Nguyen, M., Maisongrande, P.
1189	(2011). SOLS: A lake database to monitor in the Near Real Time water level and storage variations from
1190	remote sensing data. Advances in Space Research, 47(9), 1497-1507.
1191	https://doi.org/10.1016/j.asr.2011.01.004
1192	de Fleury, M., Kergoat, L., & Grippa, M. (2023). Hydrological regime of Sahelian small waterbodies from
1193	combined Sentinel-2 MSI and Sentinel-3 Synthetic Aperture Radar Altimeter data. Hydrology and Earth
1194	System Sciences, 27(11), 2189-2204. https://doi.org/10.5194/hess-27-2189-2023
1195	Desroches, D., Fjørtoft, R., Gaudin, JM., Ruiz, C., & Blumstein, D. (2016, Jun. 2016). Precise geolocation of water
1196	bodies in SWOT HR InSar data. Proceedings of EUSAR 2016: 11th European Conference on Synthetic
1197	Aperture Radar, Hamburg, Germany.
1198	Durand, M., Fu, L. L., Lettenmaier, D. P., Alsdorf, D. E., Rodriguez, E., & Esteban-Fernandez, D. (2010). The
1199	surface water and ocean topography mission: Observing terrestrial surface water and oceanic submesoscale
1200	eddies. Proceedings of the IEEE, 98(5), 766-779. https://doi.org/10.1109/JPROC.2010.2043031

1201 1202	Evans, D. G., & Jones, S. M. (1987). Detecting Voronoi (area-of-influence) polygons. <i>Mathematical Geology</i> , <i>19</i> (6), 523-537. https://doi.org/10.1007/Bf00896918
1202	Fan, C., Song, C., & TBD. (2023). An underrated abundance of young reservoirs revealed by new data. <i>Science</i>
1203	Bulletin, In review.
1204	Farr, T. G., Rosen, P. A., Caro, E., Crippen, R., Duren, R., Hensley, S., Alsdorf, D. (2007). The shuttle radar
1205	topography mission. <i>Reviews of Geophysics</i> , 45(2), 2005RG000183. https://doi.org/10.1029/2005rg000183
1200	Fergus, C. E., Lapierre, J. F., Oliver, S. K., Skaff, N. K., Cheruvelil, K. S., Webster, K., Soranno, P. (2017). The
1207	freshwater landscape: lake, wetland, and stream abundance and connectivity at macroscales. <i>Ecosphere</i> ,
1200	8(8), e01911. https://doi.org/10.1002/ecs2.1911
1210	Fisher, A., Flood, N., & Danaher, T. (2016). Comparing Landsat water index methods for automated water
1210	classification in eastern Australia. <i>Remote Sensing of Environment</i> , 175, 167-182.
1211	https://doi.org/10.1016/j.rse.2015.12.055
1212	Grosse, G., Jones, B., & Arp, C. (2013). Thermokarst lakes, drainage, and drained basins. In J. F. Shroder, R.
1213	Giardino, & J. Harbor (Eds.), <i>Treatise on Geomorphology</i> (Vol. Vol. 8, Glacial and Periglacial
1214	Geomorphology, pp. 325–353). Academic Press.
1215	Herdendorf, C. E. (1984). Inventory of the morphopmetric and limnologic characteristics of the large lakes of the
1210	world, Technical Bulletin OHSU-TB-17, The Ohio State University Sea Grant Program, March 1984.
1218	JPL internal document (2018). Surface Water and Ocean Topography Mission (SWOT) Project Science
1210	Requirements Document, Rev B. JPL D-61923, January 24, 2018. Accessed from
1220	https://swot.jpl.nasa.gov/system/documents/files/2176_2176_D-61923_SRD_Rev_B_20181113.pdf on
1220	October 16, 2023.
1222	JPL internal document (2022a). Level 2 KaRIn high rate river average vector product (short name:
1223	L2_HR_RiverAvg), Revision A, Surface Water and Ocean Topography (SWOT) Project Product
1224	Description Document. JPL D-56414, September 27, 2022. Accessed from
1225	https://archive.podaac.earthdata.nasa.gov/podaac-ops-cumulus-docs/web-misc/swot mission docs/pdd/D-
1226	56414 SWOT Product Description L2 HR RiverAvg 20220927a RevA.pdf on October 16, 2023.
1227	JPL internal document (2022b). Level 2 KaRIn high rate river single pass vector product (short name:
1228	L2_HR_RiverSP), Revision A, Surface Water and Ocean Topography (SWOT) Project Product Description
1229	Document. JPL D-56413, September 16, 2022. Accessed from
1230	https://archive.podaac.earthdata.nasa.gov/podaac-ops-cumulus-docs/web-misc/swot mission docs/pdd/D-
1231	56413 SWOT Product Description L2 HR RiverSP 20220916a RevA.pdf on October 16, 2023.
1232	JPL internal document (2022c). Level 1B KaRIn high rate single look complex data product (short name:
1233	L1B_HR_SLC), Revision A, Surface Water and Ocean Topography Mission (SWOT) Project Product
1234	Description Document. JPL D-56410, July 27, 2022. Accessed from
1235	https://archive.podaac.earthdata.nasa.gov/podaac-ops-cumulus-docs/web-misc/swot_mission_docs/pdd/D-
1236	56410 SWOT Product Description L1B HR SLC 20220727 RevA.pdf on October 16, 2023.
1237	JPL internal document (2022d). Level 2 KaRIn high rate water mask pixel cloud product (short name:
1238	L2_HR_PIXC), Revision A, Surface Water and Ocean Topography (SWOT) Project Product Description
1239	Document. JPL D-56411, July 27, 2022. Accessed from https://archive.podaac.earthdata.nasa.gov/podaac-
1240	ops-cumulus-docs/web-misc/swot_mission_docs/pdd/D-
1241	56411_SWOT_Product_Description_L2_HR_PIXC_20220727b_RevA.pdf on October 16, 2023.
1242	JPL internal document (2022e). Reference Orbit Track (RefOrbitTrack). Surface Water and Ocean Topography
1243	(SWOT) Project Auxiliary Data Description. JPL D-105500, September 13, 2022.
1244	JPL internal document (2023). Level 2 KaRIn high rate river single pass science algorithm software (short name:
1245	SAS_L2_HR_RiverSP), Initial Release. Surface Water and Ocean Topography Project Algorithm
1246	Theoretical Basis Document. JPL D-105505, July 13, 2023. Accessed from
1247	https://archive.podaac.earthdata.nasa.gov/podaac-ops-cumulus-docs/web-misc/swot_mission_docs/atbd/D-
1248	105505 SWOT ATBD L2 HR RiverSP 20230713 w-sigs.pdf on October 16, 2023.
1249	Kokelj, S. V., & Jorgenson, M. T. (2013). Advances in Thermokarst Research. Permafrost and Periglacial
1250	<i>Processes</i> , 24(2), 108-119. https://doi.org/10.1002/ppp.1779
1251	Lacroix, M. P., Prowse, T. D., Bonsal, B. R., Duguay, C. R., & Menard, P. (2005, Sept. 15-16, 2005). <i>River ice</i>
1252	trends in Canada 13th Workshop on Ice Covered Rivers, Hanover, NH.
1253	Lehner, B., & Doll, P. (2004). Development and validation of a global database of lakes, reservoirs and wetlands.
1254	Journal of Hydrology, 296(1-4), 1-22. https://doi.org/10.1016/j.jhydrol.2004.03.028

- Lehner, B., & Grill, G. (2013). Global river hydrography and network routing: baseline data and new approaches to
   study the world's large river systems. *Hydrological Processes*, 27(15), 2171-2186.
   https://doi.org/10.1002/hvp.9740
- Lehner, B., Liermann, C. R., Revenga, C., Vorosmarty, C., Fekete, B., Crouzet, P., ... Wisser, D. (2011). High resolution mapping of the world's reservoirs and dams for sustainable river-flow management. *Frontiers in Ecology and the Environment*, 9(9), 494-502. https://doi.org/10.1890/100125
- Lehner, B., Verdin, K., & Jarvis, A. (2008). New global hydrography derived from spaceborne elevation data. *Eos, Transactions American Geophysical Union*, 89(10), 93-104. https://doi.org/10.1029/2008EO100001
- Li, J., & Sheng, Y. (2012). An automated scheme for glacial lake dynamics mapping using Landsat imagery and
   digital elevation models: a case study in the Himalayas. *International Journal of Remote Sensing*, 33(16),
   5194-5213. https://doi.org/10.1080/01431161.2012.657370
- Luo, S. X., Song, C. Q., Ke, L. H., Zhan, P. F., Fan, C. Y., Liu, K., . . . Zhu, J. Y. (2022). Satellite laser altimetry reveals a net water mass gain in global lakes with spatial heterogeneity in the early 21st century.
   *Geophysical Research Letters*, 49(3), e2021GL096676. https://doi.org/10.1029/2021GL096676
- Lyons, E. A., & Sheng, Y. W. (2018). LakeTime: Automated seasonal scene selection for global lake mapping using
   Landsat ETM plus and OLI. *Remote Sensing*, 10(1), 54. https://doi.org/10.3390/rs10010054
- Manasypov, R. M., Pokrovsky, O. S., Kirpotin, S. N., & Shirokova, L. S. (2014). Thermokarst lake waters across the permafrost zones of western Siberia. *Cryosphere*, 8(4), 1177-1193. https://doi.org/10.5194/tc-8-1177-2014
- 1273 Mandelbrot, B. B. (1982). *The Fractal Geometry of Nature*. WH Freeman.
- McFeeters, S. K. (1996). The use of the normalized difference water index (NDWI) in the delineation of open water
   features. *International Journal of Remote Sensing*, 17(7), 1425-1432.
   https://doi.org/10.1080/01431169608948714
- Mendonca, R., Muller, R. A., Clow, D., Verpoorter, C., Raymond, P., Tranvik, L. J., & Sobek, S. (2017). Organic
   carbon burial in global lakes and reservoirs. *Nature Communications*, 8, 1694.
   https://doi.org/10.1038/s41467-017-01789-6
- Messager, M. L., Lehner, B., Grill, G., Nedeva, I., & Schmitt, O. (2016). Estimating the volume and age of water
   stored in global lakes using a geo-statistical approach. *Nature Communications*, 7, 13603.
   https://doi.org/10.1038/ncomms13603
- Nie, Y., Sheng, Y. W., Liu, Q., Liu, L. S., Liu, S. Y., Zhang, Y. L., & Song, C. Q. (2017). A regional-scale
   assessment of Himalayan glacial lake changes using satellite observations from 1990 to 2015. *Remote Sensing of Environment*, 189, 1-13. https://doi.org/10.1016/j.rse.2016.11.008
- Oki, T., & Kanae, S. (2006). Global hydrological cycles and world water resources. *Science*, *313*(5790), 1068-1072.
   https://doi.org/10.1126/science.1128845
- Papa, F., Crétaux, J. F., Grippa, M., Robert, E., Trigg, M., Tshimanga, R. M., . . . Calmant, S. (2023). Water
   resources in Africa under global change: Monitoring surface waters from space. *Surveys in Geophysics*,
   44(1), 43-93. https://doi.org/10.1007/s10712-022-09700-9
- Pekel, J.-F., Cottam, A., Gorelick, N., & Belward, A. S. (2016). High-resolution mapping of global surface water
   and its long-term changes [Letter]. *Nature*, 540(7633), 418-422. https://doi.org/10.1038/nature20584
- Pi, X. H., Luo, Q. Q., Feng, L., Xu, Y., Tang, J., Liang, X. Y., ... Bryan, B. A. (2022). Mapping global lake
  dynamics reveals the emerging roles of small lakes. *Nature Communications*, *13*(1), 5777.
  https://doi.org/10.1038/s41467-022-34140-9
- Pickens, A. H., Hansen, M. C., Hancher, M., Stehman, S. V., Tyukavina, A., Potapov, P., . . . Sherani, Z. (2020).
   Mapping and sampling to characterize global inland water dynamics from 1999 to 2018 with full Landsat time-series. *Remote Sensing of Environment*, 243(15), 111792. https://doi.org/10.1016/j.rse.2020.111792
- Riggs, R. M., Allen, G. H., Brinkerhoff, C. B., Sikder, M. S., & Wang, J. (2023). Turning lakes into river gauges
  using the LakeFlow algorithm. *Geophysical Research Letters*, 50(10), e2023GL103924.
  https://doi.org/10.1029/2023GL103924
- Schindler, D. W. (2009). Lakes as sentinels and integrators for the effects of climate change on watersheds, airsheds, and landscapes. *Limnology and Oceanography*, 54(6), 2349-2358.
   https://doi.org/10.4319/lo.2009.54.6 part 2.2349
- Schwatke, C., Dettmering, D., Bosch, W., & Seitz, F. (2015). DAHITI an innovative approach for estimating water
   level time series over inland waters using multi-mission satellite altimetry. *Hydrology and Earth System Sciences*, 19(10), 4345-4364. https://doi.org/10.5194/hess-19-4345-2015
- Sheng, Y. W., Song, C. Q., Wang, J. D., Lyons, E. A., Knox, B. R., Cox, J. S., & Gao, F. (2016). Representative
   lake water extent mapping at continental scales using multi-temporal Landsat-8 imagery. *Remote Sensing* of Environment, 185, 129-141. https://doi.org/10.1016/j.rse.2015.12.041

- Shilts, W. W., Aylsworth, J. M., Kaszycki, C. A., & Klassen, R. A. (1987). Canadian Shield. In W. L. Graf (Ed.),
   *Geomorphic systems of North America* (Vol. Centennial Special Volume 2, pp. 119-161). Geological
   Society of America.
- Shugar, D. H., Burr, A., Haritashya, U. K., Kargel, J. S., Watson, C. S., Kennedy, M. C., ... Strattman, K. (2020).
   Rapid worldwide growth of glacial lakes since 1990. *Nature Climate Change*, *10*(10), 939-945.
   https://doi.org/10.1038/s41558-020-0855-4
- Sikder, M. S., Wang, J., Allen, G. H., Sheng, Y., Yamazaki, D., Song, C., . . . Pavelsky, T. M. (2023). LakeTopoCat: A global lake drainage topology and catchment database. *Earth System Science Data*, *15*, 3483–
  3511. https://doi.org/10.5194/essd-15-3483-2023
- Slater, J. A., Garvey, G., Johnston, C., Haase, J., Heady, B., Kroenung, G., & Little, J. (2006). The SRTM data
   "finishing" process and products. *Photogrammetric Engineering and Remote Sensing*, 72(3), 237-247.
   https://doi.org/10.14358/Pers.72.3.237
- Smith, L. C., Sheng, Y., MacDonald, G. M., & Hinzman, L. D. (2005). Disappearing Arctic lakes. *Science*, 308(5727), 1429-1429. https://doi.org/10.1126/science.1108142
- Song, C., Sheng, Y., Wang, J., Ke, L. H., Madson, A., & Nie, Y. (2017). Heterogeneous glacial lake changes and
   links of lake expansions to the rapid thinning of adjacent glacier termini in the Himalayas. *Geomorphology*,
   280(1), 30-38. https://doi.org/10.1016/j.geomorph.2016.12.002
- Tranvik, L. J., Downing, J. A., Cotner, J. B., Loiselle, S. A., Striegl, R. G., Ballatore, T. J., . . . Weyhenmeyer, G. A.
  (2009). Lakes and reservoirs as regulators of carbon cycling and climate. *Limnology and Oceanography*,
  54(6), 2298-2314. https://doi.org/10.4319/lo.2009.54.6\_part\_2.2298
- 1331 U.S. Geological Survey. (2013). National Hydrography Geodatabase: Alaska. http://nhd.usgs.gov/
- 1332 Verdin, K. L., & Verdin, J. P. (1999). A topological system for delineation and codification of the Earth's river
   1333 basins. *Journal of Hydrology*, 218(1-2), 1-12. https://doi.org/10.1016/S0022-1694(99)00011-6
- 1334 Verpoorter, C., Kutser, T., Seekell, D. A., & Tranvik, L. J. (2014). A global inventory of lakes based on high 1335 resolution satellite imagery. *Geophysical Research Letters*, *41*(18), 6396-6402.
   1336 https://doi.org/10.1002/2014gl060641
- Wang, J. D., Sheng, Y. W., & Tong, T. S. D. (2014). Monitoring decadal lake dynamics across the Yangtze Basin
   downstream of Three Gorges Dam. *Remote Sensing of Environment*, 152, 251-269.
   https://doi.org/10.1016/j.rse.2014.06.004
- Wang, J. D., Song, C. Q., Reager, J. T., Yao, F. F., Famiglietti, J. S., Sheng, Y. W., ... Wada, Y. (2018). Recent
  global decline in endorheic basin water storages. *Nature Geoscience*, *11*(12), 926-932.
  https://doi.org/10.1038/s41561-018-0265-7
- Wang, J. D., Walter, B. A., Yao, F. F., Song, C. Q., Ding, M., Maroof, A., . . . Wada, Y. (2022). GeoDAR:
  georeferenced global dams and reservoirs dataset for bridging attributes and geolocations. *Earth System Science Data*, 14(4), 1869-1899. https://doi.org/10.5194/essd-14-1869-2022
- Wik, M., Varner, R. K., Anthony, K. W., MacIntyre, S., & Bastviken, D. (2016). Climate-sensitive northern lakes
  and ponds are critical components of methane release. *Nature Geoscience*, 9(2), 99-105.
  https://doi.org/10.1038/ngeo2578
- 1349 WMO. (2022). The 2022 GCOS Implementation Plan. GCOS-244. World Meteorological Organization.
- Wu, Q., Ke, L., Wang, J., Pavelsky, T. M., Allen, G. H., Sheng, Y., . . . Song, C. (2023). Satellites reveal hotspots of global river extent change. *Nature Communications*, 14, 1587. https://doi.org/10.1038/s41467-023-37061-3
- Wurtsbaugh, W. A., Miller, C., Null, S. E., DeRose, R. J., Wilcock, P., Hahnenberger, M., . . . Moore, J. (2017).
  Decline of the world's saline lakes. *Nature Geoscience*, 10(11), 816-821. https://doi.org/10.1038/ngeo3052
- Yamazaki, D., Ikeshima, D., Sosa, J., Bates, P. D., Allen, G. H., & Pavelsky, T. M. (2019). MERIT Hydro: A High Resolution Global Hydrography Map Based on Latest Topography Dataset. *Water Resources Research*,
   55(6), 5053-5073. https://doi.org/10.1029/2019wr024873
- Yang, X., O'Reilly, C. M., Gardner, J. R., Ross, M. R. V., Topp, S. N., Wang, J. D., & Pavelsky, T. M. (2022). The
   Color of Earth's Lakes. *Geophysical Research Letters*, 49(18), e2022GL098925.
   https://doi.org/10.1029/2022GL098925
- Yang, X., Pavelsky, T. M., Bendezu, L. P., & Zhang, S. (2022). Simple method to extract lake ice condition from
   Landsat images. *IEEE Transactions on Geoscience and Remote Sensing*, 60, 4202010.
   https://doi.org/10.1109/Tgrs.2021.3088144
- Yao, F., Livneh, B., Rajagopalan, B., Wang, J., Crétaux, J.-F., Wada, Y., & Berge-Nguyen, M. (2023). Satellites
  reveal widespread decline in global lake water storage. *Science*, *380*, 743-749.
  https://doi.org/10.1126/science.abo2812

1366 Zimnitskaya, H., & Geldern, J. v. (2011). Is the Caspian Sea a sea; and why does it matter? *Journal of Eurasian* 1367 *Studies*, 2(1), 1-14. https://doi.org/10.1016/j.euras.2010.10.009
 1368

1369

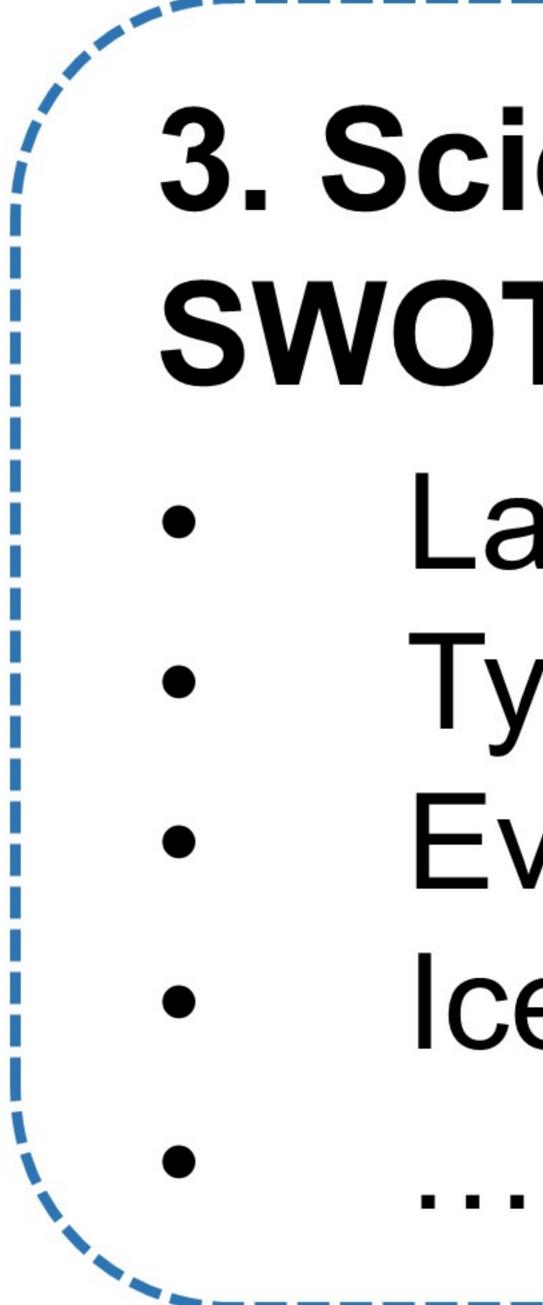
Figure 1.

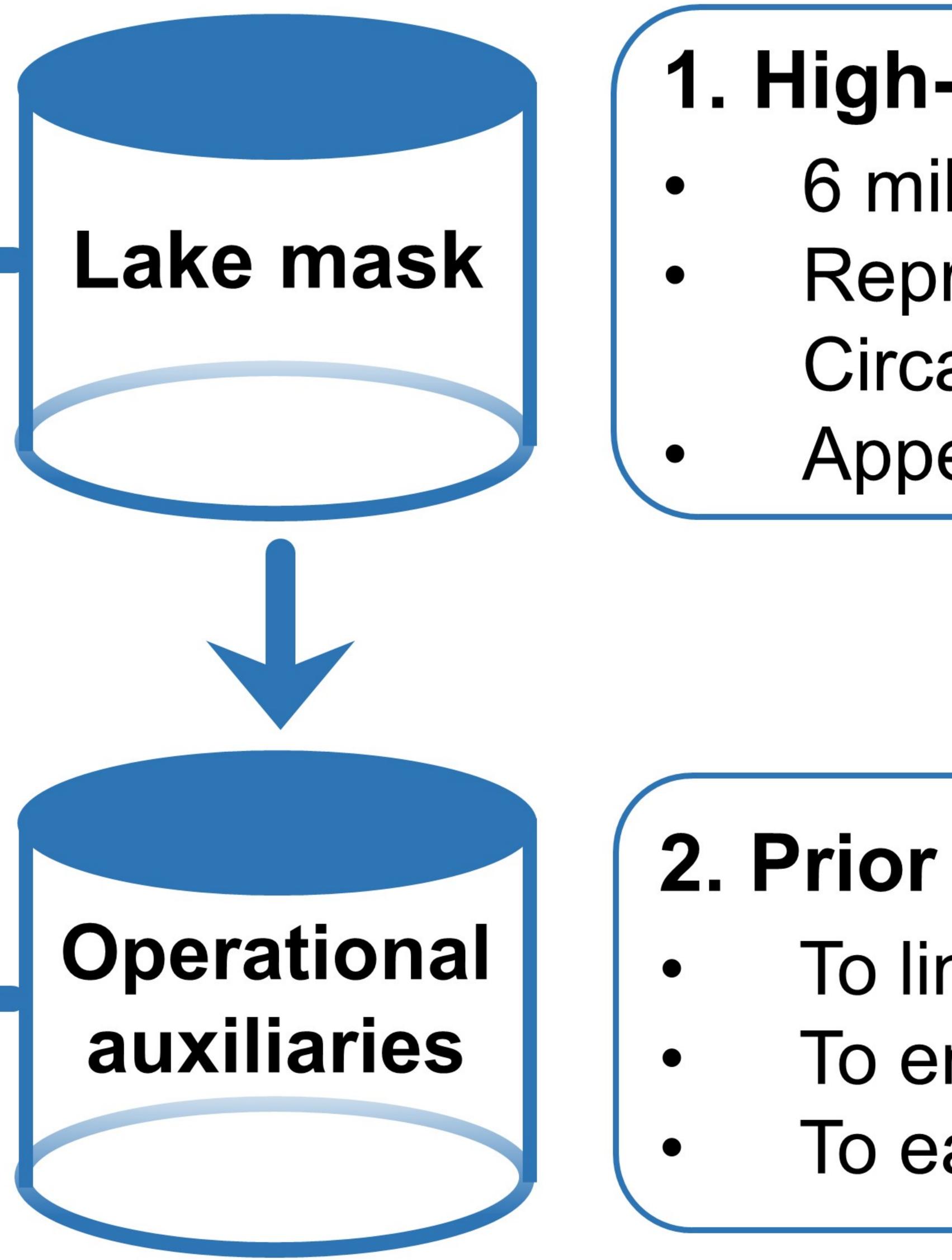
## **Operational PLD** (paper I)



## Scientific PLD (paper II)







## 3. Scientific metadata to facilitate SWOT data product applications Lake topology and catchments Typology Evaporation

Ice phenology

## 1. High-resolution global lake and reservoir polygons 6 million prior lakes >1 ha (SWOT science goal) Representative inundation extents based on the UCLA Circa-2015 Global Lake Dataset Appended by recently constructed reservoirs

## 2. Prior information to ease SWOT lake data production To link SWOT observations to prior lakes To enable computation of lake storage changes To ease lake processing and populate the lake products

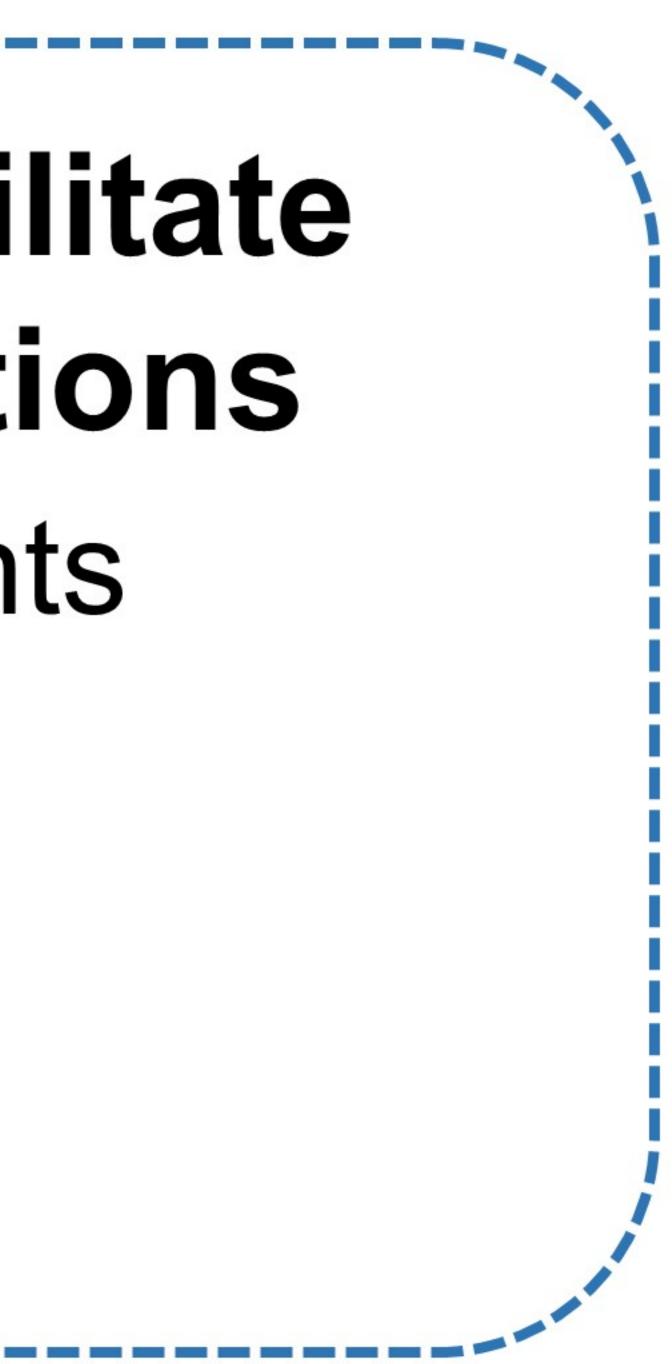
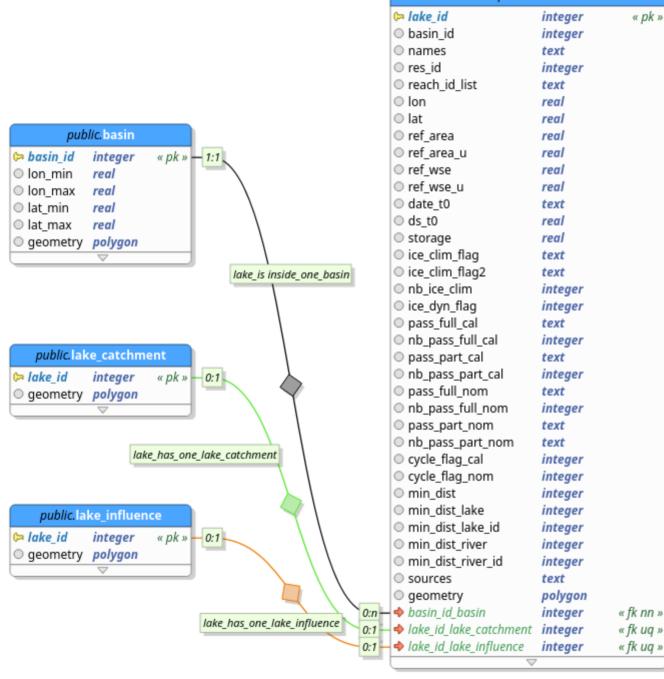


Figure 2.



public.lake

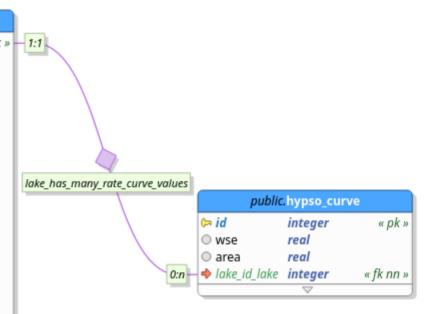
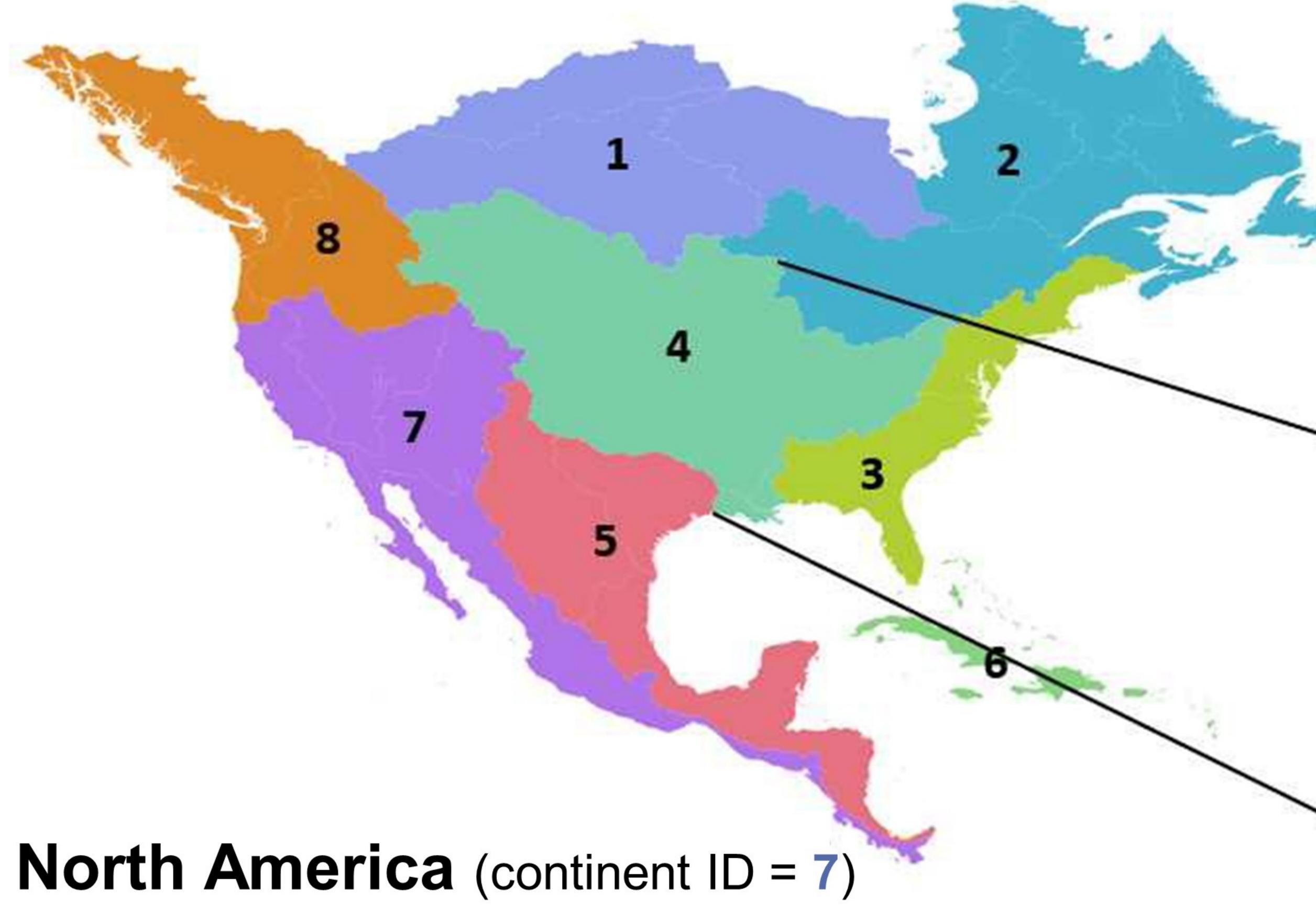


Figure 3.



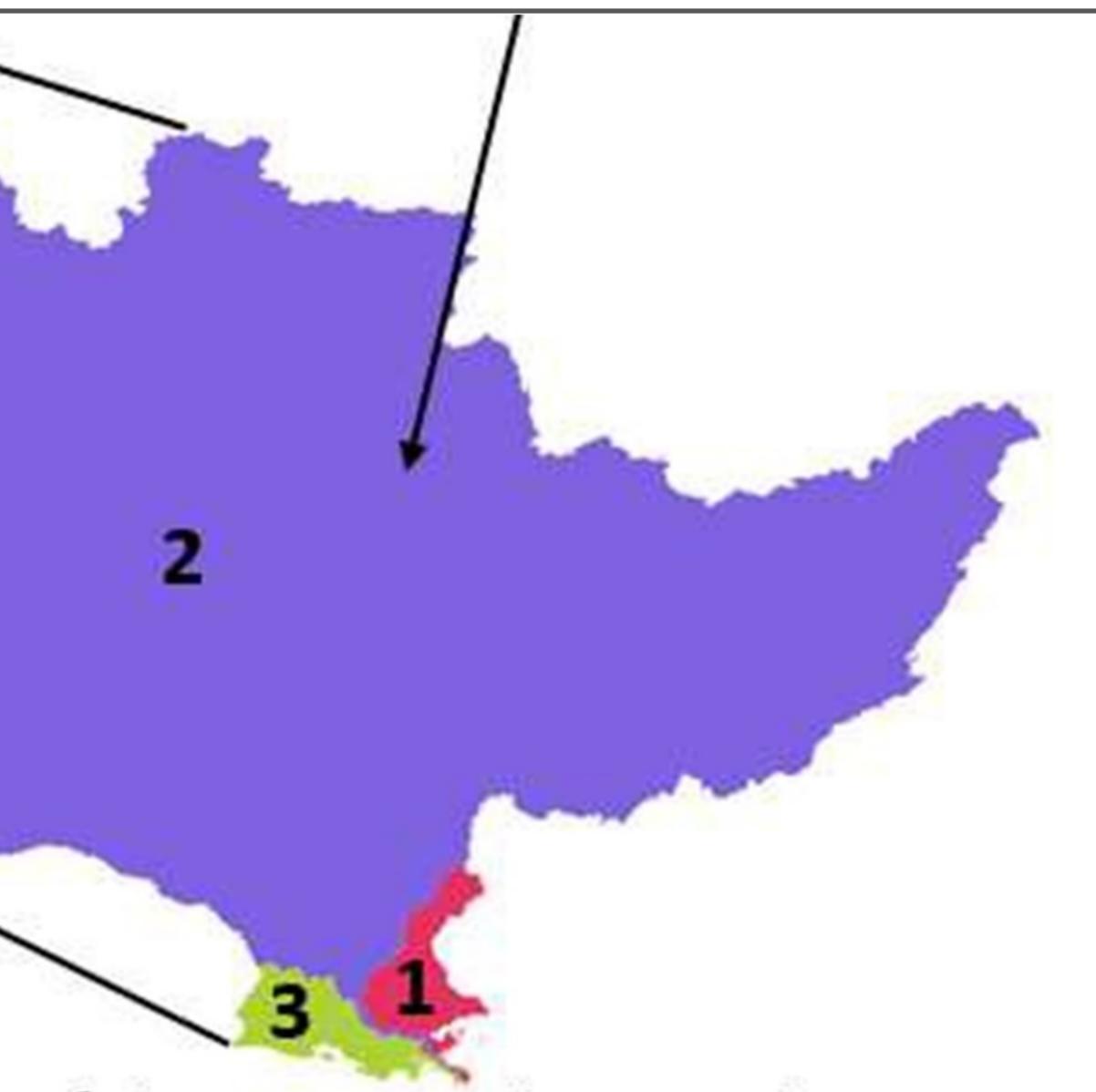
# Sub-basins (level 2)

### **CBBNNNNNT** (*lake\_id*) C – Continent **B** – Basin code ٠ • T – Type



N – Lake index in the basin

### Example for a lake in this basin: *lake\_id* = **742**046960**2**



### Mississippi (basin 1<sup>st</sup> digit = 4) Sub-basins (level 3)

Figure 4.

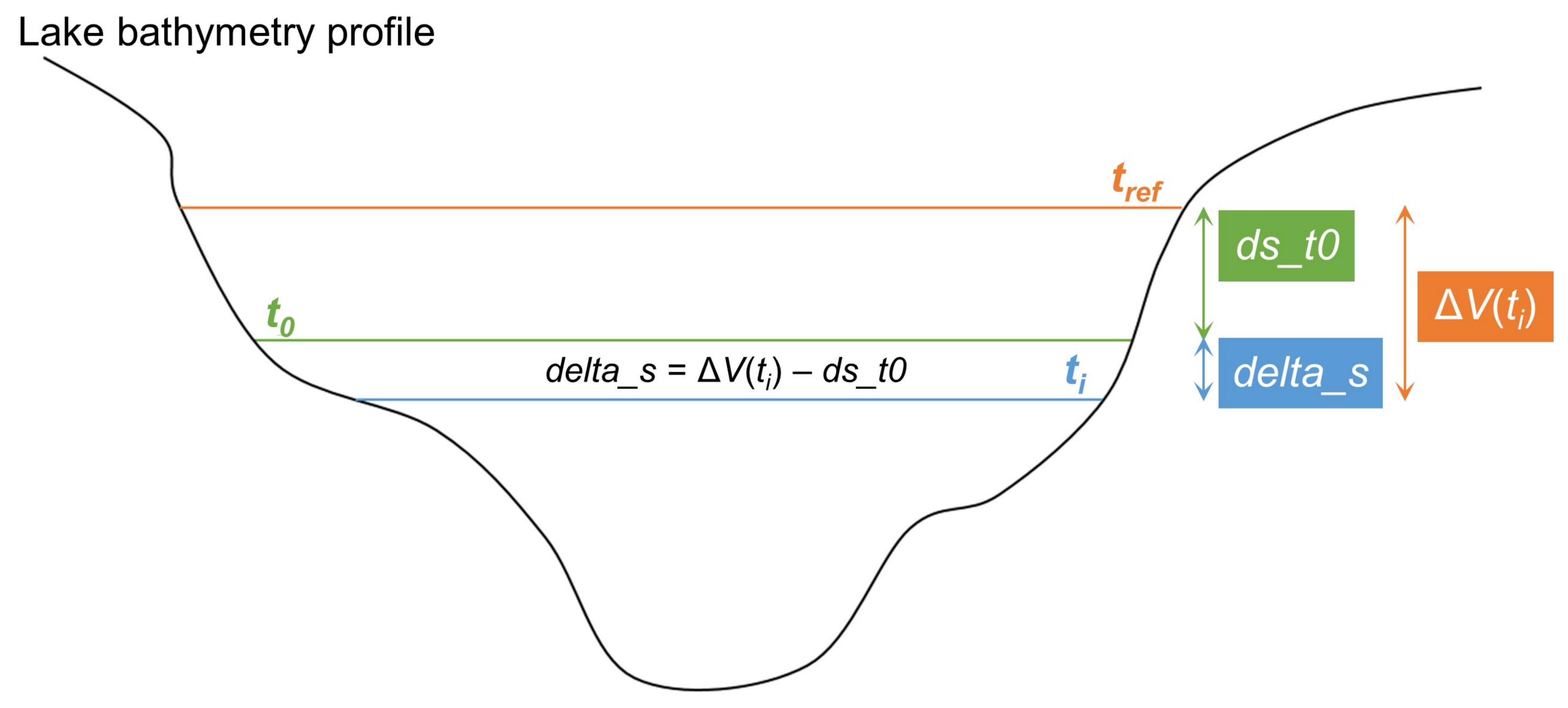


Figure 5.

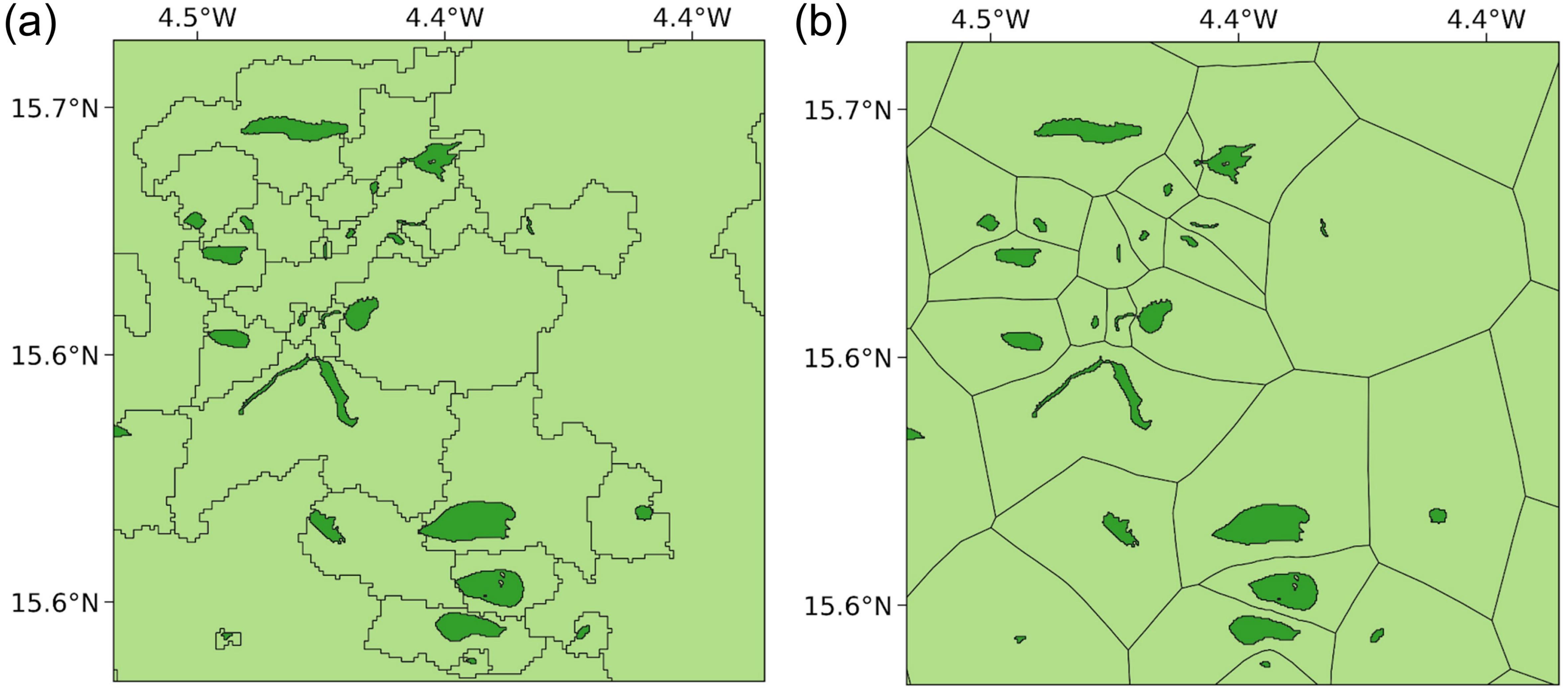


Figure 6.

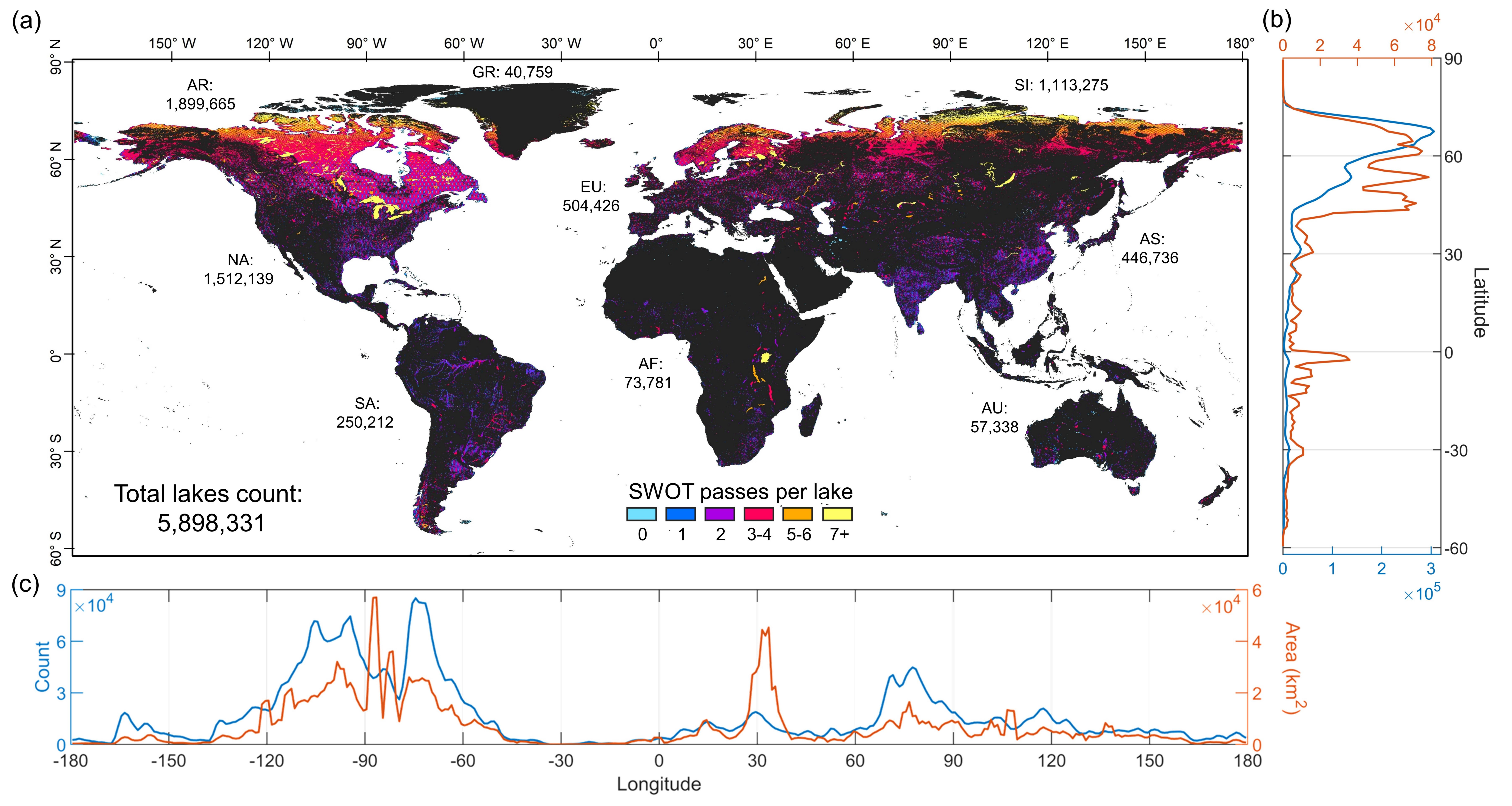
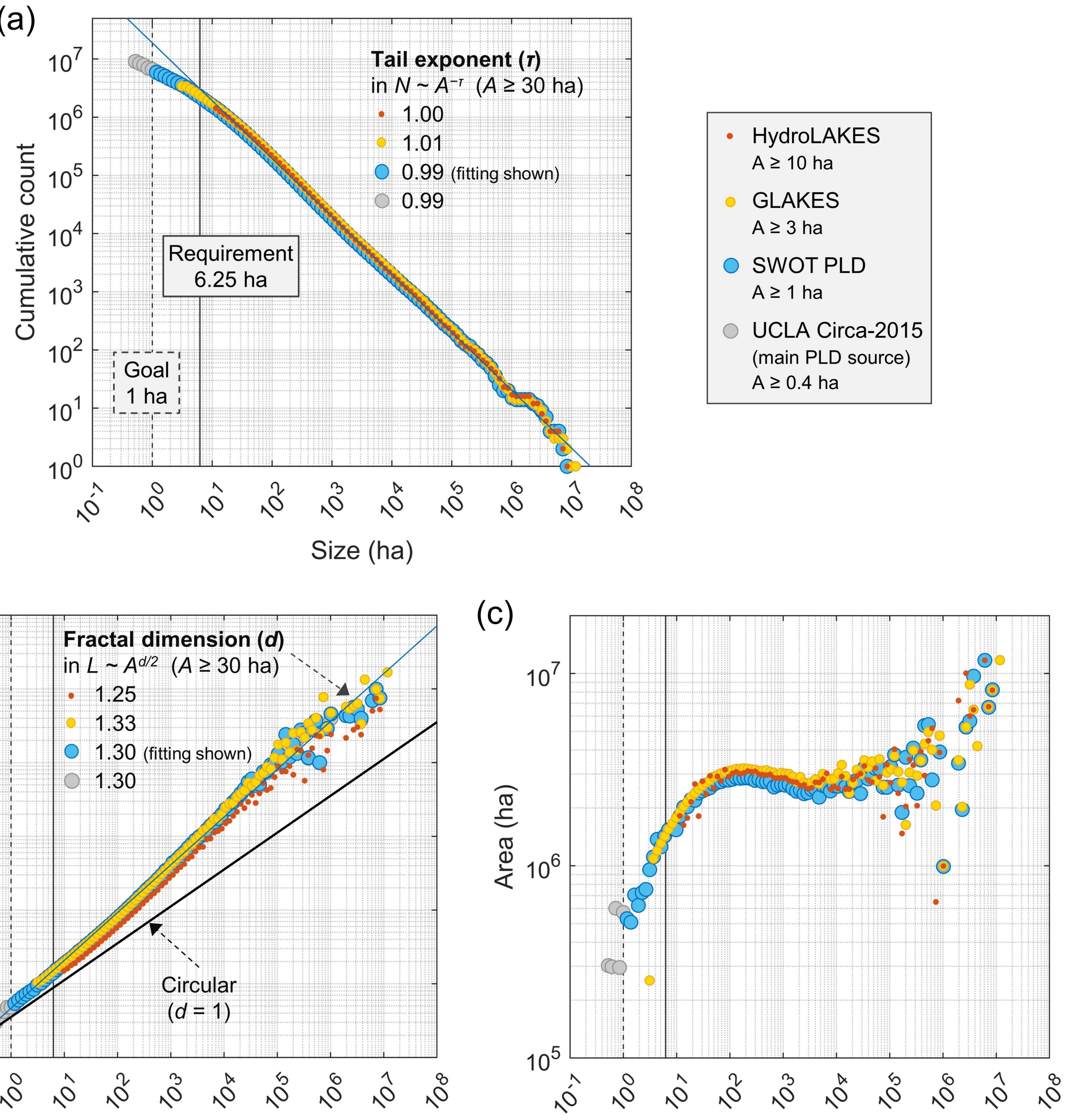
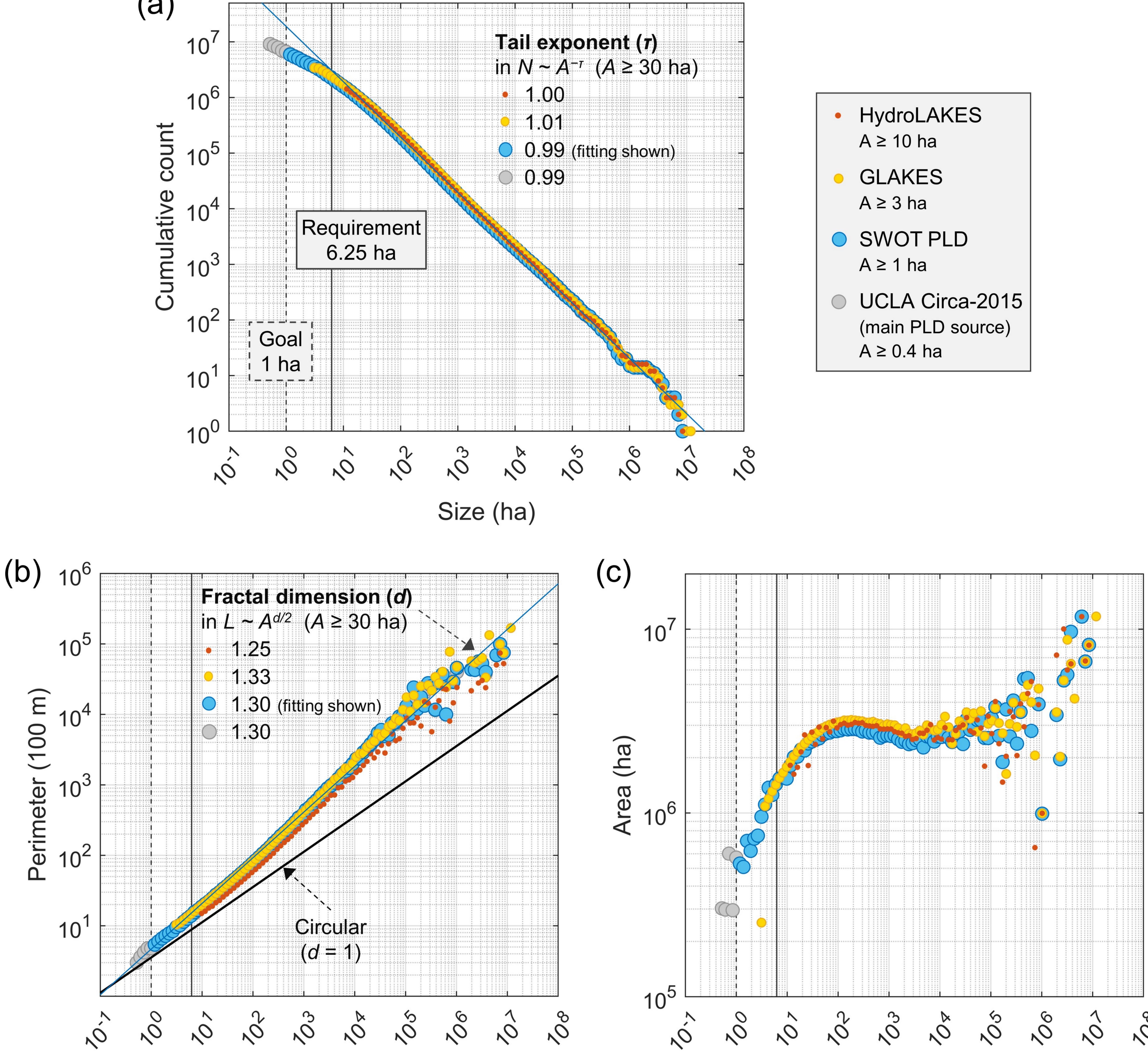
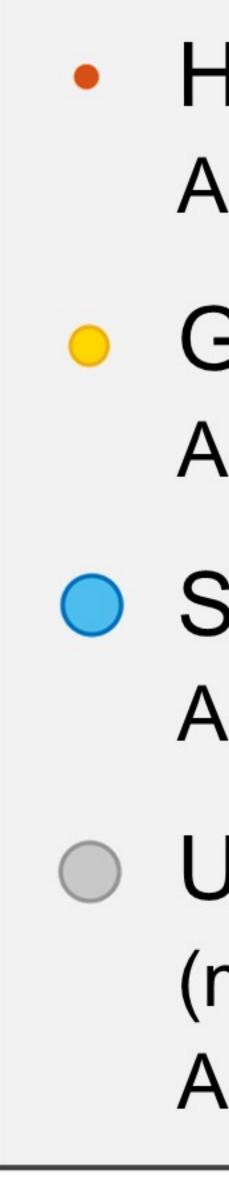


Figure 7.



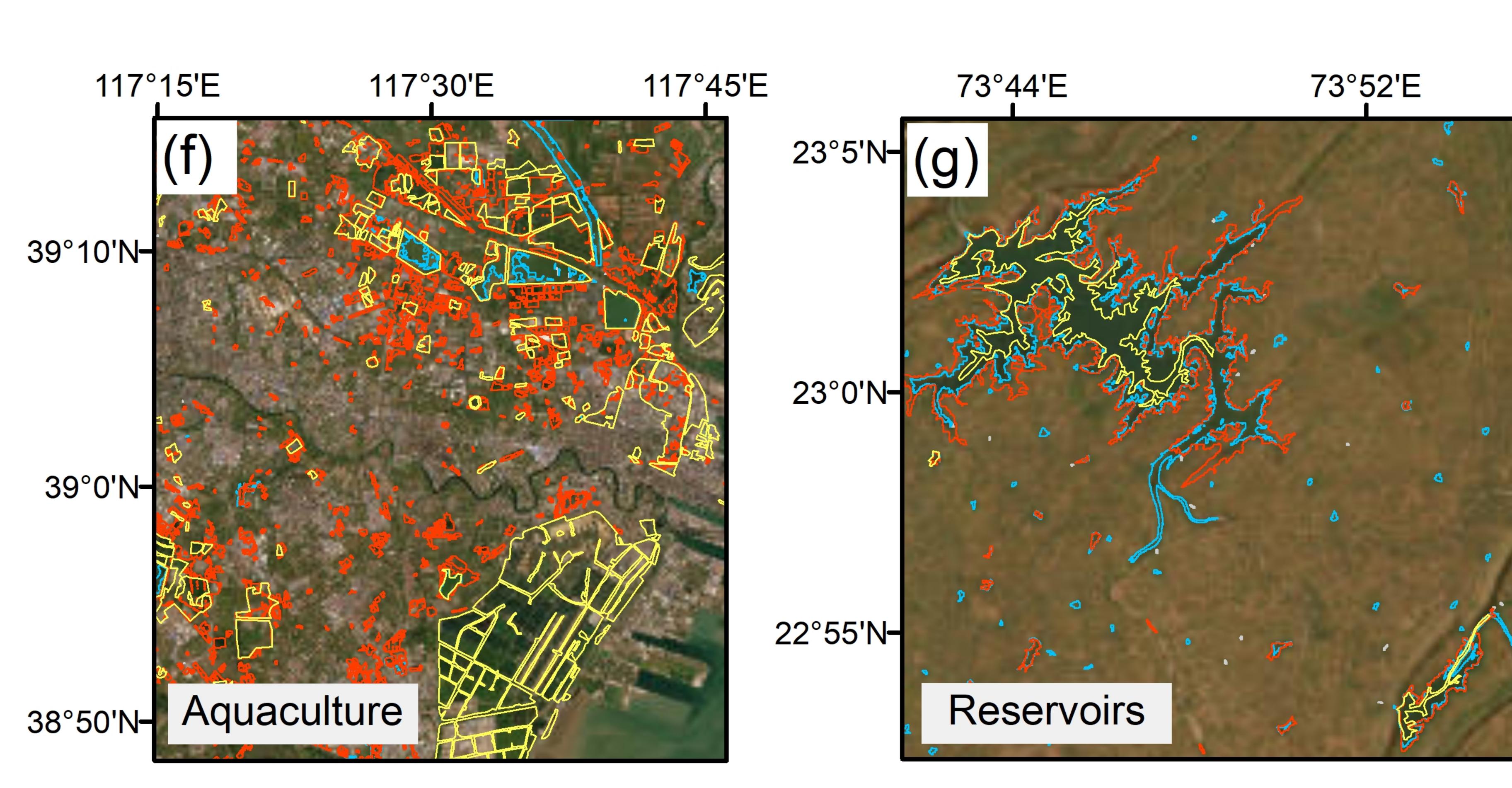


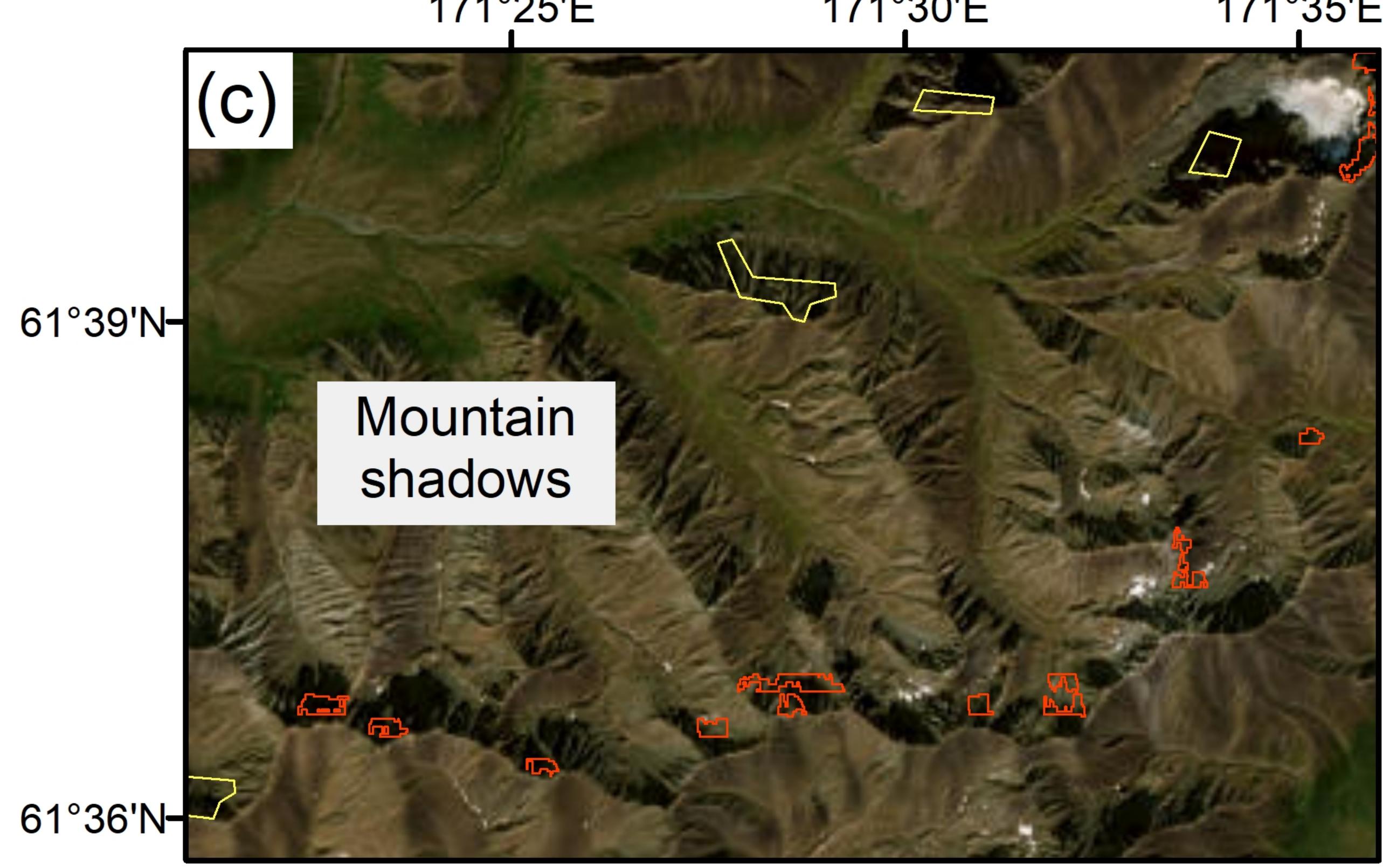
Size (ha)



### Size (ha)

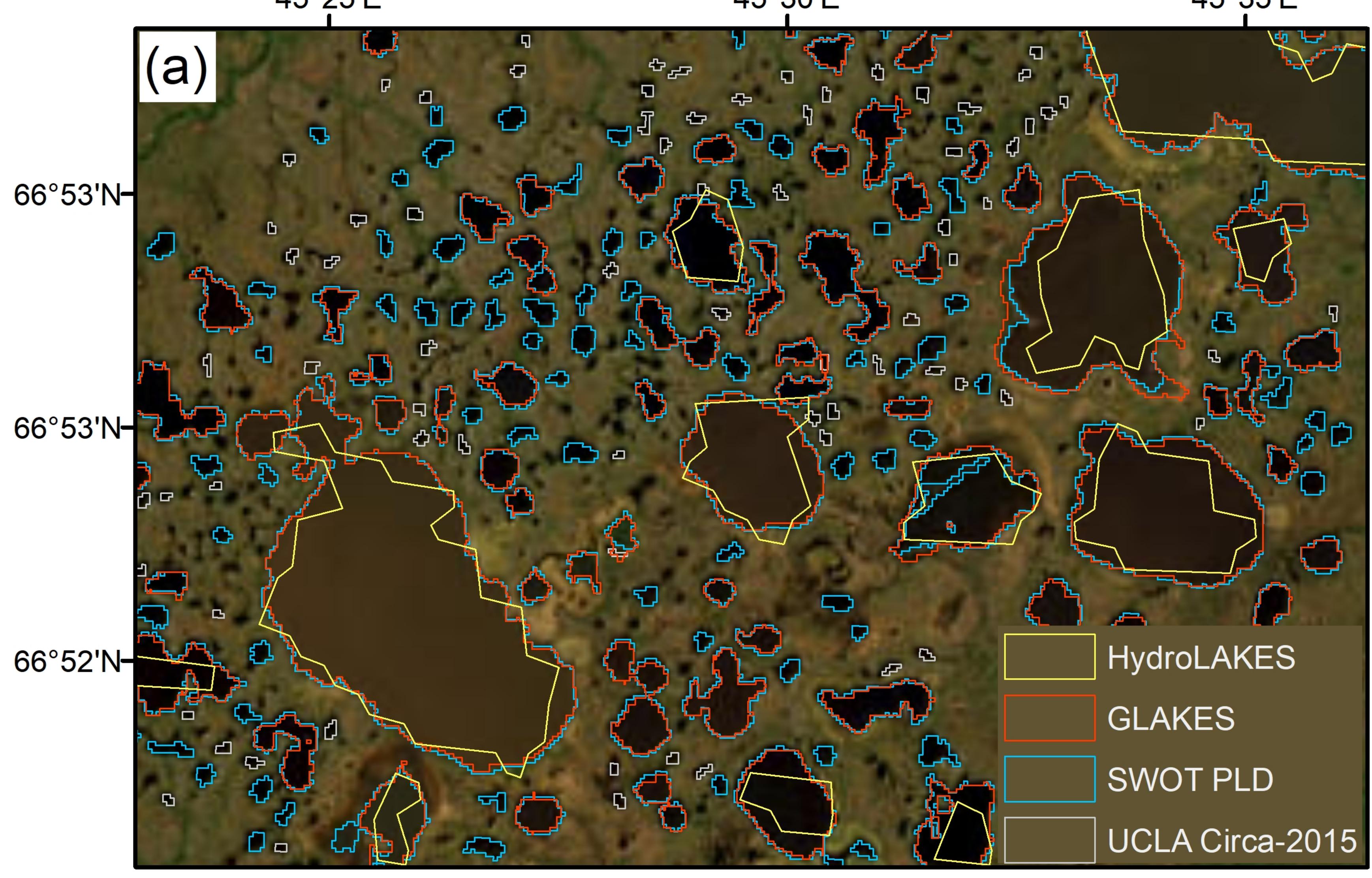
Figure 8.

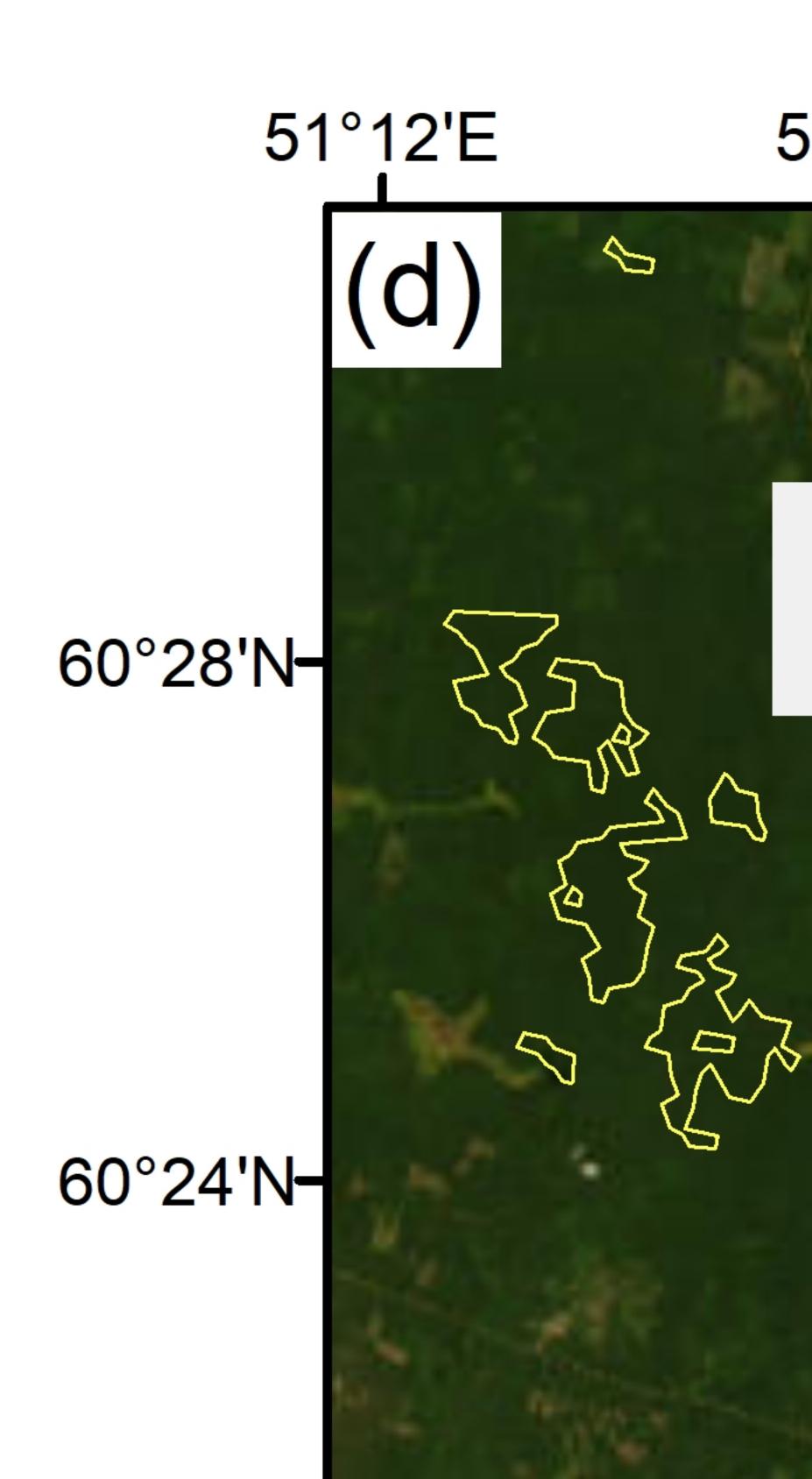




171°25'E

171°30'E





171°35'E

$$54^{\circ}10'S$$

$$54^{\circ}12'S$$

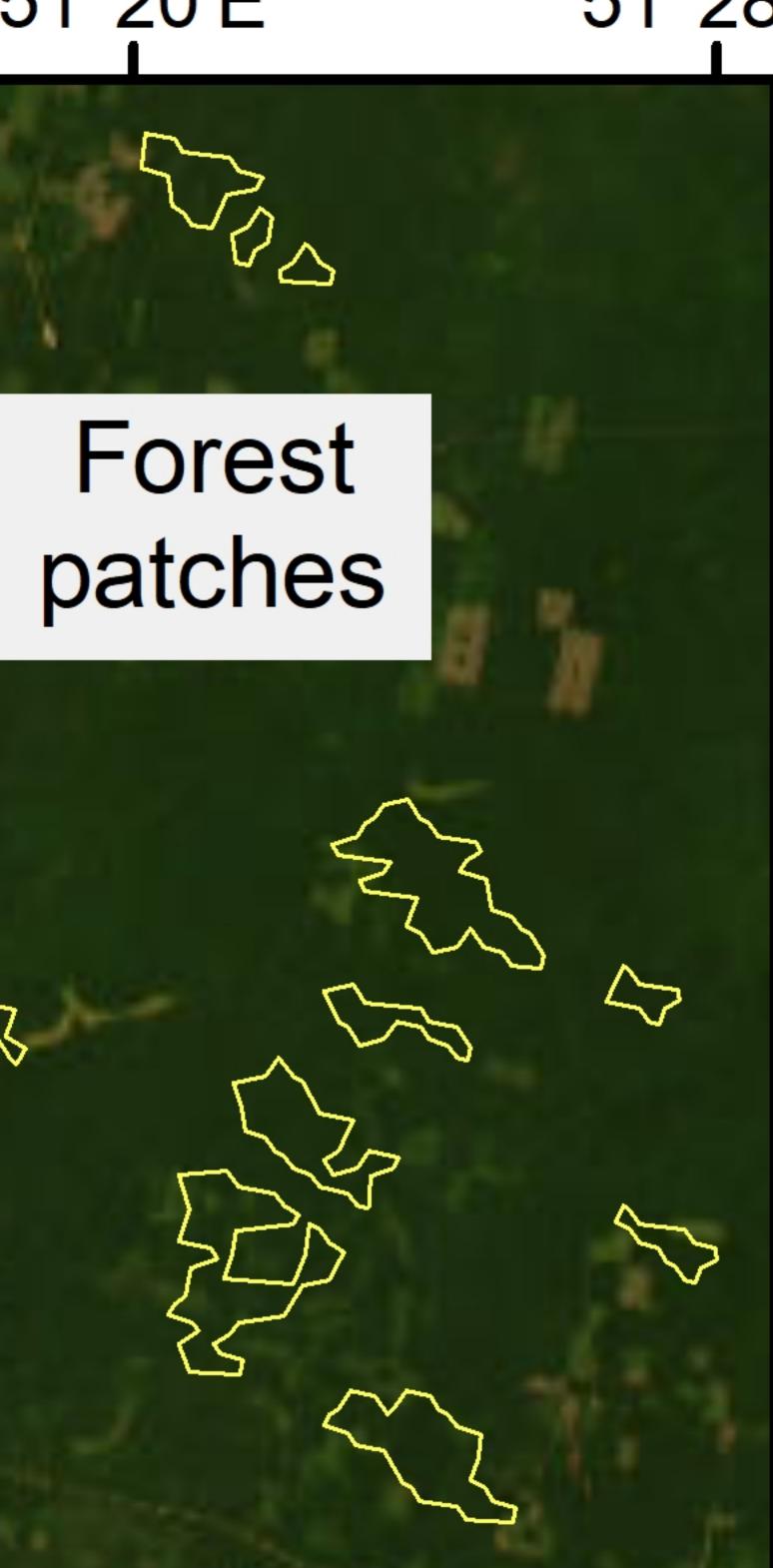
$$54^{\circ}12'S$$

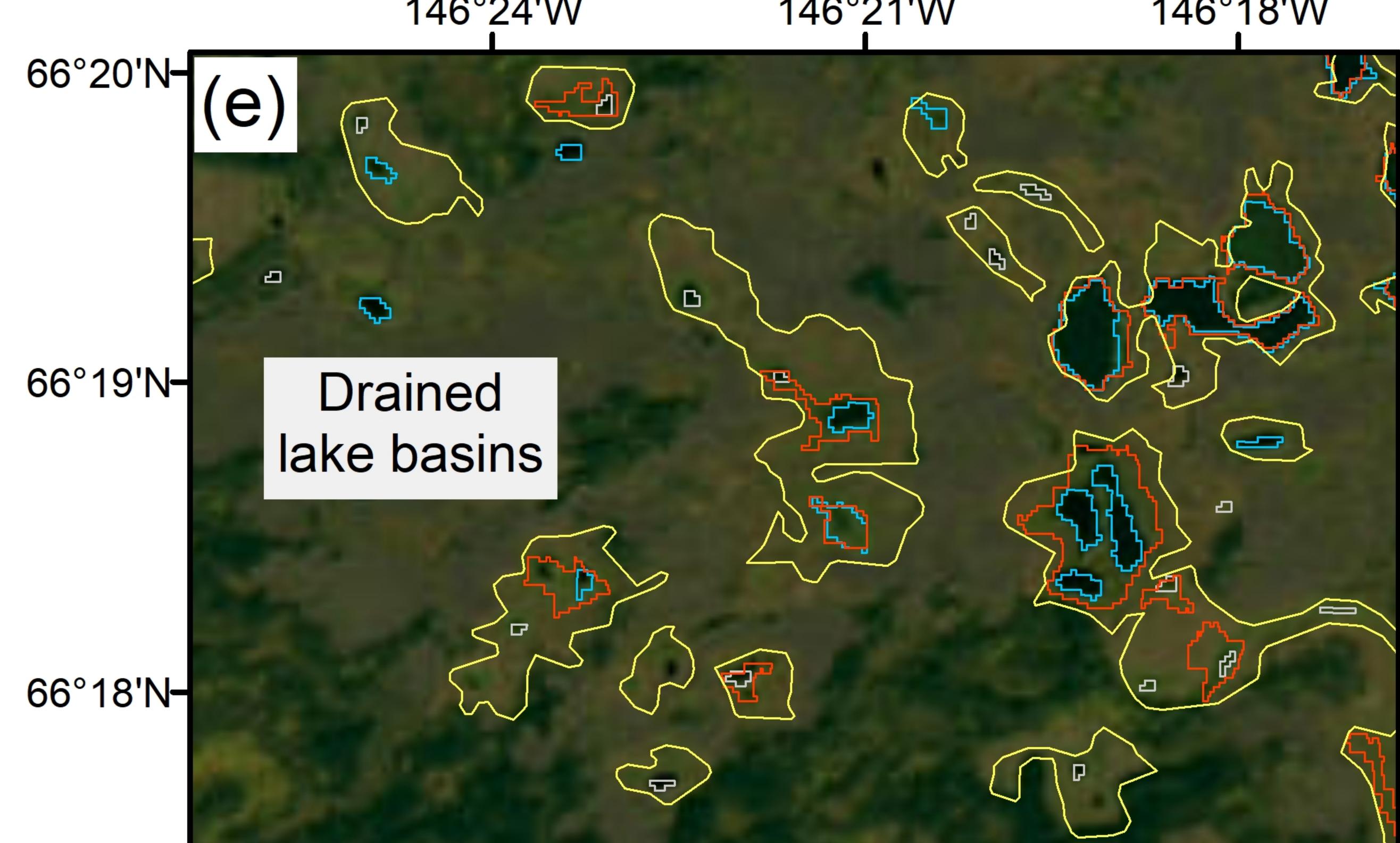
$$54^{\circ}12'S$$

$$54^{\circ}12'S$$

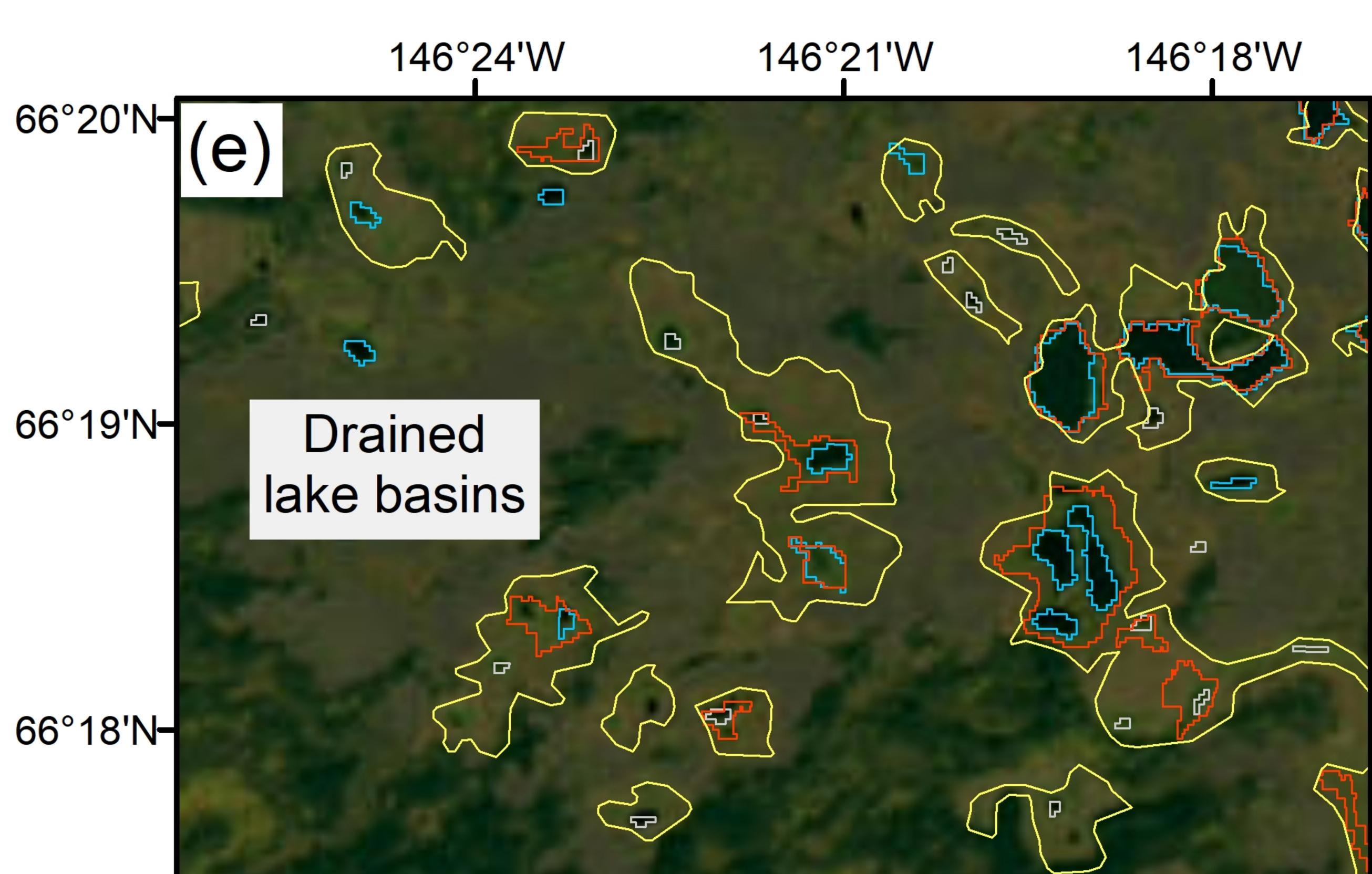
$$54^{\circ}12'S$$

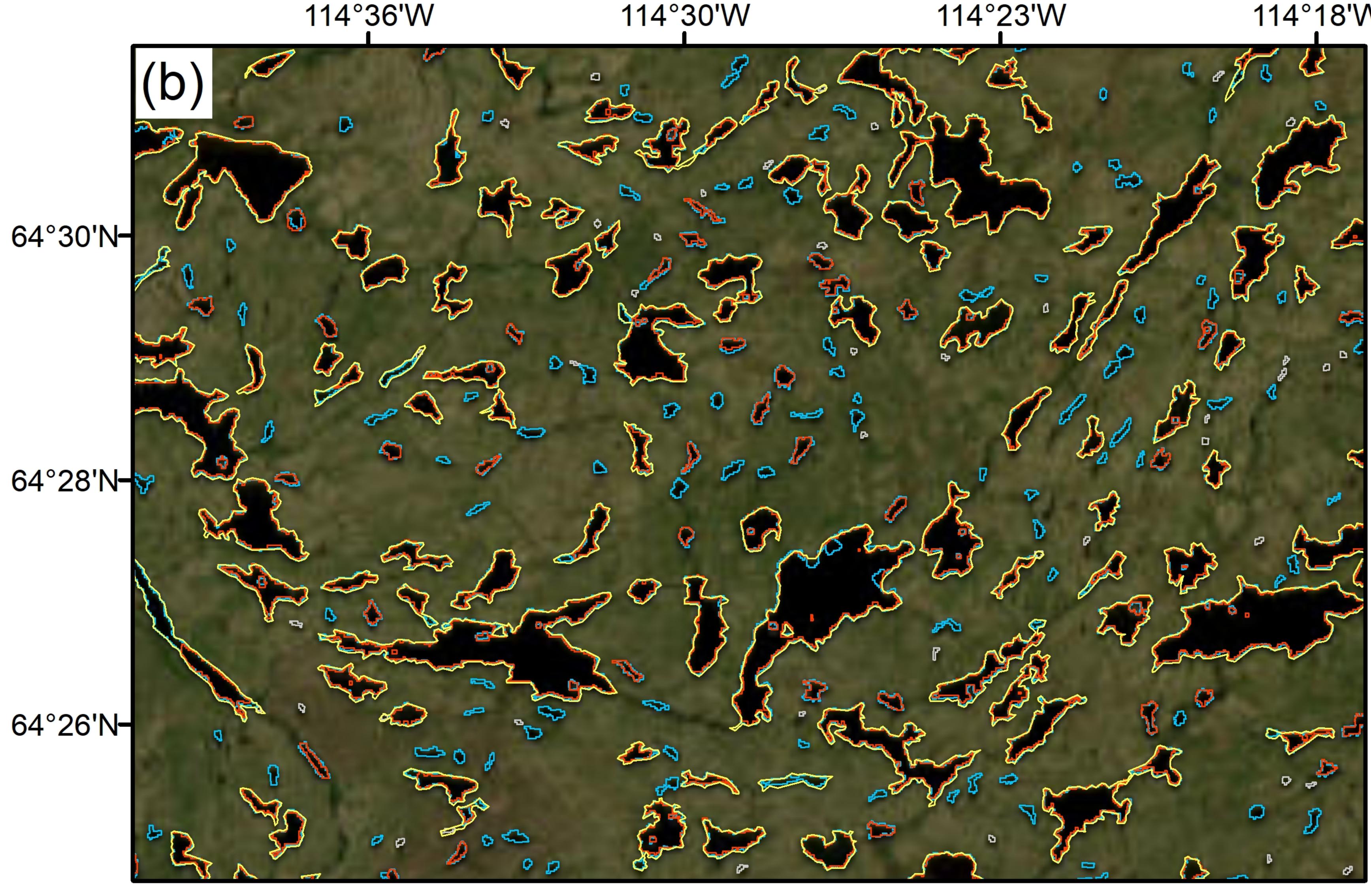
$$54^{\circ}12'S$$











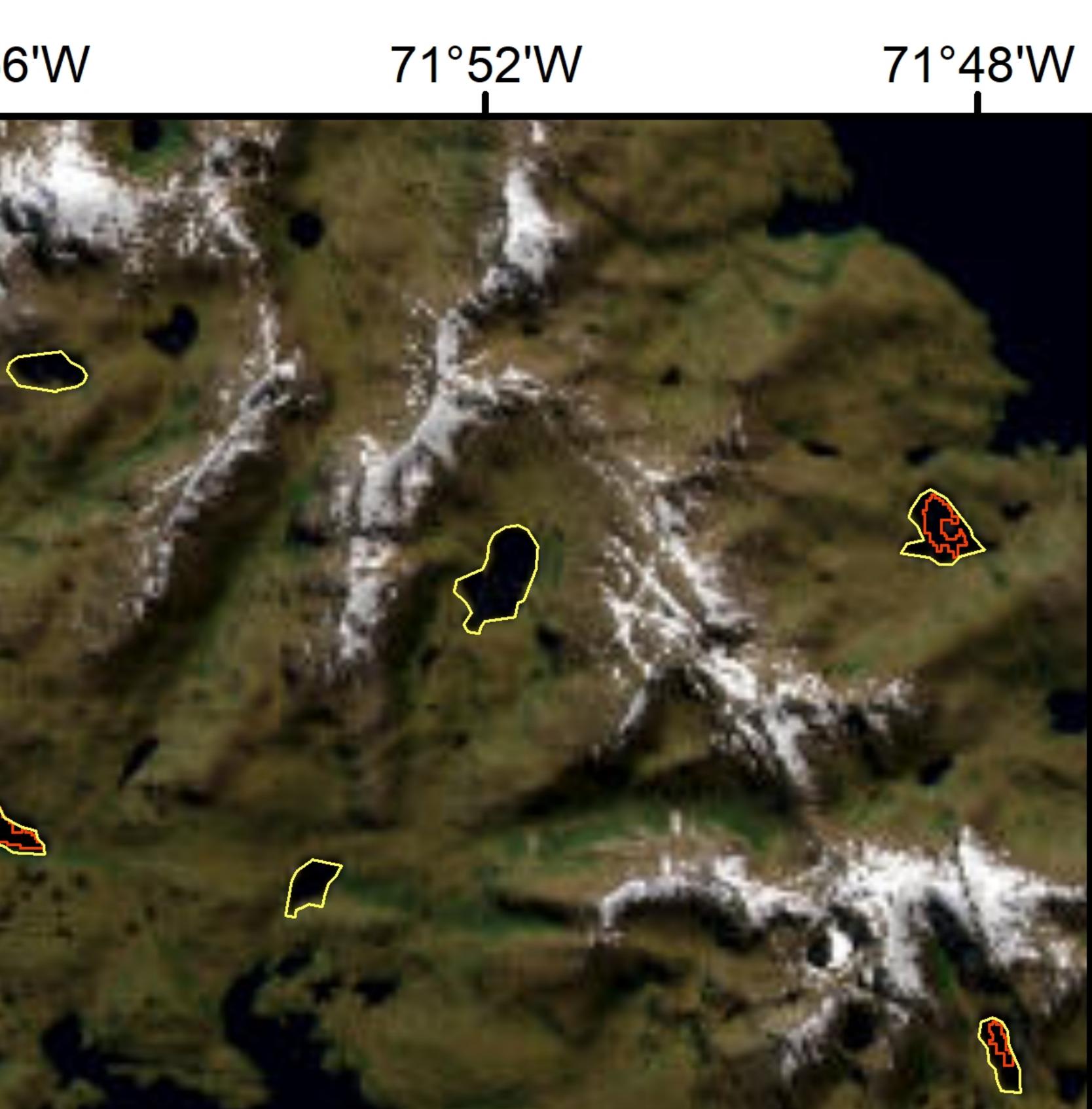


Figure 9.

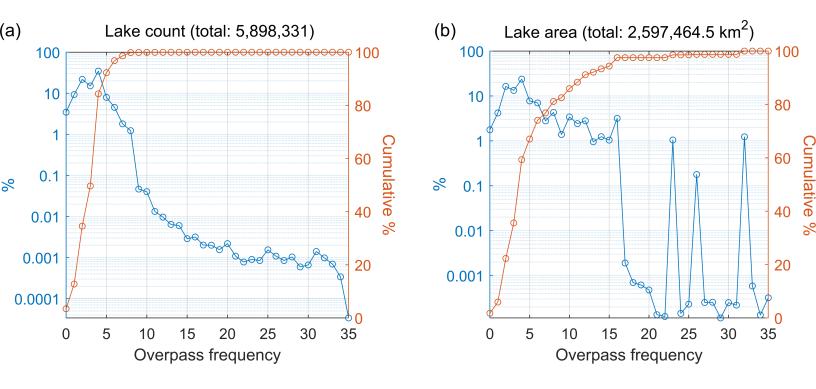


Figure 10.

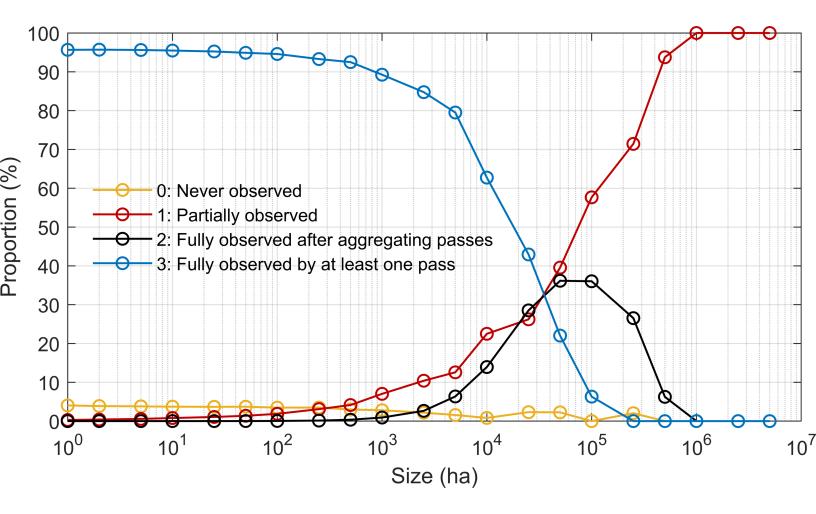
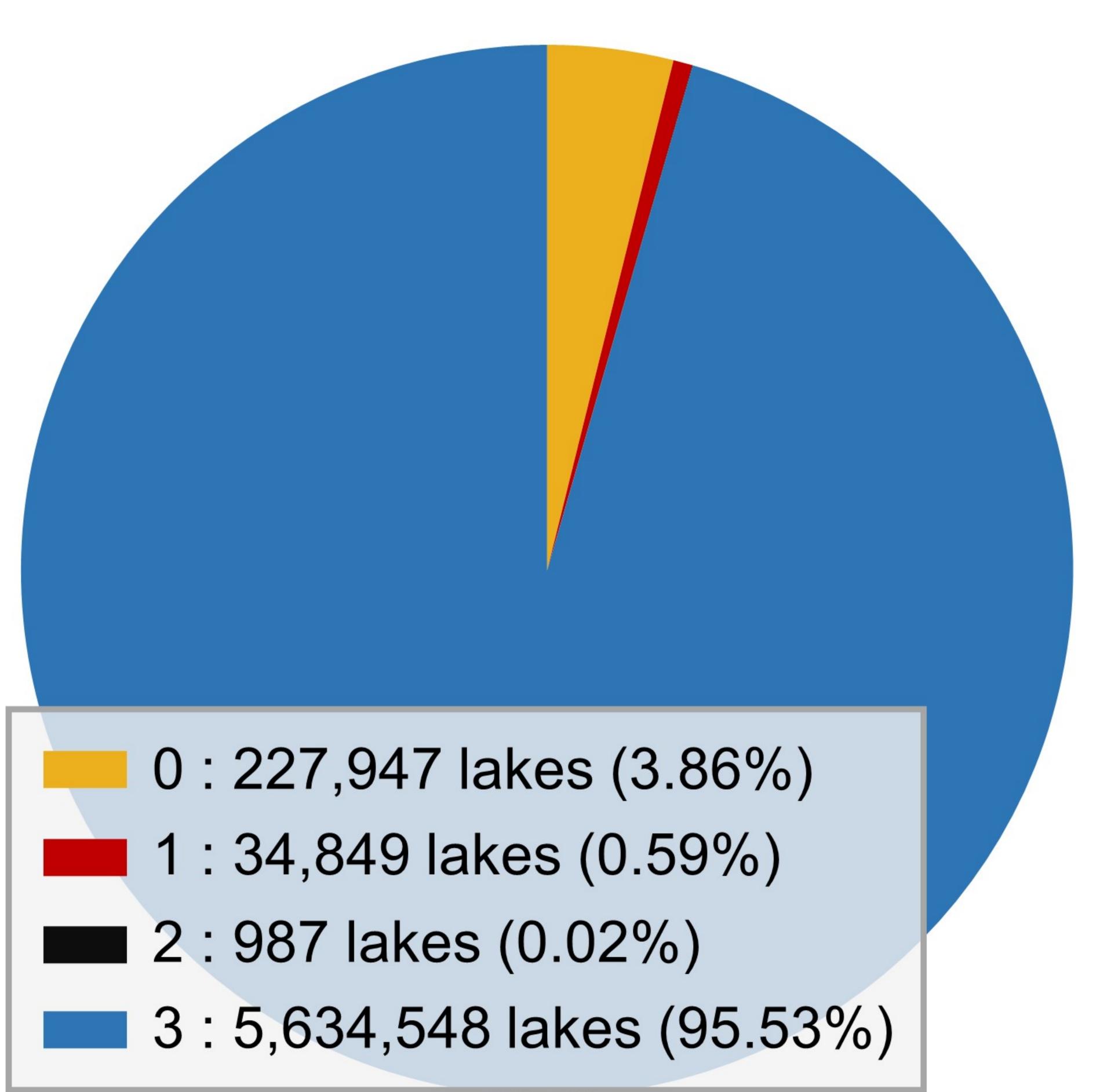


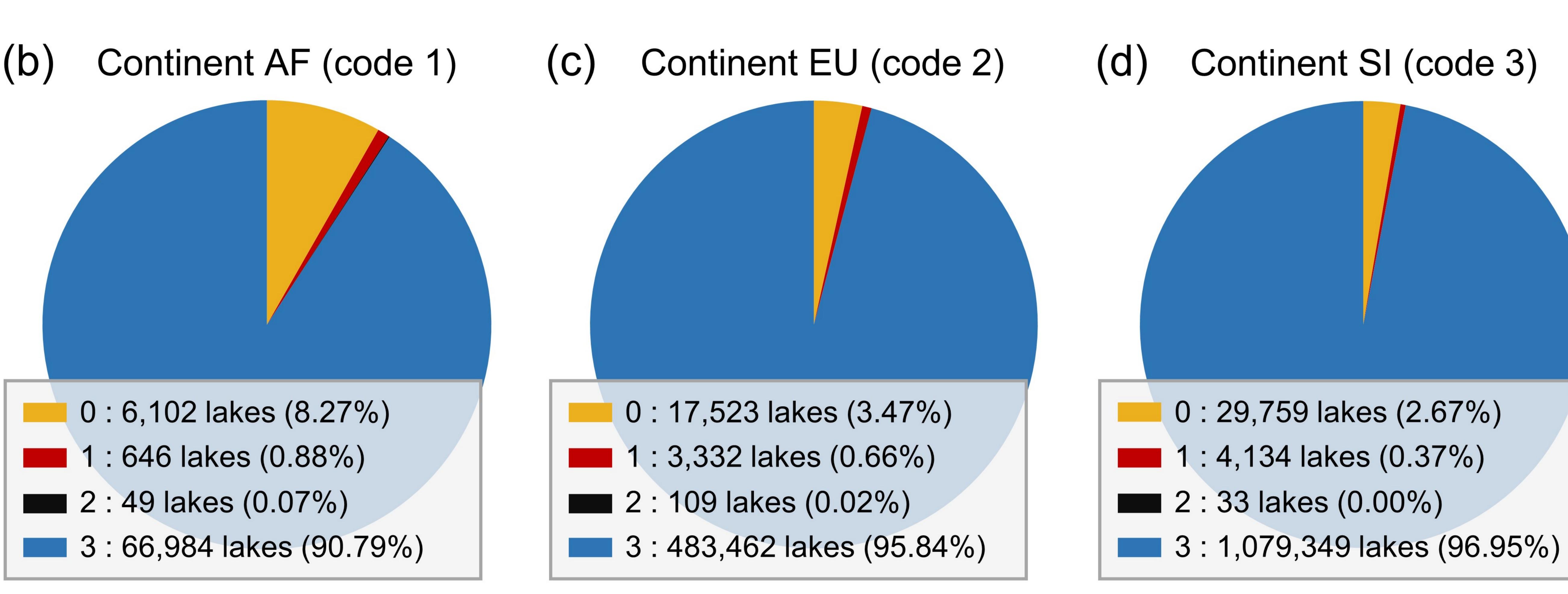
Figure 11.

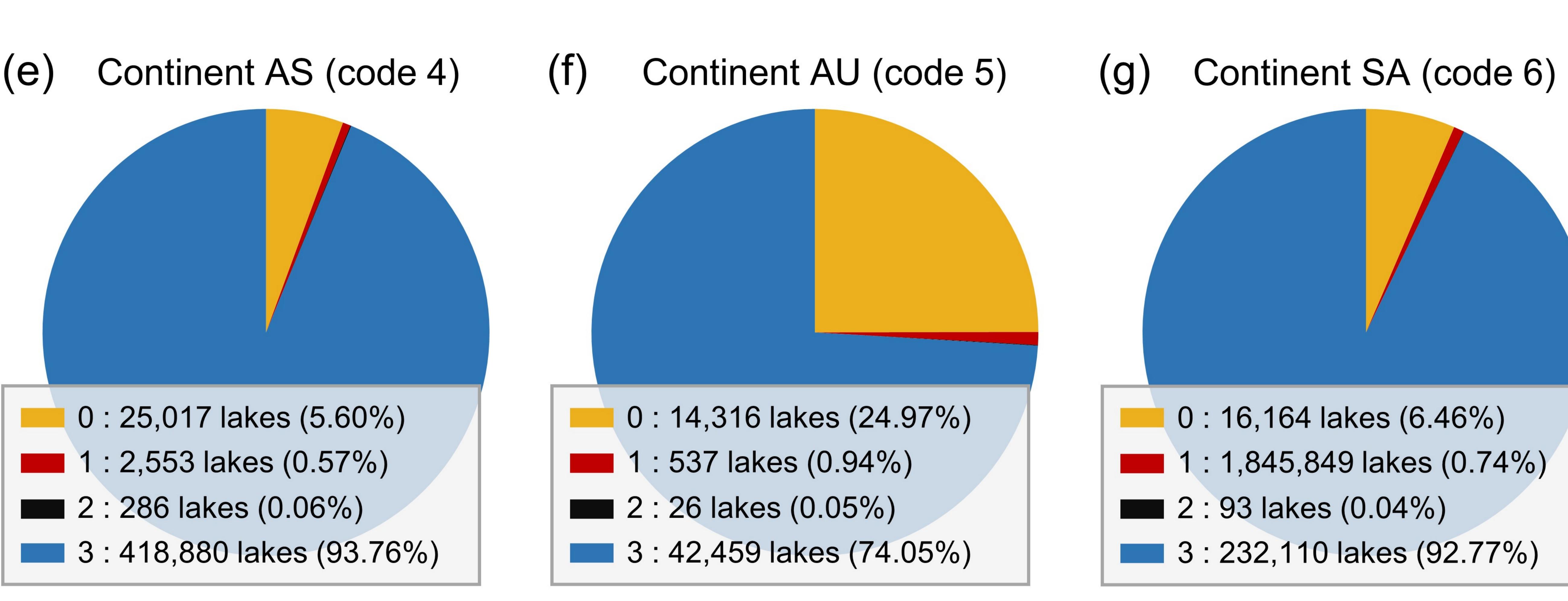
### (a) Global composition of each cycle flag

### SWOT cycle flag for prior lakes

- 0: Never observed
- 1 : Partially observed
- 2 : Fully observed after aggregating passes3 : Fully observed by at least one pass







### (h) Continent NA (code 7) (i) Continent AR (code 8) Continent GR (code 9) 0:24,583 lakes (1.29%) 0:90,146 lakes (5.96%) 0:4,337 lakes (10.64%) 1:7,870 lakes (0.41%) 1 : 13,030 lakes (0.86%) 1:902 lakes (2.21%) 2 : 293 lakes (0.02%) 2:97 lakes (0.01%) 2 : 1 lakes (0.00%) 3: 1,867,115 lakes (98.29%) 3 : 1,408,670 lakes (93.16%) 3:35,519 lakes (87.14%)

Figure 12.

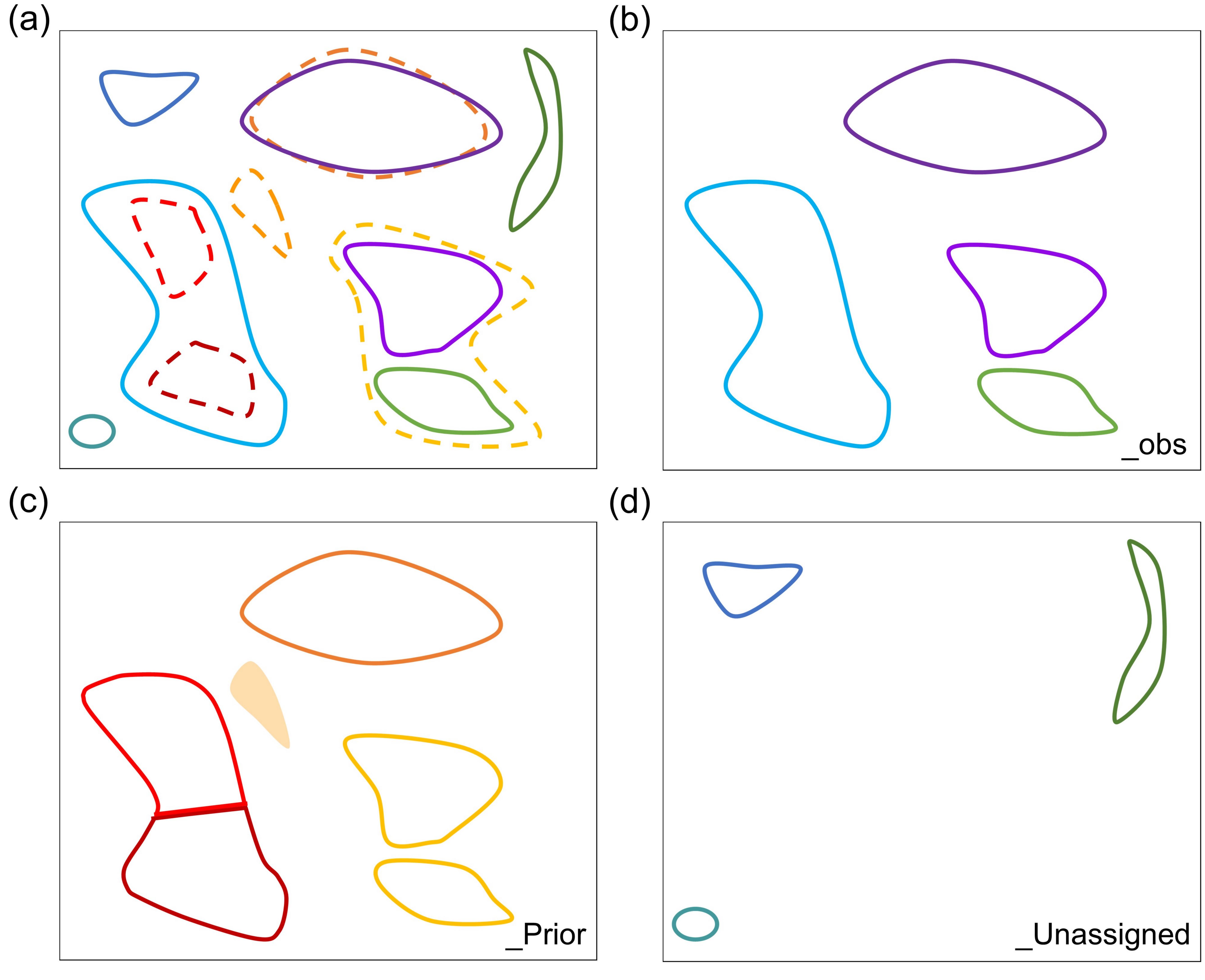


Figure 13.

## (a)



